750269

AEROSPACE REPORT NO.
ATR-75(7470)-1

# Firebrand Investigation

Prepared by
A. MURASZEW and J. B. FEDELE
Vehicle Engineering Division
The Aerospace Corporation
El Segundo, Calif. 90245
and
W. C. KUBY
University of California, Santa Barbara

31 March 1975

Designated Station Representative: R. C. ROTHERMEL
Northern Forest Fire Laboratory
Intermountain Forest and Range Experiment Station
Missoula, Montana 59801

Prepared for
USDA FOREST SERVICE
Washington, D.C.

INT Grant No. 12

THE AEROSPACE CORPORATION

Report No.
ATR-75(7470)-1

# FIREBRAND INVESTIGATION

by

A. Muraszew and J. B. Fedele
The Aerospace Corporation

and

W. C. Kuby
University of California, Santa Barbara

Vehicle Engineering Division
The Aerospace Corporation
El Segundo, California 90245

31 March 1975

Designated Station Representative: R. C. Rothermel

Northern Forest Fire Laboratory
Intermountain Forest and Range Experiment Station
Missoula, Montana 59801

Prepared for

USDA FOREST SERVICE
Washington, D. C.

INT Grant No. 12

FIREBRAND INVESTIGATION

Approved

E. G. Hertler, Director
Aero Engineering Subdivision
Vehicle Engineering Division

P. M. Stevens, Director
Forest Programs
Energy and Resources Division

## ACKNOWLEDGEMENT

The authors would like to acknowledge the help received from the Northern Forest Fire Laboratory in Missoula in the timely reduction of firebrand burning data, and for helpful suggestions from R. C. Rothermel to improve the quality and interpretation of the data.

CONTENTS

TABLES

FIGURES

FIGURES (concluded)

# I. INTRODUCTION

The rate of spread of wildfires was the object of investigation of various research workers such as Fons [1946], Byram [1959], Von Wagner [1967], Albini [1966], Rothermel [1972], and others. This work was prompted by the fire managers' need for a means of predicting fire spread in real time, based on some model correlating fuel properties, topography and meteorological data, rather than on just an educated guess. Although this work is not completed, much was done in this direction in the form of Fire Spread Simulation Program (Stevenson, et al [1973]), based on earlier Forest Service investigations. This model, as others in existence, only simulated the continuous progress of a fire as a function of the variables mentioned above. However, in real life, fire progress, particularly in large fires (see Anderson [1968], Rothermel [1967]), is characterized by hitherto unpredicted spot fires generated at some distances from the main front by flying firebrands which, in turn, often form another dangerous fire front.

The work described in this report concerns the investigation of firebrands. From earlier work (Muraszew [1974]), it appeared that generally two-dimensional convection formed above the fire front did not possess sufficient uplift velocity to lift large firebrands high enough so that the prevailing wind could carry them ahead of the main fire front to present a hazard. It appeared also from the historical data on some large fires that fire whirls created in such fires were able to lift large pieces of fuels to considerable heights.

Thus, the mechanism of spot fire formation can be attributed to these phenomena: meteorological conditions leading to fire whirls; generation and lifting of firebrands which continue to burn in flight; and continuous burning of the firebrand after fall in a recipient fuel from which a spot fire can start.

The work undertaken under Forest Service Grant INT No. 12 consisted of a) investigation of firebrand burning in flight and b) the generation and lifting of firebrands in a simulated fire whirl.

## II. SCOPE OF WORK

### A. INVESTIGATION OF FIREBRAND WIND BURNING

The objective of this work was to obtain data for prediction of the trajectory of firebrands as a function of their initial size, uplift velocity in a convection column, and of the prevailing wind outside of the column. To reach this objective, the burning history of a firebrand in flight had to be experimentally established.

This work consisted of burning wooden dowels, plates, and natural fuels in a wind tunnel with varying velocities under simulated flight conditions. The weight of the firebrands was measured continuously and their volume was estimated from photographs taken during burning. From these two values the density of the firebrands was calculated as a function of time and wind velocity.

The experimental work was carried on in the Northern Forest Fire Laboratory (NFFL) in Missoula, Montana; the analytical interpretation of the data was done at The Aerospace Corporation.

### B. INVESTIGATION OF FIRE WHIRLS/FIREBRANDS CORRELATION

The objective of this work was to obtain a functional relationship between the fire whirl intensity and the size and number of firebrands generated. As a first step in that direction, analytical and experimental work on fire whirls was performed under this Grant.

The analytical work consisted of formulation of equations coupling the vortex characteristics with the burning fuel properties, and with the air inflow through the boundary layer at the ground.

The experimental work consisted of building a test rig for formation of subscale vortices, characterizing their intensity using acetone as the burning fuel, and performing preliminary tests burning wood cribs.

The experiments were performed at the University of California at Santa Barbara under the direction of Professor W. C. Kuby, who was retained as a consultant to the program. The data analysis and correlation with the theoretical model was performed at The Aerospace Corporation.

The duration of the program was seven months, from 14 July 1974 through 31 January 1975.

## III. INVESTIGATION OF FIREBRAND WIND BURNING

### A. ANALYSIS

Considerable work on firebrands in flight was performed by Tarifa [1965]. Tarifa found that firebrands with usually large drag-to-weight ratios are accelerated very quickly to the wind velocity and while flying they continue to drop with an instantaneous fall velocity, $w_{f(t)}$, which is a function of time. The fall velocity can be expressed as

$$w_{(t)} = \left( \frac{m_{(t)} \cdot g}{\frac{1}{2} C_D \cdot \rho_a A_{(t)}} \right)^{1/2} \qquad (1)$$

$w_{(t)}$ - fall velocity, cm/sec
$g$ - gravitational constant, 98/cm/sec$^2$
$m_{(t)}$ - firebrand mass, g
$C_D$ - drag coefficient
$A_{(t)}$ - firebrand maximum cross section, cm$^2$
$\rho_a$ - ambient air density, g/cm$^2$.

Tarifa made three important observations: the value of coefficient $C_D$, as determined for the initial form of firebrand, changed very little during the burning period until the firebrands became very small; the change in weight and size of burning firebrands in a free fall was the same as if they were burning in a fixed position in the wind at a velocity equal to $w_f$; drag force of a firebrand tumbling in flight was very close to that based on maximum cross-section (maximum drag).

It was further found by Tarifa that the ratio of instantaneous fall velocity, $w_{(t)}$, to initial fall velocity, $w_o$, is a unique function of a parameter, Z, for various firebrand sizes, shapes and types of wood. The parameter Z is expressed as:

$$Z = \frac{w_o \cdot t}{C_D} \left( \frac{w_o \cdot D_o \quad \rho_a}{\mu_a} \right)^{-0.4} \cdot \left( \frac{\rho_a}{\rho_o} \right)^{1.3} \cdot \left( \frac{L_o}{D_o} \right)^{-0.4} \cdot K \qquad (2)$$

The subscript, o, refers to initial firebrand conditions at time, $t = 0$.

$D_o$ - initial firebrand diameter, cm

$\mu_a$ - ambient air viscosity, poise

$L_o$ - initial firebrand length, cm

K - shape factor.

The plot of parameter Z vs. $w_{(t)}/w_o$, from Tarifa [1955], is shown in Fig. 1. Since Z can be calculated as a function of time once the initial characteristics of the firebrand are known, then from Fig. 1 (or equivalent algebraic expression representing this curve) the value of $w_{(t)}/w_o$ can be obtained.

This was the main scope and extent of Tarifa's work. A few curves were given in his report showing a change of mass, volume and surface for a sphere with the burn time, but no burn data were presented on the more conventional forms of firebrands, viz.: cylinders, plates or natural woods. Thus, while trajectories of firebrands can be calculated from Tarifa's work, no data are obtainable on the size and weight of the firebrand at the end of its trajectory.

Yet, knowledge of the condition of a firebrand reaching the ground is essential for assessment of its capability to ignite the surrounding fuel. This was recognized by researchers studying the firebrand problem and, for instance, Lee and Hellman [1969] assumed that the density of the firebrand remains constant and, based on Tarifa's data, developed formulae for the change in diameter. Tarifa, in his paper presented to the Combustion Institute (Tarifa [1965]), made the observation that the law of variation of a spherical firebrand radius is similar to that of a combustion of a liquid sphere.

It became apparent that more experimental data have to be provided on firebrands burning in wind, and obtaining such data was one of the objectives of this program. The emphasis was not put on the measurement of fall velocity, which was covered extensively by Tarifa, but on the measurement of weight and volume of various types and sizes of wood at various wind velocities.

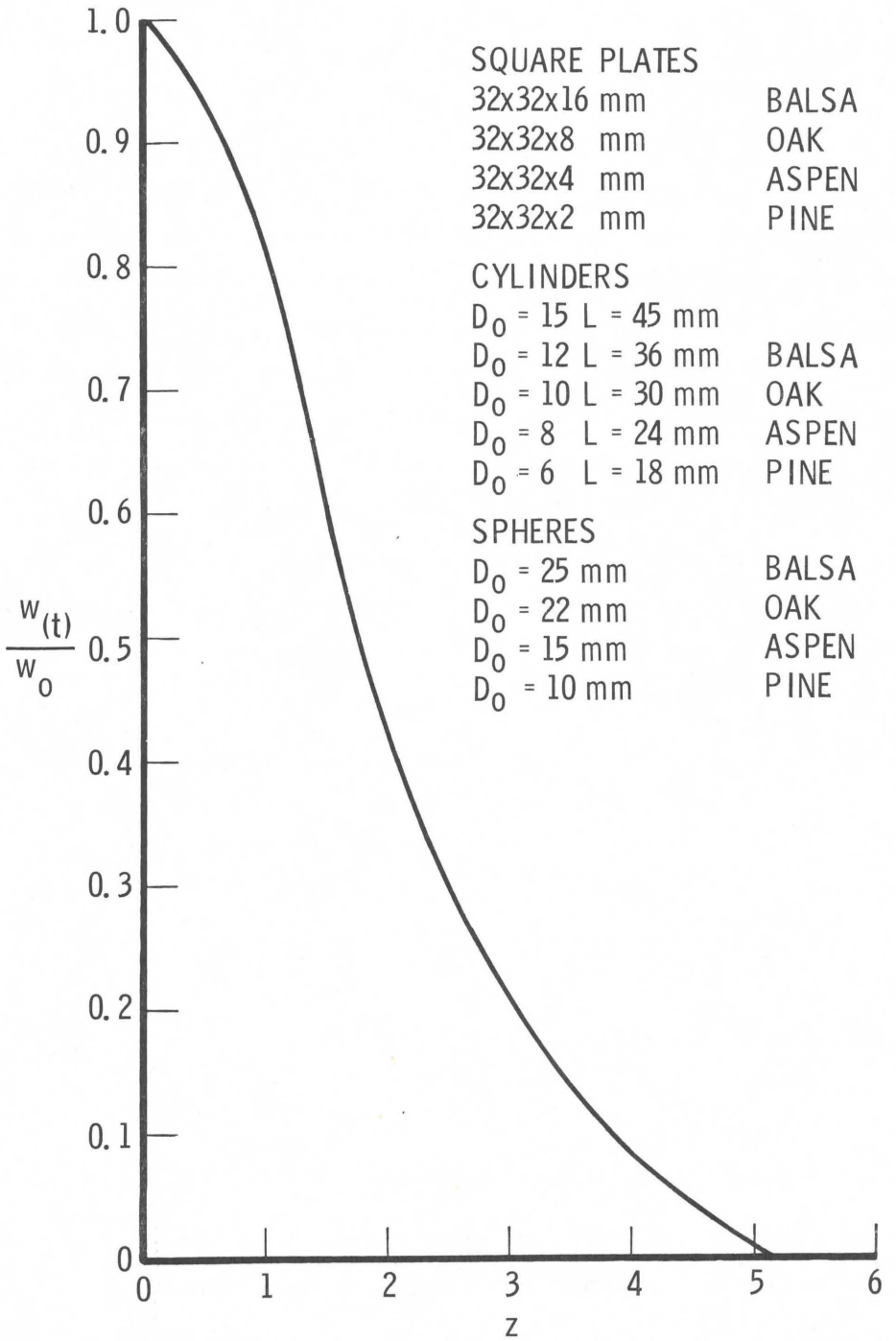


Fig. 1. Dimensionless Correlation of Experimental Results for the Combustion of Firebrands at Final Velocity of Fall

Substituting in Eq. (1) the product of volume and density for m, and taking the ratio of instantaneous to initial fall velocity, one obtains

$$\frac{w_{(t)}}{w_o} = \left(\frac{D_{(t)}}{D_o} \cdot \frac{\rho_{(t)}}{\rho_o}\right)^{1/2} \tag{3}$$

where, for cylinders and spheres $D_{(t)}$ and $D_o$ represent the actual diameter; for other shapes $D_o$ can be regarded as a dimension representing volume/maximum cross-section ratio. Since the ratio of fall velocity can be defined from Tarifa's work, and if the ratio of $\rho_{f(t)}/\rho_{fo}$ is experimentally established, then the diameter of the firebrand could be calculated at any time instant of firebrand burning. The choice of density as the variable to be determined experimentally is deliberate. The burning rate of firebrands is mainly controlled by the rate of cellulose (and lignin) pyrolysis, and analytical expressions for that rate were evaluated and proposed in the past by various research workers. Secondly, the determination of the dimension D for irregular shapes would be difficult since not only volume but also a total surface area must be known.

From the past work on wood pyrolysis summarized by Muraszew [1974], it was established that the pyrolysis reaction is of first order and it can be written as

$$\frac{d\rho_{(t)}}{dt} = -\rho_{(t)} \cdot a \exp\left(\frac{-E}{RT}\right) \tag{4}$$

where E - activation energy in cal/g mole
T - pyrolysis temperature, $^{o}R$
a - pre-exponential constant, $sec^{-1}$
R - universal gas constant, 1.987 cal/g-mole-$^{o}K$.

Previous investigations by other researchers led to the observation that the fuel burn rate (and rate of density change) is mostly affected by the fuel element diameter. From experiments of burning various shapes and types of wood in quiescent air, Muraszew [1974] determined that the general form of Eq. (4) should be modified to include sample diameter and that a reasonable agreement was obtained with a correlation

$$\frac{\rho_{(t)} - \rho_c}{\rho_o - \rho_c} = \exp^{-\frac{t}{D_o K}} \qquad (4a)$$

$\rho_c$ - final burning wood density, $g/cm^3$

The constant K was determined to be equal to 55 sec/cm when t was expressed in seconds and $D_o$ in cm. A computer program for firebrand trajectories, based on Tarifa's work, and firebrand burn history, based on Eq. (4a), was written at Aerospace (Young [1973]).

It is, however, not known whether Eq. (4a) applies to in-wind burning. If the burning of wood in wind is controlled by the rate of the pyrolysis process, then the basic relationship of Eq. (4a) should be valid, although the values of the parameter, K, could be different. This will be determined experimentally in the work described below.

An important parameter in the repeatability of the results was the ignition time. Variations in the time resulted in different rates of burning (varying values of K), although the basic first order reaction relationship was retained.

Another significant parameter in Eq. (4a) is the final wood density on completion of burning, $\rho_c$. It was found that for all types of wood burned in quiescent air, the value $\rho_c/\rho_o = f(D_o)$. For small wood elements, ($\leq 0.6$ cm), the burning was completed down to ash ($\rho_c/\rho_o \sim 0.06$); for medium sized (0.6 - 4 cm) the value of $\rho_c/\rho_o$ varied as a function of $D_o$; for large elements above, say, 5 cm in diameter, burning stopped as soon as the ignition source was removed and $\rho_c/\rho_o \sim 1$. Further experimental data on $\rho_c$ are required in quiescent air as well as in wind burning, and such experiments were performed in the work described below.

The effect of air temperature and relative humidity, and the effect of fuel moisture are other parameters which may affect the wood burning in quiescent air and in wind. Investigation of these parameters was included in the experimental work.

## B. EXPERIMENTS

The experimental work was performed at the NFFL in Missoula, Montana, under the direction of R. C. Rothermel. The detailed description of the apparatus, instrumentation and test techniques, including fuel ignition, will be described in a NFFL report and, therefore, will be only briefly discussed here.

### 1. APPARATUS

The in-wind burning of wood elements was performed in a horizontal wind tunnel with controlled air temperature and humidity. A load cell weighing system was built to introduce a minimal flow disturbance around the burning sample, which was placed horizontally. During the burning of the sample, photographs of it were taken through the wind tunnel windows at specific intervals, for volume measurements. The sample ignition system, which was developed in several steps, consisted of a shielded gas burner with gaseous oxygen addition. The objective of the igniter development was to provide a complete ignition of the sample along its full length in the shortest possible time. The ignition time aimed at was $t_i = 12 \cdot D_o$ sec, with $D_o$ expressed in cm.

The test procedure was as follows: The sample was placed in the tunnel. The sample had been preconditioned to the required moisture content weighed, and its size measured before its placement in the tunnel. Air velocity in the tunnel was set at the required value. Temperature and relative humidity were adjusted as required. Weighing instrumentation and photo graphic equipment were previously placed in position and their calibration and operation checked. The igniter was placed upstream of the sample and ignited. After a fixed, predetermined time, the igniter was turned off and removed from the tunnel while the sample continued burning. During the burning time, weight measurements and photographs were taken.

### 2. INSTRUMENTATION

The weighing equipment consisted of a single load cell thermally isolated from the sample holder, a Statham amplifier, and a strip chart recorder.

The photographs of the sample were taken during the sample burning by two 35 mm cameras viewing the top and the end of the sample. The cameras were synchronized for simultaneous exposures, the time interval between the exposures being manually controlled. Timing marks were simultaneously made on the weight loss recorder when the cameras were triggered.

The sample ignition system after development consisted of a shielded igniter using natural gas boosted with oxygen.

The accuracy of weight measurement is estimated at $\pm$ 2% and of the volume measurements at $\pm$ 20%.

## 3. RESULTS

The wood samples were either oven-dry or they were preconditioned to the required moisture content. The wood samples included: birch, white pine, Ponderosa pine, in 1/2-inch and 1-inch diameter; and various natural fuels in sizes up to 3.5 cm.

Two problems were encountered in the course of tests which affected the accuracy and consistency of results. One was asymmetrical burning in the wind tunnel with reference to the horizontal plane through the sample axis which created an airfoil effect; i.e., added negative or positive component to the weight measurement (the sample was burned in a horizontal position). The onset of "airfoiling" could be detected by discontinuity in weight measurements and such measurements were then neglected. This effect was unexpected and could be avoided by mounting the sample vertically.

In the last phase of this program, the test setup will be modified and the samples mounted in a vertical position; a few check runs will be performed to verify the previously acquired data.

The second problem stemmed from the sample ignition. Since the objective of this work was to establish a firebrand burn law, both in quiescent air and in wind, it was important to ascertain that each sample was fully ignited, i.e., uniformly burning along its full length. On the other hand, the ignition period had to be short in comparison with total sample burn time so that the data taken could indeed represent a self-burning condition. An ideal arrangement would be instantaneous and

complete ignition but, since that was not possible, a goal of ignition time was set for dry fabrication samples, as mentioned before, at $t_i = 12 \cdot D_o$ seconds where $D_o$ is expressed in cm. A development of the ignition system was carried out at Missoula to reach this goal, and this work will be described separately in a NFFL report. It has to be realized that this ignition time will be different for natural fuels because of the insulating effect of the bark, and also it will be different for fuels with high moisture content. Therefore, for each family of fuels it is necessary to adjust the ignition system in such a way that a complete ignition is obtained in the shortest possible time and that this time does not exceed 10% of the total burn time of the sample.

The importance of consistent, complete and short ignition time on the repeatability and consistency of the results cannot be overemphasized. It is realized that in real life the ignition may be incomplete, particularly with long fuel elements, but once the basic burn law is established, a coefficient accounting for partial burning can be introduced.

The burn tests carried out can be divided into three categories:

(1) Basic tests with oven-dry fuels at constant air relative humidity and temperature, but at various air velocities (0, 5, 10, 15, 20 and 25 mph). Fuels included dowels and plates of pine and birch and various natural fuels.

(2) Tests with varying air relative humidity with pine and birch dowels.

(3) Tests with the same fuels at varying moisture content. More details on the size of fuels used are shown in Appendix I.

In addition, a series of tests was carried out to obtain the value of final fuel density ($\rho_c$) corresponding to completion of burning. In quiescent air, the burning stopped at some $\rho_c$ which depended on the diameter of the sample whereas, in wind, with complete initial ignition, the burning of oven-dry samples continued to ash. Initially, final density was determined by burning samples in a wind tunnel at zero wind velocity and calculating density from weight and volume measurement as for the wind case.

To improve the accuracy of following tests, the samples were taken out of the tunnel and their volume calculated from physical measurements; finally, for further improvement of accuracy, samples after completion of burn were immersed in water and their volume established with a proper correction for any water absorbed by the sample. Table 1 summarizes the results.

Table 1. Final Density Ratio of Wood Samples Burning in Quiescent Air (each value is a mean of three or more samples)

| Wood Type | Dia • length, cm | $\rho_c/\rho_o$ | | | |
|---|---|---|---|---|---|
| | | Volume from photographs | Volume from measurements | Volume from water displacement | Eq. (5) |
| Birch | 1.25 • 12.5 | 0.32 | 0.33 | 0.24 | 0.27 |
| Birch | 1.25 • 6.3 | 0.29 | - | - | 0.27 |
| Birch | 2.5 • 12.5 | - | 0.43 | 0.48 | 0.50 |
| Pond. pine | 1.25 • 12.5 | 0.43* | 0.41* | - | 0.27 |
| Pond. pine | 1.25 • 6.3 | 0.38 | - | - | 0.27 |
| White pine | 2.5 • 12.5 | 0.42 | 0.57 | 0.60 | 0.50 |
| Birch | 0.65 • 5.2 | - | 0.07 | - | 0.15** |

* Incomplete ignition suspected
** From Aerospace experiments

On the basis of these data, neglecting the data for Ponderosa pine (1.25 • 12.5), an empirical equation for $\rho_c/\rho_o$ oven-dry fuel was derived, correcting the previous relationship given by Muraszew [1974].

$$\frac{\rho_c}{\rho_o} = 1 - 0.014\left(8.45 - D_o\right)^2 \qquad (5)$$

where $D_o$ is expressed in cm.

Further verification of this equation for natural fuels is required, and experiments with 1.25 cm Ponderosa pine also merit repetition. Probably a correction will be required to account for fuel moisture, although this will be confirmed in experiments performed in the future.

The instantaneous density for in-wind burning was calculated, as mentioned before, from measurements of burning sample weight and volume. These values were then plotted with the aid of a Hewlett-Packard plotter, as shown in Fig. 2. Three or more samples were burned at one set of conditions. The first attempt to obtain a best-fit value for a constant K used in Eq. (4a) by a nonlinear regression program which provided a least-square fit to the data was not satisfactory.

After further study of the data, it became apparent that some samples were not ignited completely and burned too slowly, while in a few others ignition time was too long, giving erroneous self-burning results. Inclusion of such samples in the statistical analysis led to erroneous and varied values of K. Consequently, in the alternative approach, the data were screened and the volume and weight curves smoothed to one set of curves for each set of samples remaining after screening. Such a set of curves was used to determine the best correlation.

Data so obtained are shown in Figs 3 through 6. The values of $(\rho_{(t)} - \rho_c)/(\rho_o - \rho_c)$ are plotted vs. $t/D_o$ in Fig. 3 for zero wind velocity, with $\rho_c$ calculated from Eq. (5). For wind velocity $\geq$ 5 mph, burning continues to the ash stage and for these conditions it is assumed that

$$\frac{\rho_{(t)} - \rho_c}{\rho_o - \rho_c} \simeq \frac{\rho_{(t)}}{\rho_o}$$

and these values are plotted vs. $t/D_o$ in Figs. 4, 5 and 6.

Further data on the effect of air relative humidity and on the effect of fuel moisture are being analyzed and will be reported later. Also, flat plates, pine cones, bark plates are being tested and the results will be included in a later report.

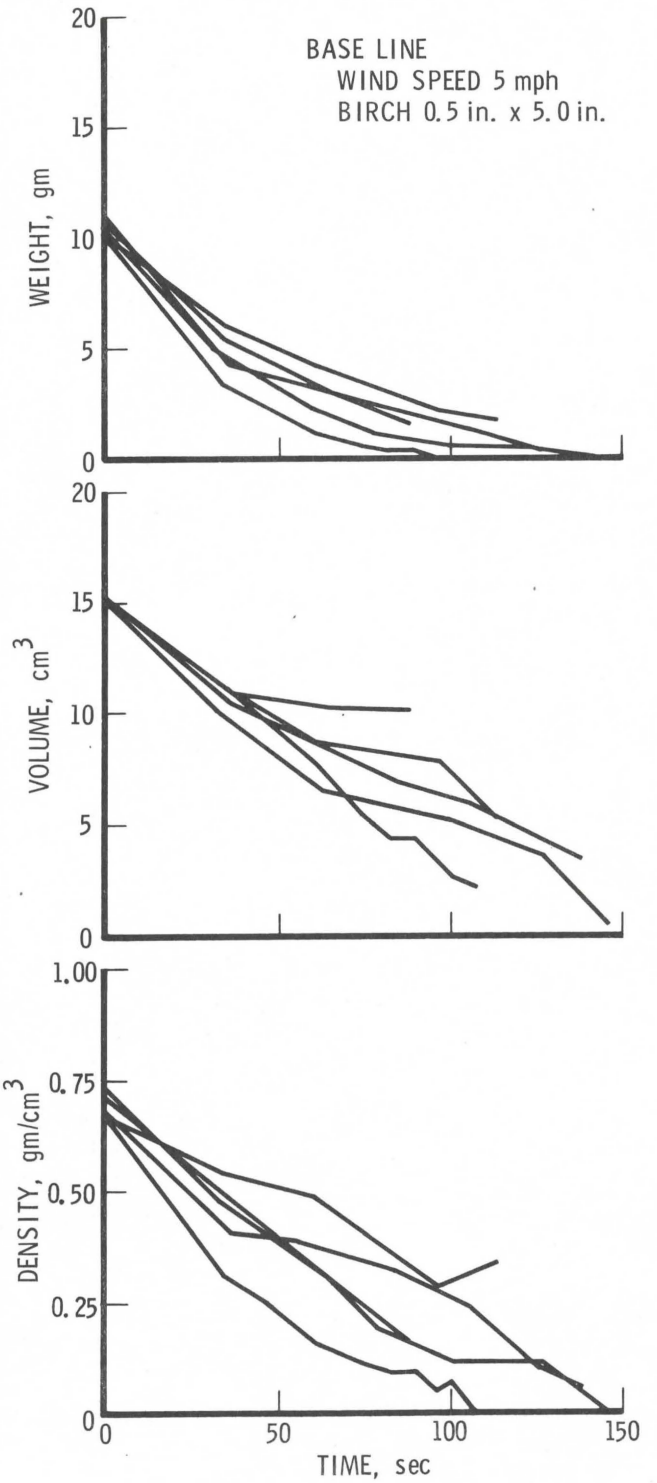


Fig. 2. Plots of Weight, Volume and Density of Burning Wood Samples

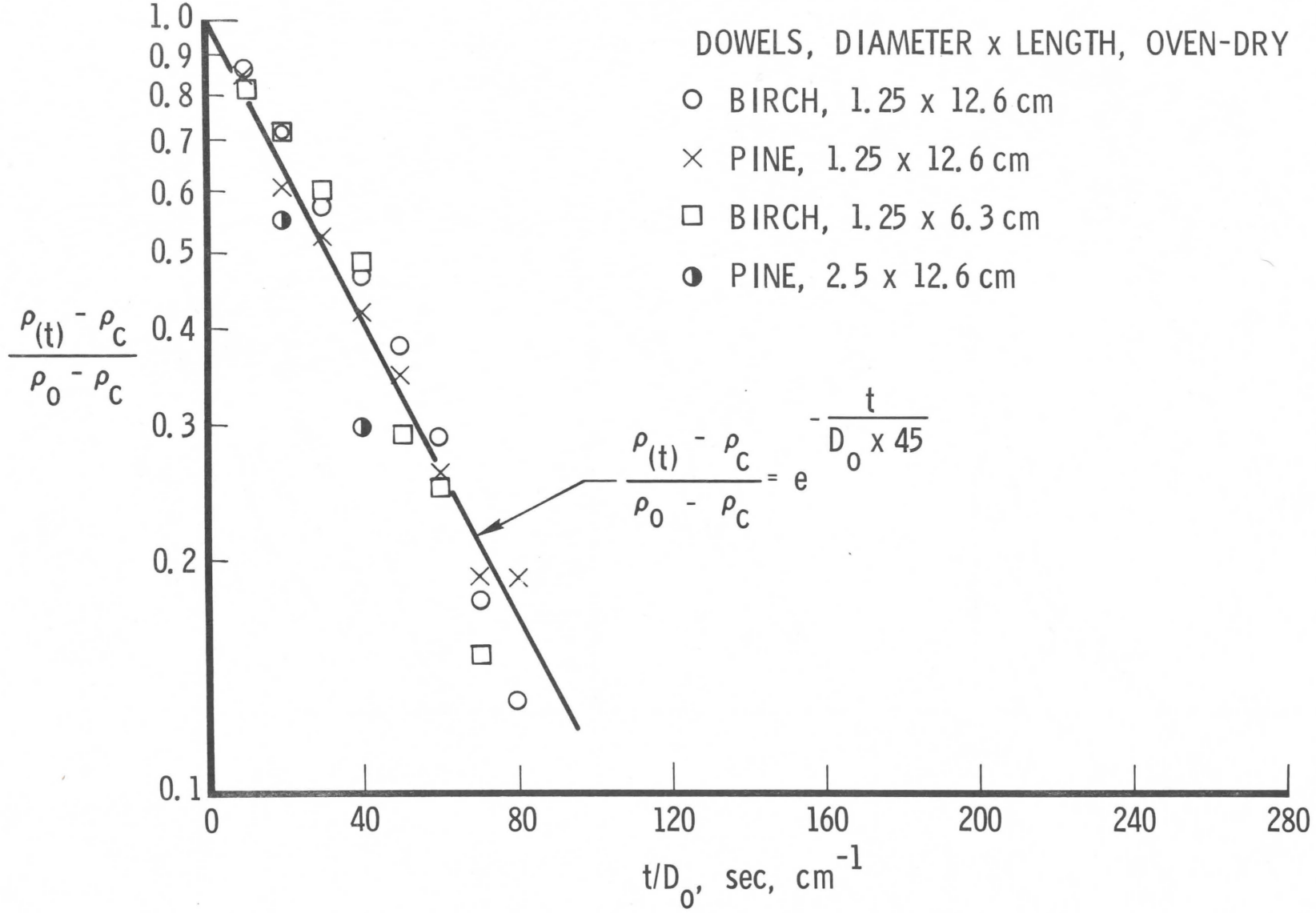


Fig. 3. Density Change of Burning Wood Samples at Wind Velocity = 0 mph

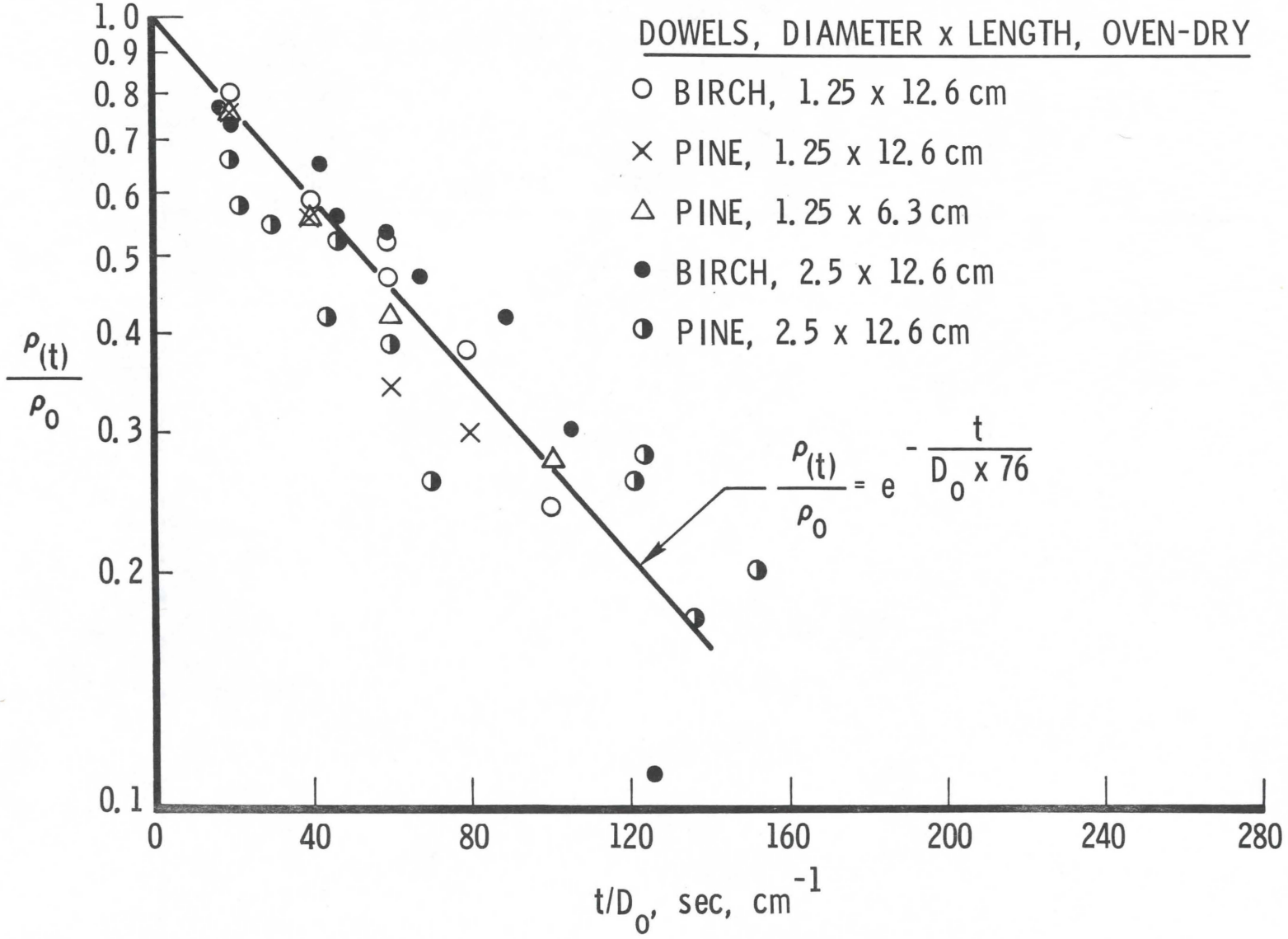


Fig. 4. Density Change of Burning Wood Samples at Wind Velocity = 10 mph

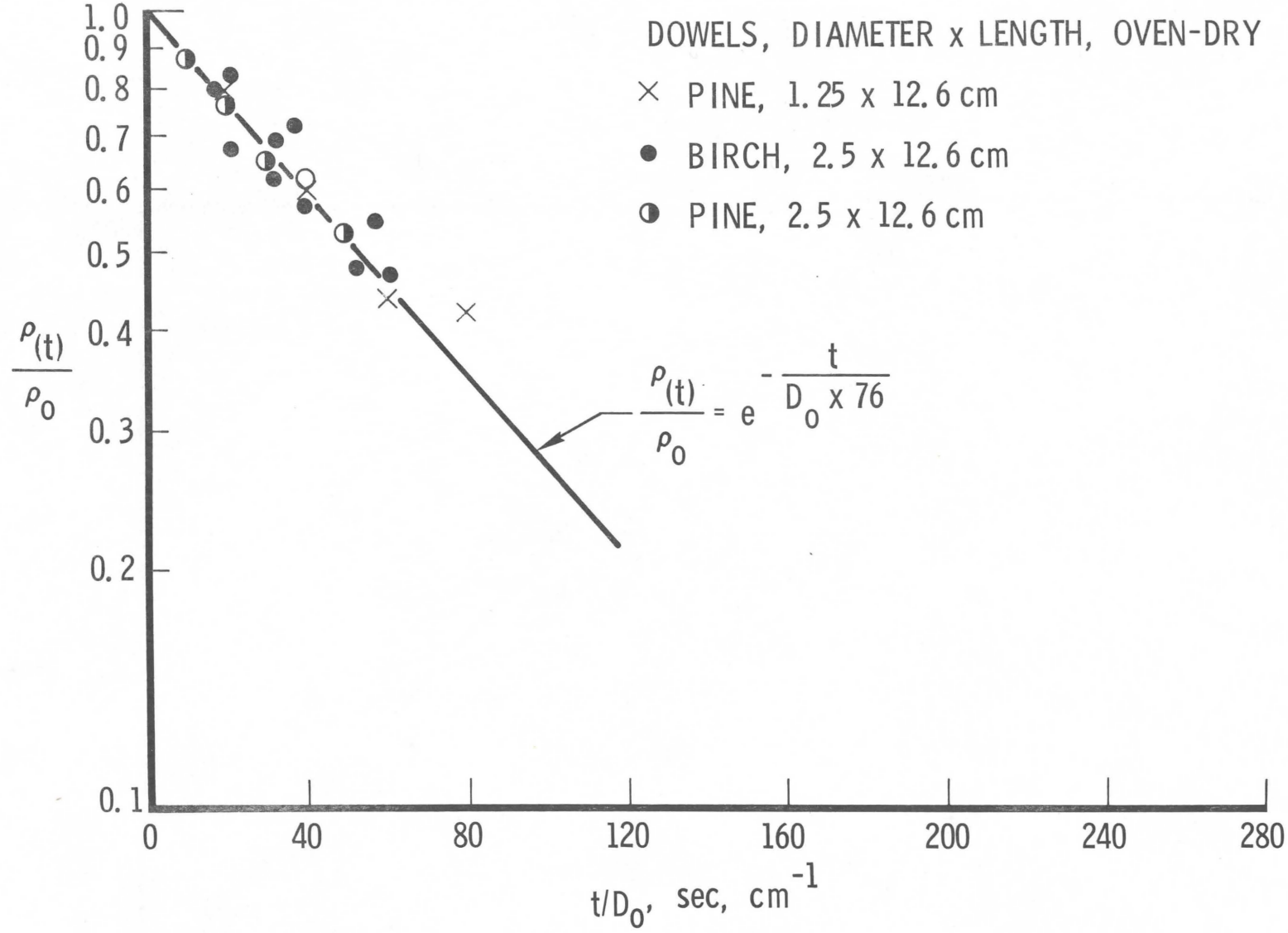


Fig. 5. Density Change of Burning Wood Samples at Wind Velocity = 15 mph

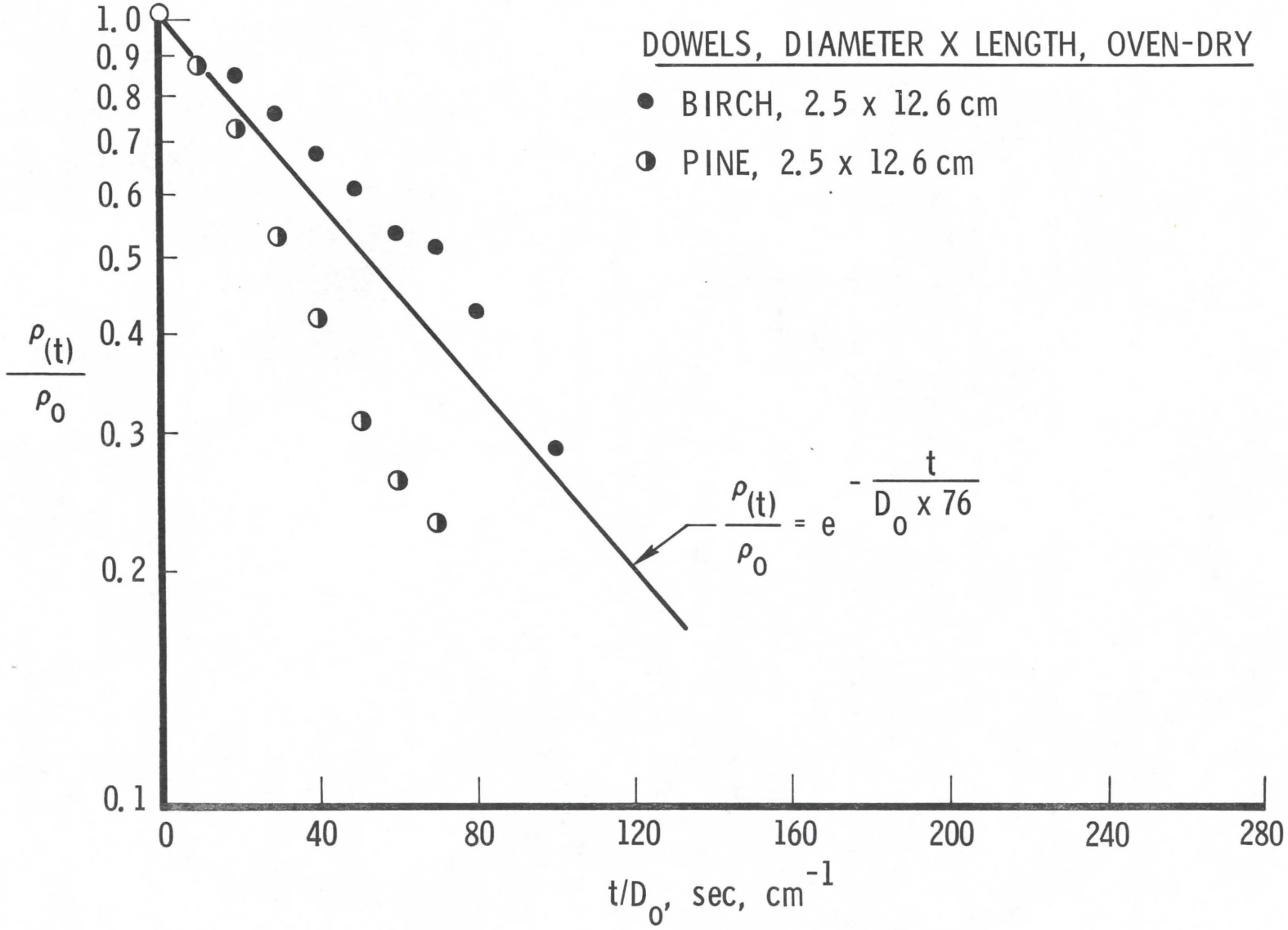


Fig. 6. Density Change of Burning Wood Samples at Wind Velocity = 20 mph

## 4. DISCUSSION

### a. Final Density

The interpretation of final fuel density, $\rho_c$, for quiescent air burning, as defined in Eq. (5), would indicate that when

$$D_o = 8.45 \text{ cm}, \quad \frac{\rho_c}{\rho_o} = 1,$$

i.e., no self-burning will continue after the ignition source is removed. This was not verified in ignition of samples of exactly that size, but in previous tests carried out at The Aerospace Corporation with sample diameter > 5 cm, a brief period of glowing was observed after the removal of the ignition source, followed by extinction, with a very small weight loss. Final air density cannot be determined accurately from sample burning in a wind tunnel at some wind velocity because, with a fixed sample position, burning is concentrated at the leading edge only, and upon removal from the tunnel the sample extinguishes quickly. In reality, a wood sample will tumble in flight with most of the surface remaining hot; upon reaching the ground, it will continue smoldering or glowing. It is postulated that final density can be calculated in such a case by substituting in Eq. (5) for $D_o$ the fall diameter, $D_f$. Final density calculated from Eq. (5) with some experimental data is shown in Fig. 7.

For irregular shapes, the value of $D_o$ or $D_f$ can be derived from sample volume-to-surface ratio. This will be confirmed in further tests with natural fuels. The tests will also include the effect of fuel moisture.

### b. Instantaneous Density

In trying to establish a correlation for the change in instantaneous fuel density, $\left(\rho_{(t)}/\rho_o\right)$, it is important to keep in mind that for such a correlation to be useful in the final determination of spot fire hazard, it must be able to predict with reasonable accuracy the density history for all shapes, types and commonly encountered sizes of firebrands from fuel data normally available to fire managers. Such data consist only of the knowledge of initial fuel conditions ($\rho_o$, size, shape, type of wood, moisture content).

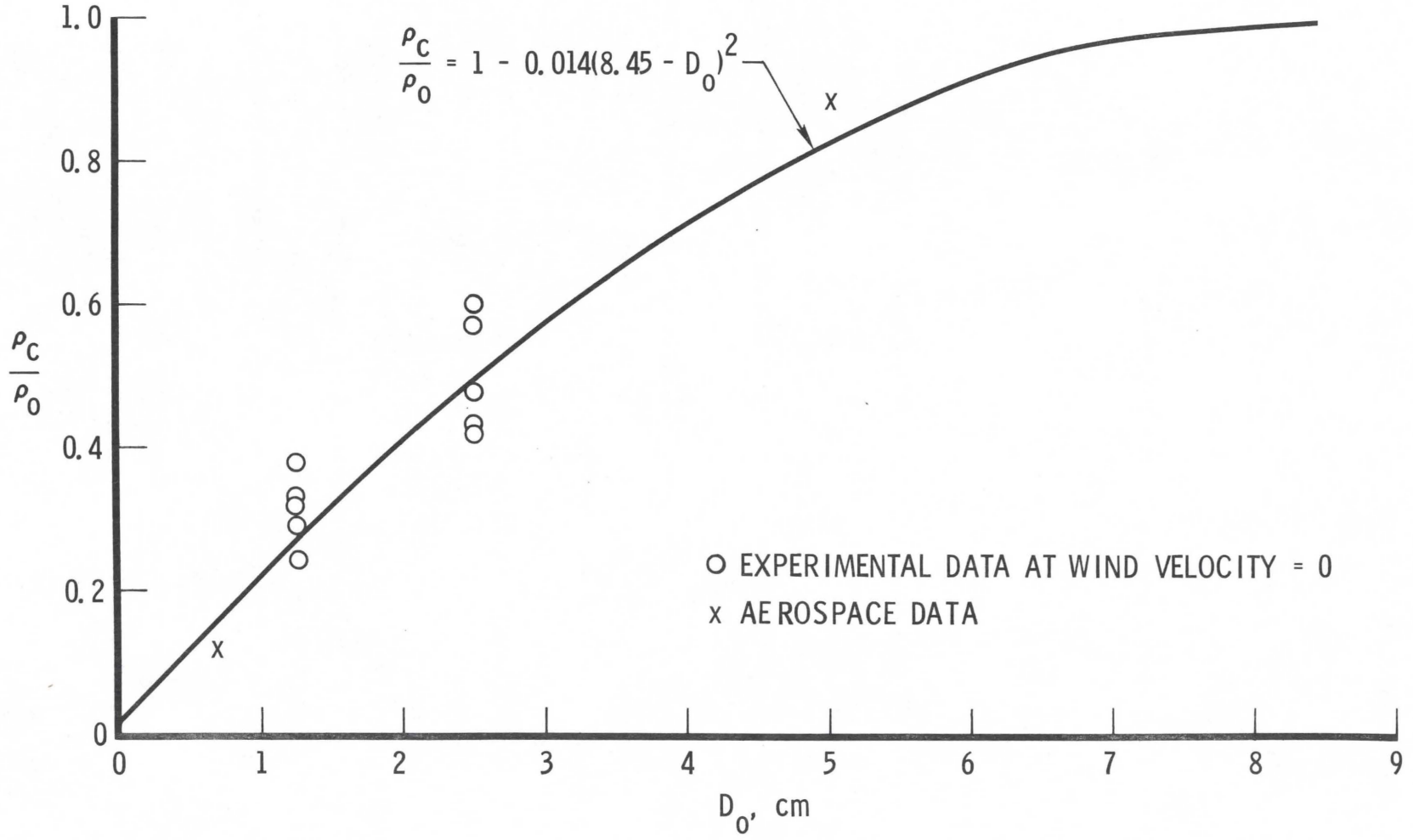


Fig. 7. Final Wood Density as a Function of Initial Diameter at Wind Velocity, v = 0

In trying to satisfy this requirement and the basic law of wood pyrolysis process, correlation for quiescent air burning was derived as:

$$\frac{\rho_{(t)} - \rho_c}{\rho_o - \rho_c} = e^{-\frac{t}{D_o \cdot 45}} \quad . \tag{6}$$

For burning at any wind velocity $\geq$ 5 mph:

$$\frac{\rho_{(t)}}{\rho_o} = e^{-\frac{t}{D_o \cdot 76}} \quad . \tag{7}$$

The value $\rho_c$ was neglected in Eq. (7) since it was found that it became small (ash equivalent) for in-wind burning.

It should be noted that Eqs. (6) and (7) become invalid when $\rho_{(t)}/\rho_o$ becomes small (probably less than 0.2) since it requires $t \longrightarrow \infty$ for $\rho \longrightarrow \rho_c$.

Fortuitously, when a firebrand reaches that stage with accompanying size decrease, it usually does not constitute a fire hazard. Perusal of Figs 3 through 6, in which the correlation equations are plotted, indicates a reasonable agreement at all air velocities. They indicate that the burning of a fuel sample in the air is mainly a function of its characteristic dimensions (volume/surface) and of its initial density, $\rho_o$. As a matter of interest, Tarifa also made the observation that instantaneous fuel density is a weak function of wind velocity. At 20 mph wind velocity (Fig. 8), white pine burning appears faster and birch slower than predicted by the correlation. Since this trend is not pronounced at 15 mph, some of the 20 mph tests may need repetition.

In reconstruction of firebrand burning <u>after</u> it reaches the ground, Eq. (6) applies with substitution of $D_o$ for fall diameter $D_f$ and $\rho_{(t)}$ for fall density. Calculation of final density, $\rho_c$, was discussed before.

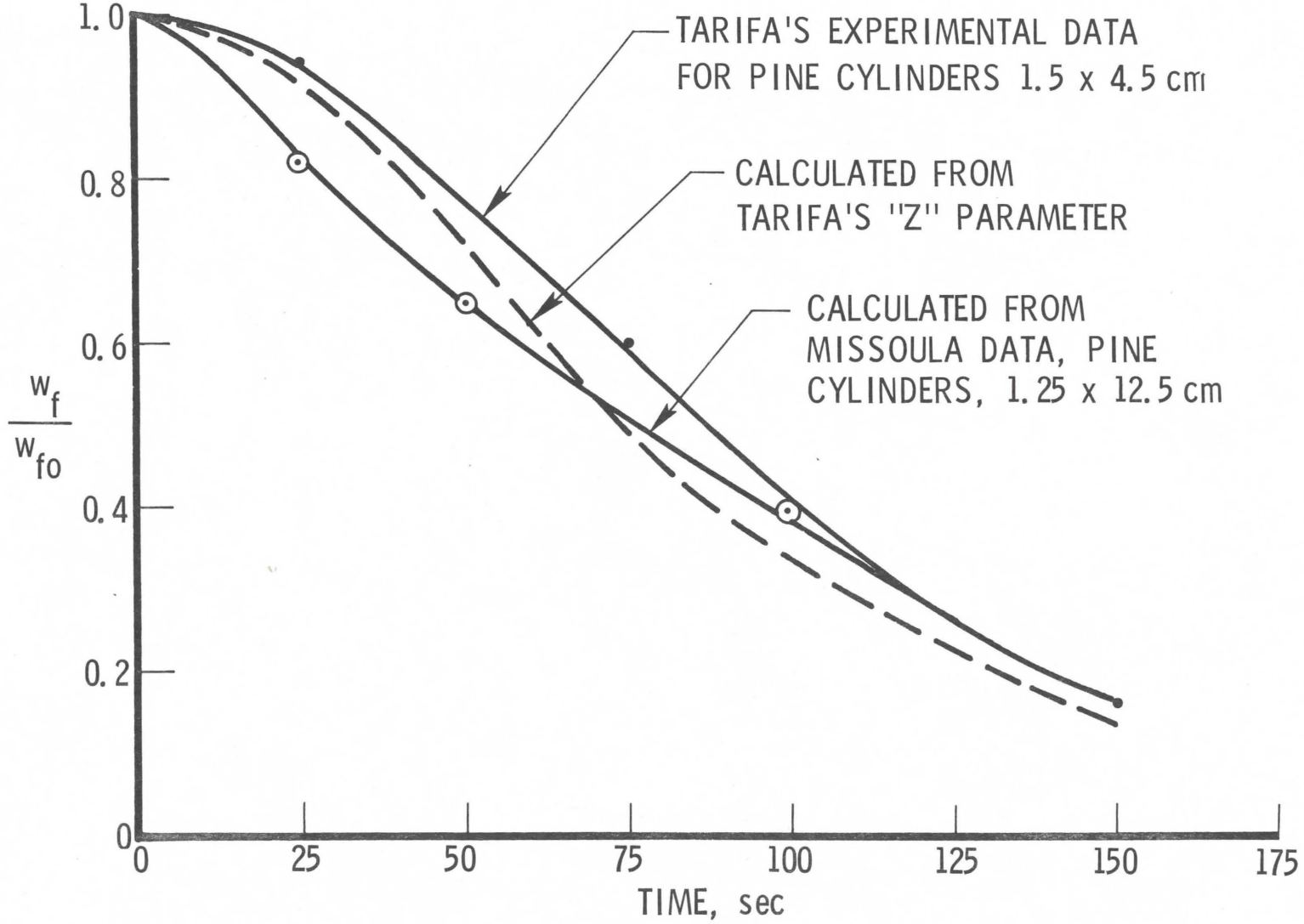


Fig. 8. Comparison of Fall Velocity Ratio ($w_f/w_{fo}$) Between Tarifa's Experimental Values and Calculations Based on Missoula Data (Pine)

To compare Missoula experimental data and the correlations presented here with Tarifa's data (Tarifa [1967]), $D_{(t)}/D_o$ in Eq. (3) can be substituted by

$$\frac{D_{(t)}}{D_o} = \left(\frac{m_{(t)}}{m_o} \cdot \frac{\rho_{(o)}}{\rho_{(t)}}\right)^{1/2}$$

and Eq. (3) becomes

$$\frac{w_{(t)}}{w_o} = \left(\frac{\rho_{(t)}}{\rho_o} \cdot \frac{m_{(t)}}{m_o}\right)^{1/4} \quad . \tag{8}$$

Data for $w_{(t)}/w_o$ were compared on three different bases. One set of data was from calculations performed using Missoula experimental data for $m_{(t)}/m_o$ with $\rho_{(t)}/\rho_o$ calculated from Eq. (7). The second set of experimental data for $w_f/w_o$ was taken from Tarifa's report (Tarifa [1967]); the third set of data was obtained from the use of his unique Z parameter vs. $w_f/w_o$ relationship with the values of Z determined for the samples considered. Table 2 gives the measured summary and Figs. 8 and 9 illustrate the comparison for the pine and birch samples, respectively. The main difference between Tarifa's experimental values and those obtained from Missoula experiments consists of approximately 5-10% lower fall velocity in the latter during the first 25-50 seconds of burning. This is, no doubt, associated with the influence of the ignition period which, in the Missoula tests, accelerated the sample weight and size loss during the ignition period more than in Tarifa's tests. Otherwise, the data agreement is good.

Data on natural fuels and on the effect of fuel moisture will be analyzed and reported later.

c. Burning Process

The burning process of cellulose-type fuels can proceed either in flaming or glowing combustion. Very often the combination of the two occurs and a transient, flaming combustion period is followed by a

Table 2. Comparison of Feirbrand Fall Velocity Ratios, $w_{(t)}/w_o$

| t, sec | $m_{(t)}$, g | $m_{(t)}/m_o$ | $\rho_{(t)}/\rho_o$, Eq. (7) | $w_{(t)}/w_o$ Eq. (8) | $w_{(t)}/w_o$, Tarifa Experiments | | Z, from Eq. (2)* | $w_{(t)}/w_o$, from Z (Tarifa |
|---|---|---|---|---|---|---|---|---|
| Pine, 1.25 • 12.5 cm, $\rho$ = 0.5 g/cm$^3$, wind vel = 10 mph | | | | | Pine, 1.5 • 4.5 cm | | | Pine, 1.25 • 12.5 cm |
| 0 | 7.70 | 1.00 | 1.00 | 1.00 | 1.00 | | - | 1.00 |
| 25 | 4.50 | 0.58 | 0.77 | 0.82 | 0.94 | | 0.58 | 0.92 |
| 50 | 2.40 | 0.31 | 0.59 | 0.65 | 0.76 | | 1.16 | 0.75 |
| 75 | 1.00 | 0.13 | 0.45 | 0.49 | 0.60 | | 1.74 | 0.48 |
| 100 | 0.60 | 0.08 | 0.35 | 0.40 | 0.40 | | 2.53 | 0.33 |
| 150 | - | - | - | - | 0.16 | | 3.50 | 0.10 |
| Birch, 1.25 • 12.5 cm, $\rho_o$ = 0.66 g/cm$^3$, wind vel = 10 mph | | | | | Oak | | | Birch, 1.25 • 12.5 cm |
| | | | | | 1.5 • 4.5 | 1.2 • 3.6 | | |
| 0 | 10.00 | 1.00 | 1.00 | 1.00 | 1.00 | 1.00 | - | - |
| 25 | 6.20 | 0.62 | 0.82 | 0.85 | 0.95 | 0.93 | 0.40 | 0.95 |
| 50 | 3.50 | 0.35 | 0.65 | 0.69 | 0.85 | 0.77 | 0.81 | 0.85 |
| 75 | 2.25 | 0.23 | 0.49 | 0.58 | 0.71 | 0.53 | 1.21 | 0.72 |
| 100 | 1.50 | 0.15 | 0.40 | 0.49 | 0.56 | 0.34 | 1.62 | 0.50 |
| 125 | 0.80 | 0.08 | 0.27 | 0.38 | 0.40 | 0.22 | 2.00 | 0.38 |
| 180 | - | - | - | - | 0.18 | 0.03 | 2.92 | 0.19 |

* shape factor, K = 6.75

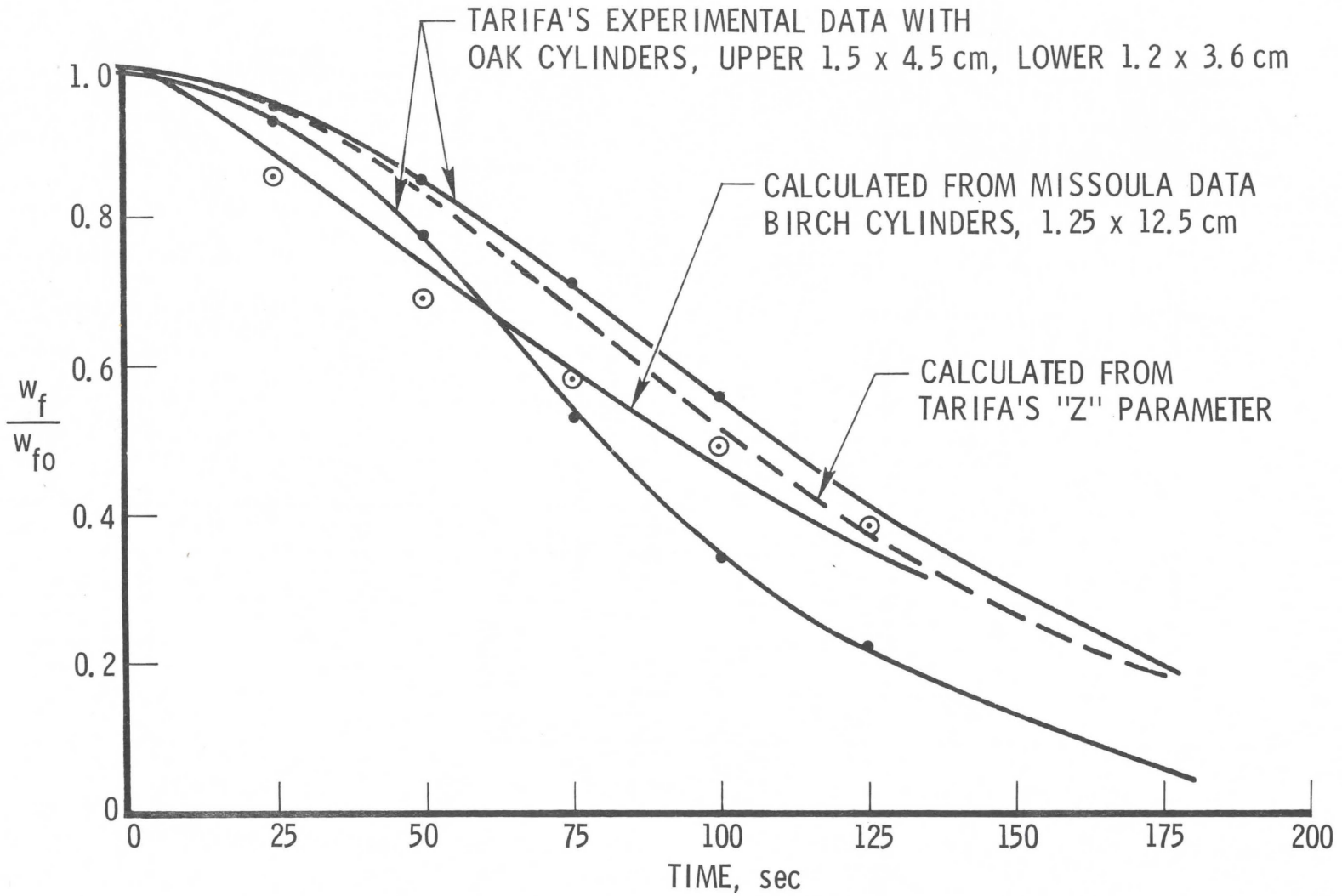


Fig. 9. Comparison of Fall Velocity Ratio ($w_f/w_{fo}$) Between Tarifa's Experimental Values and Calculations Based on Missoula Data (Birch)

glowing combustion. Martin [1964], Emmons [1965], and others tried to define analytically each of the combustion regimes as a function of heat input and fuel thermal properties.

In our investigation of firebrands, the importance of flaming vs. glowing periods is secondary. The mass change while burning in wind was defined by Eq. (7) irrespective of whether the fuel was flaming and glowing and, similarly, Eq. (6) defined the burning in quiescent air.

Observations of fuel samples burning in the wind indicated that after ignition, flaming continued for a short period of time (10-15 seconds) and that thereafter the combustion was maintained in a glowing stage at the windward part of the sample. At high wind velocities (greater than 15 mph), there was no flaming at all and the entire combustion process continued by glowing. The concentration of the combustion in the windward part of the sample is understood since it is near and at the stagnation point that the heat transfer from the heated gas in the boundary layer to the fuel sample is the greatest. The dilution of the combustible gases with air as the flow around the sample proceeds prevents formation of any durable flame and causes a rapid cooling of the fuel sample walls in its leeward part. The higher the air velocity, the greater will be this dilution effect.

Another effect of the stagnation point high heat transfer combined with an adequate supply of oxygen is the continued glowing until all material is consumed. Of course, the size effect of the sample still plays an important part in the rate of mass loss (see Eq. (7)) since the ratio of sample volume-to-surface represents also the ratios of heat required to pyrolyze the fuel volume to the heat transferred through the surface. There will be some difference in the condition of a real firebrand flying and tumbling in the air. The windward part will vary all the time and the total surface of the firebrand will remain hot although the burning will at any time be concentrated at the windward part. Tarifa's observation that the burning rate of a tumbling and fixed fuel sample in wind was similar confirms that assumption; whether this assumption is correct for firebrands of irregular shape is not known and it requires experimental verification.

The mechanism of quiescent air burning is slightly different. There, the heat transfer coefficient of the buoyant gases flowing around the sample increases with gas velocity and becomes highest at the top of the sample. The concentration of combustible gases with air is sufficient to maintain flame over the sample as long as the pyrolysis rate is high enough. As this rate decreases (with time or with increased diameter), the flame will gradually disappear and will be replaced by glowing. The disappearance of the flame reduces the heat input into the sample walls which causes further reduction in the pyrolysis rate which, depending on the sample size, may terminate combustion altogether (see Eq. (5) for $\rho_c$).

From this, some conclusions can be drawn regarding the continuous burning of a firebrand after it reaches the ground. Since, in most cases, it will be in the glowing phase, our observations indicate that any subsequent flaming will not occur. The glowing will continue, depending on the size of the firebrand at impact, until a final density $\rho_c$, calculated from Eq. (5), is reached. Knowing the density at impact and $\rho_c$, the duration of firebrand burning on the ground can be calculated from Eq. (6).

# IV. INVESTIGATION OF FIRE WHIRLS/FIREBRANDS CORRELATION

## A. ANALYSIS

Intense fires can produce fire whirls, which are tornado-like regions of hot swirling gas. Large fires create convection columns of hot, rising air. Ordinarily, the small pressure differential between the hot buoyant column and the surrounding air will create a horizontal flow of air into the convection column which replaces the hot air flowing upward in the column. This bulk mixing, as well as turbulent diffusion along the vertical extent of the column, tends to rapidly diffuse the column, limiting its height and upward gas velocity. However, in the presence of ambient vorticity, or circulation, the horizontal pressure difference due to buoyancy is counteracted by the centrifugal force due to the circulation, limiting any bulk motion of ambient air into the rising air column. Furthermore, turbulent mixing of the column air with the ambient air can initially concentrate the vorticity of the ambient air into the column, creating a swirling core. The rotation then reduces the turbulent mixing between the rising, swirling core and the ambient circulating air. Hence, the steady-state core height can become very large before the core is dispersed due to mixing. The convection column can thus be concentrated into a long, narrow core of swirling hot gas.

This vortex core region can be maintained, with little influx of ambient air along its vertical extent, by the influx of air into the core from the ground boundary layer. The inhibiting influence of a solid boundary (the ground) on the rotating air results in a ground boundary layer. The reduced rotational motion in the boundary layer removes the centrifugal force which inhibits the inward flow of air. The radial pressure gradient arising due to the pressure differential between the ambient air and the hot core is impressed upon the boundary layer and results in a radial inflow of air within the ground boundary layer into the core. Both air and new fuel (fire material) is brought into the core through the ground boundary layer, and the core, or fire whirl, is maintained. This radial influx greatly increases the vertical velocity in the

buoyant core. The decreased turbulent mixing at the core-ambient air interface results in maintaining large upward velocities within the core up to large heights.

The purpose of this current effort is to analytically characterize the fire whirl parameters which are pertinent to the uplift of firebrands (vertical gas velocity, etc.), in terms of quantities which would be available to fire managers in the field. These quantities are the properties of the burning material (the natural burn rate, etc.), and the strength and size of the ambient circulation , and they will be the controlling parameters in the generation of firebrands.

It is anticipated that subsequent studies would provide for determination of the strength and vertical extent of the ambient circulation in terms of the local terrain and wind conditions. These data combined with the current analysis will determine the fire whirl properties. These fire whirl properties, along with the ambient wind properties, would then be employed in a firebrand generation and trajectory model for the statistical prediction of probable spot fires caused by firebrands emanating from the fire whirl.

## 1. ANALYTICAL FORMULATION

The objective of the analytical effort is to characterize the relevant fire whirl gas dynamic unknowns in terms of the ambient circulation and the known physical properties of the fuel material, and then to correlate the results with the data obtained from the experimental phase of this study. A complete solution of the fire whirl gas dynamics requires an analysis which couples the fire whirl vortex core flow, the boundary layer flow, and the heat transfer between the burning fuel and the fire whirl flow.

The fully coupled fire whirl problem is highly complex. Past analyses directed at obtaining fire whirl core properties have circumvented attacking the full coupled problem by solving for the core properties in terms of their unknown values at some starting point in the core

above the boundary layer. Emmons and Ying [1966] obtained a solution for radially averaged core properties as a function of height and in terms of their value at the initial starting height. Lee [1966a] assumed similarity profiles for the radial dependence of the core variables and solved for them in terms of their ground-plane (above the boundary layer) values. Thus, both studies eliminated the need for coupling the ground boundary layer and fuel surface heat transfer to the core flow by solving for the core variables nondimensionalized with respect to their unknown values at the base of the core just above the fuel surface. Both Emmons [1966] and Lee [1966b] conducted laboratory fire whirl experiments from which the unknown values at the core base could be obtained, and their values along the core height could then be calculated. However, while the nondimensionalization parameters necessary for these solutions can be readily measured in a controlled laboratory experiment, they are not available to fire managers in the field.

In order to obtain a self-contained fire whirl theory, the coupling between the boundary layer, fuel heat transfer, and the core flow needs to be considered. Fortunately, a very high degree of numerical accuracy is not required. Reasonable estimates of the upward gas velocity and gas density are acceptable. Bearing this in mind, various simplifications were introduced into the coupled model employed in this study in order to make the problem tractable. The pertinent physical processes were retained in the theory but, where applicable, the mathematical descriptions of these processes were simplified.

A major simplification results by solving for radially averaged core quantities. In terms of utilizing a fire whirl model ultimately for the statistical prediction of spot fires, radially averaged values of the core gas density and axial (upward) velocity should suffice. Thus, the gas dynamic conservation equations for the core are radially integrated from the core centerline to the core-ambient air interface, removing the radial dependence from the equations and leaving only the height, z, as an independent variable. In performing the radial integrations,

boundary conditions at the core-ambient air interface are needed. For these, the Byram and Martin [1970] results are used. While Byram and Martin did not formulate a method to analytically predict the axial (uplift) velocity, they did develop a static core model relating the pressure, swirl (azimuthal) velocity, and radius of the vortex core in terms of the vertical extent and strength of the ambient circulation and the unknown mean core density and unknown initial core radius. In the present study, the core flow is coupled to the ground boundary layer through an overall conservation of mass, balancing the boundary layer mass inflow into the core and the mass loss by the burning fuel with the upward core mass flow. The burning fuel is further coupled to the core flow through the convective heat transfer at the fuel surface, which causes fuel ignition and evaporation, and through an overall energy balance that relates the core temperature increase to the heat released by the combusting fuel.

The geometry and coordinate system used for the fire whirl analysis was shown in Fig. 10. The critical parameters are the circulation $\Gamma$ (tangential velocity • radius) and its vertical extent, $z_e$. The region outside the fire whirl for $z < z_e$, $r > a$, is one of irrotational flow where the circulation, $\Gamma$, is constant. In that region, the swirl (azimuthal) velocity is independent of z and is given by $W = \Gamma/r$. Inside the fire whirl, $z < z_e$, $r < a$, the Byram and Martin [1970] assumption that a horizontal cross-section of the core rotates as a solid body (but that the angular velocity of rotation, $\omega$, is a function of height, z) is employed. Then, for $r < a$, evaluating $\omega$ at the core interface ($r = a$), $\omega = W(r = a)/a = \Gamma/a^2$. At any point inside the core, the tangential velocity $W = \omega(z)r = \Gamma r/a^2$. The core radius increases with height, z, and according to Byram and Martin [1970],

$$a/a_o = \left(1 - z/z_e\right)^{-1/2} \tag{9}$$

where $a_o$ is the core radius at the ground just above the ground boundary layer. These results are incorporated into the core conservation equations. The circulation $\Gamma$, and its vertical extent, $z_e$, are taken as known parameters in a given problem.

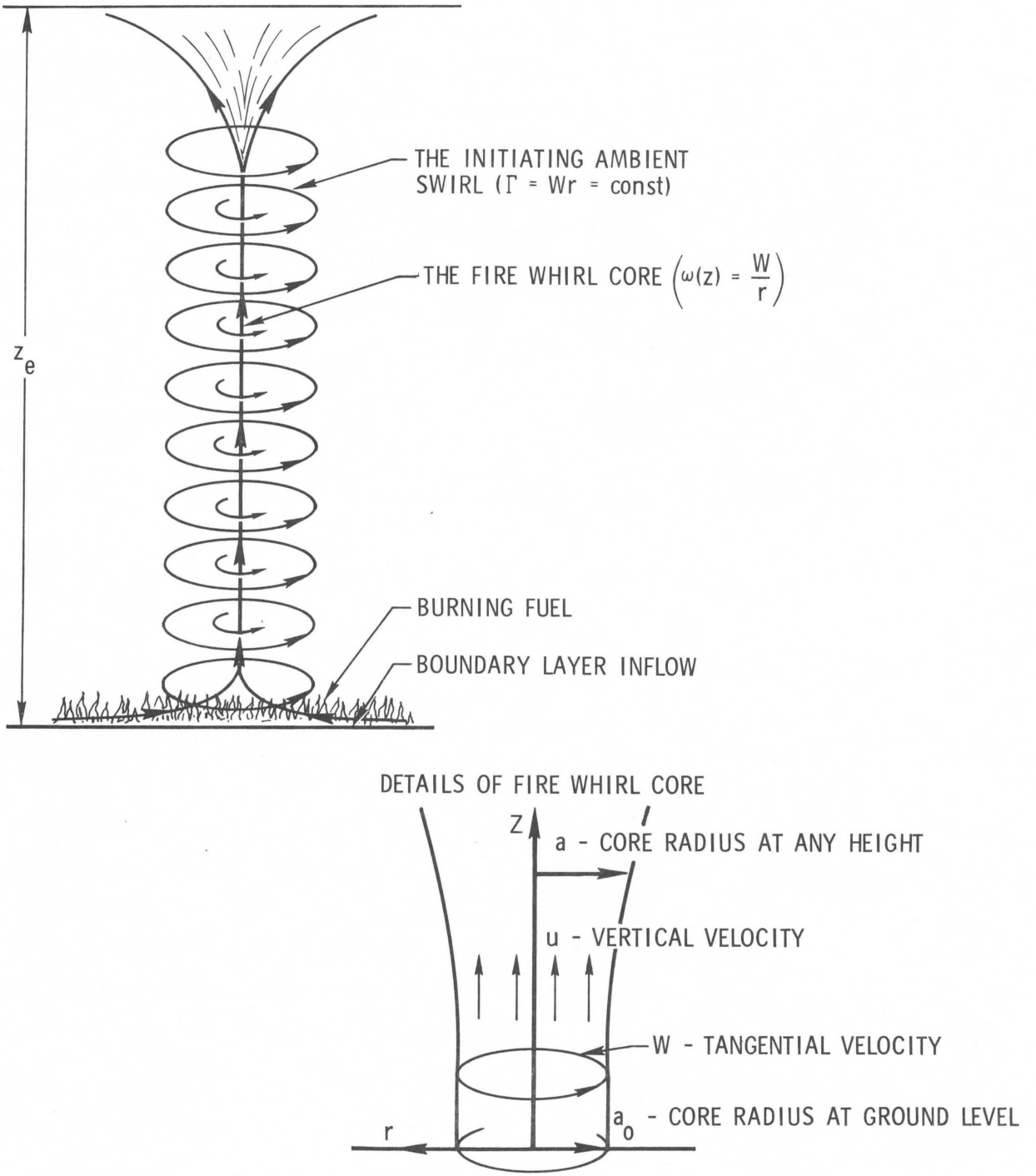


Fig. 10. Fire Whirl Geometry

Neglecting lateral entrainment of the ambient circulating air into the core, $v(r = a) = 0$. Also, since the circulating flow outside the core is taken to be a pure vortex flow, then $u(r = a) = 0$. Interchanging the order of integration and differentiation results in

$$\int_0^a \rho r u \, dr = \text{constant.} \tag{13}$$

From Byram and Martin [1970], the axial mean density between the core base and the upper surface $z = z_e$ is practically constant. Assuming that the radially averaged density is also practically a constant,

$$\rho = \bar{\rho} = \text{constant} \tag{14}$$

and that a top-hat radial profile for u is appropriate (or that u is a radial mean average of u), then Eq. (13) results in

$$\bar{\rho} u \frac{a^2}{2} = \frac{A}{2} = \text{constant.} \tag{15}$$

Eq. (15) states simply that the mass flux through the core is constant (independent of z), which results from the neglect of entrainment.

The degree of entrainment depends on the intensity of the ambient circulation. For large scale fire whirls corresponding to large values of $\Gamma$, the uplift velocity through the major part of the core height is not expected to be greatly influenced by entrainment. The greater the circulation, the smaller the steady-state turbulent diffusion of air across the core boundary since the centrifugal force inhibits the radial influx of the rotating air.

The usual entrainment hypothesis is based on investigations of nonswirling turbulent axisymmetric plumes by Morton, Taylor, and Turner [1956]. Employed here, it assumes that the value of $\rho rv$ at the core edge is proportional to the product of the local core radius and the radial mean axial velocity. The nondimensional proportionality constant,

$\alpha$, is denoted as the effective entrainment, or mixing, coefficient. The effect of swirl, $\Gamma$, on entrainment is to decrease the entrainment, as can be seen from the results of Emmons and Ying. To improve agreement between their analytical and experimental results, they allowed $\alpha$ to vary (increase) with height and they fit $\alpha$ to the data till the predicted effective plume size matched the measured results. A different fit is necessary for different values of $\Gamma$. As $\Gamma$ increases, the rate of increase of $\alpha$ with height becomes less and less, and $\alpha$ changes very little over the lower extent of the plume. Their need for allowing $\alpha$ to vary with height arises primarily in order to match the rapid increase of the plume at larger heights. However, their analysis neglects the effect of the pressure field due to the ambient circulation. They themselves show that the retention of this pressure field (and neglect of the momentum flux inertia contributions) results in a rapid increase in fire whirl radius for the upper part of the plume. Thus, the assumption of the variability of $\alpha$ with height may not be necessary if this pressure term is retained. Emmons' and Ying's results for the initial value of $\alpha$ (at the lower end of the plume) are shown in Fig. 11. As seen in the Figure, $\alpha$ decreases as $\Gamma$ increases. Values of $\Gamma$ obtained in the experimental phase of the current Aerospace Corporation effort are greater than 2.5 $ft^2/sec$, suggesting small values of $\alpha$. Also, the $\Gamma$ for full scale fire whirls are large enough so that they are not expected to be dominated by entrainment. Thus, the effect of entrainment is neglected in the present analysis.

The axial velocity, u, is given by Eq. (15) as $u a^2 = u_o a_o^2$, where the subscript zero indicates the value at the base of the core above the ground boundary layer (at z = o). Using Eq. (9), then

$$u/u_o = 1 - z/z_e. \tag{16}$$

Turning to Eq. (11), integration with respect to r from r = o to r = a is again performed. From Byram and Martin's analysis, the core pressure ($r \leq a$) can be shown as

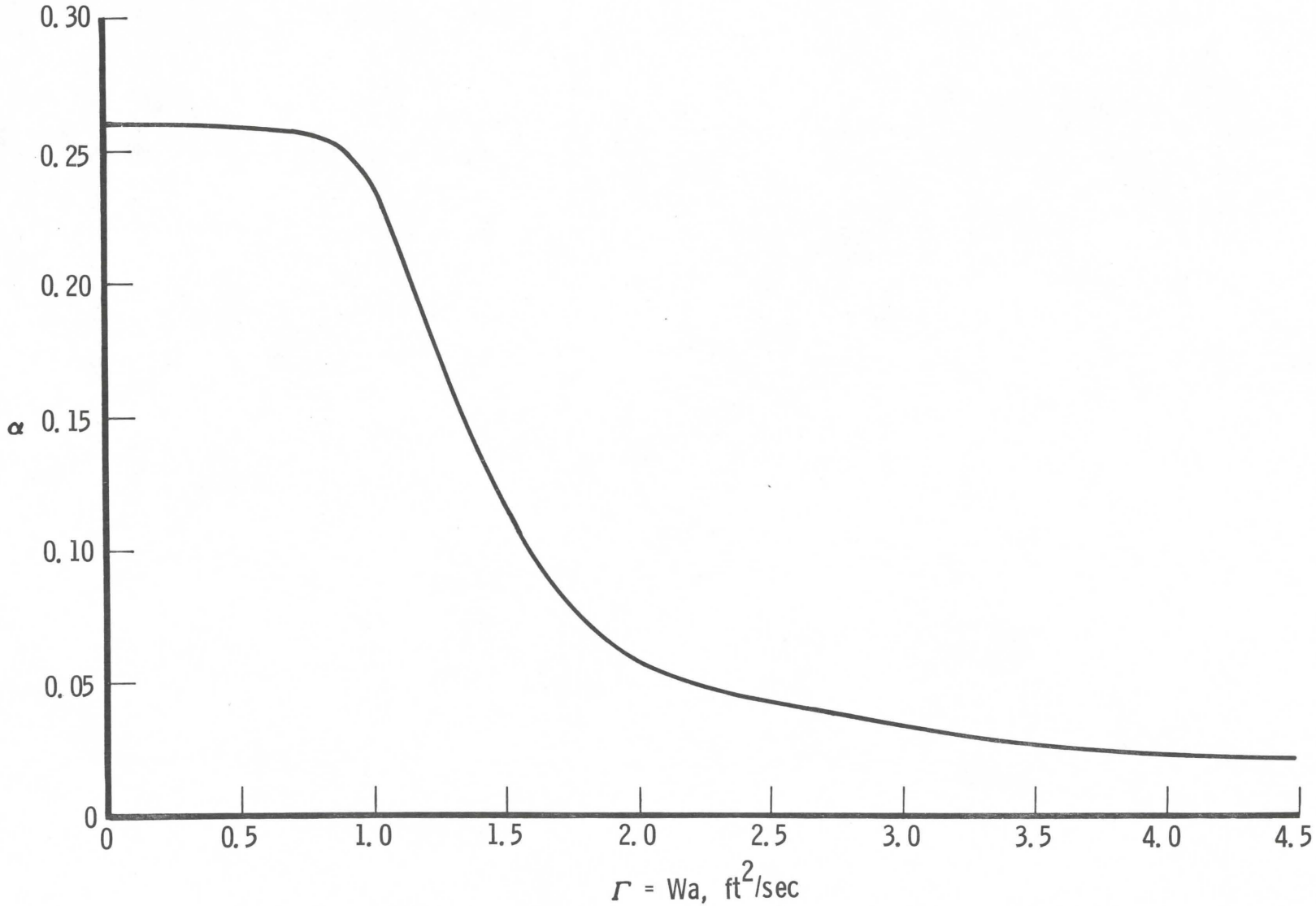


Fig. 11. Entrainment Reduction Due to Increasing Circulation

$$p = p_\infty - \rho_\infty g z - \frac{\Gamma^2}{2a^2}\left(\rho_\infty + \bar{\rho}\right) + \frac{\bar{\rho}\Gamma^2}{2a^2}\frac{r^2}{a^2} \quad . \tag{17}$$

This result can also be readily obtained from the radial momentum equation,

$$\frac{\partial p}{\partial r} = \frac{\bar{\rho} W^2}{r}$$

where the $v^2$ and uv terms were neglected relative to the $W^2$ term. Integrating from $r = \infty$ to $r = r$, and inserting $W = \Gamma/r$ for $r > a$ and $W = \Gamma r/a^2$ for $r < a$, Eq. (17) is obtained. Integration of Eq. (11), and using the Leibniz rule for interchange of integration and differentiation under the integral sign, results in

$$\frac{d}{dz}\int_o^a \rho r u^2 dr + \frac{d}{dz}\int_o^a \left[p_\infty r - \rho_\infty g z r - \frac{\Gamma^2}{2a^2} r\left(\rho_\infty + \bar{\rho}\right) + \frac{\bar{\rho}\Gamma^2}{2a^2}\frac{r^3}{a^2}\right] dr$$

$$- \frac{da}{dz}\left[p_\infty a - \rho_\infty g z a - \frac{\Gamma^2}{2a}\left(\rho_\infty + \bar{\rho}\right) + \frac{\bar{\rho}\Gamma^2}{2a}\right] + \bar{\rho} g \frac{a^2}{2} = 0,$$

$$\frac{d}{dz}\left(\bar{\rho} u^2 \frac{a^2}{2}\right) + \frac{d}{dz}\left[\frac{a^2}{2}\left(p_\infty - \rho_\infty g z\right) - \frac{\Gamma^2}{4}\left(\rho_\infty + \frac{\bar{\rho}}{2}\right)\right] + \bar{\rho} g \frac{a^2}{2}$$

$$- \frac{da}{dz}\left[\left(p_\infty - \rho_\infty g z\right) a - \frac{\rho_\infty \Gamma^2}{2a}\right] = 0,$$

$$\frac{d}{dz}\left(\frac{A\bar{u}}{2}\right) - \left(\rho_\infty - \bar{\rho}\right)\frac{g a^2}{2} + \frac{\rho_\infty \Gamma^2}{2a}\frac{da}{dz} = 0 \quad , \tag{18}$$

where A is given by Eq. (15). If the inertial term is neglected relative to the buoyancy and vortex pressure terms, and Eq. (9) is substituted for a, then

$$\left(\rho_\infty - \bar{\rho}\right) g a_o^2 = \frac{\rho_\infty}{2} \frac{\Gamma^2}{z_e} \tag{19}$$

Eq. (19) can also be obtained by combining Eqs. (3) and (7) of the Byram and Martin [1970] paper. This is not surprising, since the Byram and Martin analysis is static, and neglecting the momentum flux (inertia) term in the momentum equation is equivalent to a nondynamic (static), kinematic approach. For small z, the error arising by neglecting the inertia term can be estimated by substituting Eqs. (9) and (16) into Eq. (18). Since $\Gamma = W_o a_o$ and $A = \bar{\rho} u_o a_o^2$, it is seen that neglect of the inertia term relative to the vortex pressure field requires that $2\left(\bar{\rho}/\rho_\infty\right)\left(u_o^2/W_o^2\right)$ be small relative to one. Now, $\bar{\rho}/\rho_\infty$ is typically on the order of 1/5. Emmons and Ying [1966] state the supposition that $u_o/W_o$ is about 1/2, for which the above requirement is satisfied. Furthermore, Emmons and Ying show that neglect of the inertia term results in a core radius variation of the form given by our Eq. (9), and that this variation is consistent with the measured large z core size growth over the upper portion of the core. (In the lower portion, the measured core radius changes very slowly. For $z/z_e \ll 1$, Eq. (9) predicts that the core radius changes very little with z.)

The preliminary data taken to date for the Aerospace/UCSB acetone experiments indicate a $u_o/W_o$ ratio on the order of 0.6, which is comparable to the Emmons and Ying value, giving a value of $2\left(\bar{\rho}/\rho_\infty\right)\left(u_o^2/W_o^2\right)$ of on the order of 1/7. Thus, it appears that the neglect of the inertia term in the axial momentum equation is a reasonable as well as a useful simplification.

Only the axial component of the momentum equation is needed. The azimuthal moment equation is redundant since it, upon radial integration, reproduces Eq. (15). The radial momentum equation reproduces the Byram and Martin result for the core pressure, as demonstrated previously.

While the decrease in the core pressure from ambient is sufficient to influence the dynamic behavior of the fluid, it is not large enough to cause any significant change in the thermodynamic properties of the gas. In subscale fire whirl laboratory tests, the pressure at the core axis is less than ambient by approximately 1 psf. In full scale natural fire whirls, where the vertical extent of the ambient circulation is not more than several hundred feet, the pressure at the core axis near ground level is approximately 1% (20 psf) below ambient. For a 1000-foot vertical extent, the pressure decrease from ambient is approximately 3%. Thus, in Eq. (12), the pressure can be taken to be $p_\infty$, and Eq. (12) can be rewritten as

$$\frac{T}{T_\infty} = 1 \Big/ \left(\frac{\bar{\rho}}{\rho_\infty}\right)\left(\frac{R}{R_\infty}\right) \tag{20}$$

With the fuel types and core fuel mass fractions of interest, the changes in the core gas constant R from its ambient value are small, and R can be taken as a constant equal to its mean value in the core. For most applications, as in this present study, the value of $R/R_\infty$ can be taken as unity. Thus, the temperature given by Eq. (20) is a constant and is the mean temperature of the core, to be denoted by $\bar{T}$.

The use of constant mean core density and temperature as pertinent variables facilitates the application of an overall core energy equation in which the energy released by the combusting fuel heats the rising core gases. Equating the increase in temperature of the rising core gases (and again neglecting entrainment) with the effective heat released by the combustion of the fuel results in

$$\pi \bar{\rho} u_o a_o^2 \left( \bar{C}_p \bar{T} - Cp_\infty T_\infty \right) = \dot{M}_f Q_c \qquad (21)$$

where $\dot{M}_f$ = burn rate of fuel (within core) in swirl environment ($lb_m/sec$). $\dot{M}_f$ is one of the unknown variables in the problem.

$Q_c$ = net heat of combustion of the fuel which is effective in heating the core gas ($Btu/lb_m$).

A value of 10,000 $Btu/lb_m$ was used for acetone. The gross value is 13,000, but this includes the energy released by the formation and condensation of water. Also, some of the energy released by the fuel is radiated away from the core. Generally, the net effective heat of combustion is 75-80% of the gross.

The above value of $Q_c$ also neglects the heat required to vaporize and ignite the fuel. Since the heat of ignition is small relative to the net heat of combustion, it is neglected in the present acetone calculation. However, the wood ignition and pyrolysis heat would be included for the case of wood fuels.

A separate energy balance relating the steady-state fuel ignition to the heat convected to the burning fuel surface at the core-fuel surface interface is employed. In the absence of swirl, with the energy required for steady-state fuel ignition being supplied by the heat convection from the hot buoyant column immediately above the fuel,

$$\left( \bar{T} - T_s \right) h_o = \rho_F G_o Q_i \, .$$

In the presence of swirl, with the energy required for ignition supplied by the swirling core just above the fuel,

$$\left( \bar{T} - T_s \right) h = \rho_F G Q_i, \quad h = h_o + h_w$$

where

$T_s$ = fuel surface burning temperature (the boiling temperature of acetone is approximately $600^{\circ}R$)

$h$, $h_o$ = heat transfer coefficients between the swirling flow and the burning fuel surface, with and without swirl, respectively ($Btu/ft^2\text{-}sec\text{-}^{\circ}R$). The values $h$ and $h_o$ are effective total heat transfer coefficients which include both convective and radiative terms. It is assumed that the radiative term is the same with and without swirl and that the added contribution of swirl is in the convective heat transfer coefficient, $h_w$ (see Appendix II).

$h_w$ = added contribution due to the swirl

$\rho_F$ = bulk density of the fuel ($lb_m/ft^3$)

$G$, $G_o$ = linear burn rate of the fuel (ft/sec), in the presence of swirl and without swirl, respectively

$Q_i$ = effective heat of ignition of the fuel, including both vaporization and ignition ($Btu/lb_m$). For acetone, $\rho_F G_o = 0.00536\ lb_m/ft^2\text{-}sec$, $Q_i = 260\ Btu/lb_m$.

Eliminating $h_o$, one finds

$$\frac{G}{G_o} = 1 + \frac{h_w\left(\bar{T} - T_s\right)}{\rho_F G_o Q_i} \tag{22}$$

The swirl contribution to the convection coefficient is related to the ambient circulation as follows: the coefficient of heat transfer (convection coefficient) is defined in terms of the Stanton number ($S_t$) as $h_w = \rho_\infty V_\infty \bar{C}_p (S_t)$. The characteristic velocity for the flow, $V_\infty$, is taken as the velocity at the core-ambient circulating air interface near ground level (near the fuel surface), $V_\infty = \Gamma/a$. Using Reynolds' analogy between heat transfer and skin friction, then for a Prandtl

number ($P_r$) near one, $S_t = (1/2)C_f(P_r)^{-2/3}$, where $C_f$ is the skin friction coefficient at the core-air interface. The skin friction coefficient is related to the fuel surface shear stress ($\tau_o$) by definition as

$$C_f = 2\tau_o/\rho_\infty V_\infty^2$$

and

$$\tau_o = \bar{\nu}\bar{\rho}\left.\frac{\partial W}{\partial z}\right|_{z=o},$$

where the relevant velocity for determination of $\tau_o$ is the azimuthal component within the boundary layer above the fuel surface. The analysis in Schlichting [1960] for a pure rotating (constant $\omega$) flow above the ground is used to determine this velocity. Following Schlichting,

$$W = a_o \omega N(\zeta) = \Gamma N/a_o,$$

$$\zeta = z(\Gamma/\bar{\nu})^{1/2}/a_o,$$

where N is a nondimensional velocity profile variable. Thus,

$$\tau_o = \bar{\rho}\bar{\nu}^{1/2}\Gamma^{3/2} N'(o)/a_o^2$$

and

$$C_f = 2(\bar{\rho}/\rho_\infty) N'(o)/(\Gamma/\bar{\nu})^{1/2}.$$

The quantity $\Gamma/\nu$ is the Reynolds number of the swirling flow above the fuel surface based on the velocity at the core-air interface ($\Gamma/a_o$), the kinematic viscosity of the flow above the fuel surface, and the characteristic distance over which heat transfer is taking place, which is

$a_o$ for the burning pool of acetone. (The appropriate Reynolds number for wood involves the size of the wood material. The analysis for wood will not be discussed in the report, but will be discussed in connection with the follow-on study.) The heat transfer coefficient then becomes

$$h_w = \rho_\infty \frac{\Gamma}{a_o} C_p \frac{C_f}{2} = \bar{\rho}\,\bar{C}_p P_r^{-2/3} N'(o)\sqrt{\bar{\nu}\Gamma}/a_o \qquad (23)$$

The value of N'(o) from Schlichting for the case of a rotating flow over the ground, with no burning or combustion, is about 0.76. For the present case of a burning ground plane and a hot buoyant core, it is expected that the vertical gradient of the characteristic azimuthal velocity would be different from the case considered in Schlichting. It will be considered an unknown parameter (dependent on $\Gamma$) to be determined from the experiments. Calling this parameter C [instead of N'(o)], Eq. (22) becomes

$$\frac{G}{G_o} = 1 + \frac{C\,\bar{\rho} P_r^{-2/3} \sqrt{\bar{\nu}\Gamma}\left(\bar{C}_p \bar{T} - C_{ps} T_s\right)}{\rho_F G_o Q_i a_o} \qquad (24)$$

The formulation in Eq. (23) is specifically for the case of constant molecular properties. The variation of $\bar{C}_p$ with temperature is incorporated into Eq. (24) by considering the static enthalpy ($C_p T$) difference instead of the temperature difference.

The use of Eq. (24) assumes that the radiative heat transfer contribution to the evaporation and ignition of the fuel is small relative to the convection contribution. An estimate of the radiative and convective heat fluxes to the core-fuel surface interface reveals that the radiative contribution is probably less than 20% of the total*. Therefore, the effect of radiation of the core gases on the ignition of the fuel beneath the core is neglected in this analysis.

Referring to Eq. (21), one finds that it is convenient to express $\dot{M}_f$ in terms of the linear burn rate G. For the case of a core radius

---

* See Appendix II

($a_o$) less than the radius of the dish containing the acetone ($r_o$), the process of fuel outside the core central area being swept into the central area and evaporating and burning is envisioned. The convective heat transfer-ignition process is idealized as occurring over this central area of radius $a_o$. The linear burn rate G applies to this central core area, and $\dot{M}_f = G\rho_F \pi a_o^2$. For the case of $a_o$ greater than $r_o$, the relevant area over which the core-fuel heat transfer takes place is the area of the acetone dish, and $\dot{M}_f = G\rho_F \pi r_o^2$. If we allow $\Omega = a_o^2/r_o^2$ for $a_o < r_o$ and $\Omega = 1$ for $a_o \geq r_o$, then

$$\dot{M}_f = G\rho_F \pi r_o^2 \Omega \tag{25}$$

(For the case of wood spread over a wide area, $\dot{M}_f = G\rho_F \pi a_o^2$.) $\dot{M}_f$ is the burn rate of the fuel that is enveloped into the core. When $a_o$ is less than $r_o$, fuel outside of the core area is burning at the acetone surface. Without swirl, the burn rate of this fuel (over the dish area outside of $\pi a_o^2$) is $\rho_F G_o \pi\left(r_o^2 - a_o^2\right)$. The excess rate of fuel burning over this amount is envisioned as swept into the core area, and is included in $\dot{M}_f$. Thus, the <u>measured</u> acetone burn rate (using the dish weighing system described in the experimental apparatus section) is $\dot{M}_{f_m} = \dot{M}_f + \dot{M}_o(1 - \Omega)$, where $\dot{M}_o = \rho_F G_o \pi r_o^2$ is the steady burn rate, without swirl, of the acetone in the dish of radius $r_o$. Since the overall core energy equation [Eq. (21)] relates the heating of the core gases by the fuel which combusts within the core, $\dot{M}_f$ is the appropriate quantity (rather than $\dot{M}_{f_m}$) to use in that equation, as well as in the overall mass balance equation which is discussed in the next paragraph. The ratio of the total amount of acetone, in a dish of radius $r_o$, burned with swirl to that without swirl is

$$\dot{M}_{f_m}/\dot{M}_o = \dot{M}_f/\dot{M}_o + 1 - \Omega.$$

Relating $\dot{M}_f$ to G from Eq. (25), Eq. (21) can be rewritten as

$$\pi \bar{\rho} u_o a_o^2 \left( \bar{C}_p \bar{T} - C_{p_\infty} T_\infty \right) = \frac{G}{G_o} \rho_F G_o \pi r_o^2 \Omega Q_c , \tag{26}$$

The set of equations is closed with the addition of an overall mass balance between the radially inward ground boundary layer flow into the core, the evaporating and combusting fuel, and the upward core flow.

$$2\pi \rho_\infty \int V_{BL} \, dz = \pi \bar{\rho} u_o a_o^2 - \dot{M}_f \tag{27}$$

As discussed previously, Schlichting [1960] reports results for a rotating $\omega$ = constant flow over a fixed surface. From Schlichting, we evaluate the above integral for the radial mass influx into a cylinder of radius $a_o$,

$$2\pi \rho_\infty \int V_{BL} \, dz = B' \pi \rho_\infty a_o^2 \sqrt{\nu_\infty \omega_{(z=o)}} \equiv B' \pi \rho_\infty a_o \sqrt{\Gamma \nu_\infty} \tag{28}$$

where B' is a constant. For the case presented in Schlichting, B' = 1.38. In the present case, the value of B' would be expected to be modified by the fuel evaporation and combustion and the ensuing buoyancy forces. The influx of boundary layer air into the fire whirl core is expected to be greatly increased over the case given in Schlichting. Since an increased circulation ($\Gamma$) is expected to increase the upward mass flow in the core, a stronger increase in the ground boundary layer radial mass inflow with $\Gamma$ than appears in Eq. (28) would not be surprising. At any rate, the constant B' [and also C in Eq. (24)], while taken to be independent of the height z, will be allowed to vary with the circulation $\Gamma$. Determination of the functional form of B' (and C) will be based on fitting the analytical results to the experimental measurements.

Using Eq. (20) and writing $\dot{M}_f$ in terms of G, Eq. (27) becomes

$$B' \pi \rho_\infty a_o \sqrt{\Gamma \nu_\infty} = \pi \bar{\rho} u_o a_o^2 - \frac{G}{G_o} \rho_F G_o \pi r_o^2 \Omega \tag{29}$$

Eqs. (19), (20), (24), (26) and (29) form a complete set for the unknowns $\bar{\rho}$, $\bar{T}$, $u_o$, $a_o$, and G (or, equivalently, $\dot{M}_f$), for the case of a pool of liquid fuel. (For the case of wood as the fuel, the major modification would involve the determination of the heat transfer coefficient. The wood analysis and results are scheduled for the next phase of this effort.) The vertical profiles for a and u are given in Eqs. (9) and (16), respectively. The unknowns $\bar{\rho}$, $\bar{T}$, $u_o$, $a_o$, and G are constant for given ambient ($\Gamma$, $z_e$) conditions and a specified fuel type. The solutions to the set of equations are presented in the next section.

## 2. ANALYTICAL RESULTS AND DISCUSSION

Eqs. (19), (20), (24), (26) and (29) are solved simultaneously for $\bar{\rho}$, $\bar{T}$, $u_o$, $a_o$ and $G/G_o$. The equations also involve the gas properties $P_r$, $\bar{\upsilon}$ and $\bar{C}_p$. The Prandtl number, $P_r$, appears as $P_r^{-2/3}$ in Eq. (24). Since $P_r^{-2/3}$ has a weak temperature dependence, it can be taken as a constant. A value of one is chosen for simplicity; small departures from unity can be considered to be incorporated into the constant C. The core kinematic viscosity, $\bar{\upsilon}$, also appears in Eq. (24). Fitting the temperature dependence of $\bar{\upsilon}$ to tabulated air data,

$$\bar{\upsilon}^{1/2} = \left(\rho_\infty \upsilon_\infty / \bar{\rho}\right)^{1/2} \left(\bar{T}/T_\infty\right)^{\beta},$$

where $\beta = 0.3$ and $\upsilon_\infty = 0.00016$ ft$^2$/sec. The specific heat, $\bar{C}_p$, appears in Eqs. (21) and (24), and is given in terms of the mean core temperature as

$$\bar{C}_p = C_{p_\infty} \left(\bar{T}/T_\infty\right)^n$$

where $n = 0.14$, and $C_{p_\infty} = 0.25$ Btu/lb$_m$-$^o$R. These temperature dependencies are incorporated into the equations.

The variables $\bar{T}$, $\bar{\rho}$, G and $u_o$ are systematically eliminated from the equations, reducing the set to one equation for the unknown

$a_o$. Eq. (26) is used to eliminate G from Eqs. (24) and (29). The value of $u_o$ obtained from the resulting Eq. (24) is then substituted into the resulting Eq. (29). This equations is

$$\frac{B'\sqrt{v_\infty \Gamma}\,\rho_\infty\, C_{p_\infty} T_\infty}{\rho_F G_o Q_c r_o^2 \Omega} \frac{a_o\left[\left(\bar{T}/T_\infty\right)^{1+n} - 1\right]}{1 - \frac{C_{p_\infty} T_\infty}{Q_c}\left[\left(\bar{T}/T_\infty\right)^{1+n} - 1\right]}$$

$$= 1 + \frac{C\rho_\infty C_{p_\infty} T_\infty \sqrt{v_\infty \Gamma}\left(\bar{T}/T_\infty\right)^{\beta}\left[\left(T/T_\infty\right)^{1+n} - \left(T_s/T_\infty\right)^{1+n}\right]}{\rho_F G_o Q_i \left(\frac{\rho_\infty}{\bar{\rho}}\right)^{1/2}} \qquad (30)$$

Eliminating $\bar{T}$ in terms of $\bar{\rho}$ from Eq. (20), and $\bar{\rho}$ in terms of $a_o$ from Eq. (19), the following equation is obtained.

$$\frac{C_2 C_3}{\Omega} \frac{a_o}{z_e} \Bigg/ \left[\frac{\delta^{1+n}}{1 - \delta^{1+n}} - C_7\right] = 1 + C_4 \frac{\delta^{1/2-\beta}}{C_6^{1/2} a_o/z_e}\left[\delta^{-1-n} - C_5^{1+n}\right] \qquad (31)$$

where

$$\delta = T_\infty/\bar{T} = C_6\,\bar{\rho}/\rho_\infty = C_6\left(1 - \frac{1}{2\,C_1\left(a_o/z_e\right)^2}\right),$$

$$C_1 = g\,z_e^3/\Gamma^2\,, \quad C_6 = R/R_\infty = 1, \quad C_2 = B'\sqrt{v_\infty/\Gamma}\,,$$

$$C_3 = \frac{C_{p_\infty} T_\infty \Gamma z_e}{\rho_F G_o Q_c r_o^2}\,, \quad C_4 = \frac{C\rho_\infty C_{p_\infty} T_\infty \sqrt{v_\infty \Gamma}}{\rho_F G_o Q_i z_e}$$

$$C_5 = T_s/T_\infty\,,$$

and

$$C_7 = \frac{C_{p_\infty} T_\infty}{Q_c}\,.$$

Eq. (31) is an algebraic equation for $a_o$. Once $a_o$ has been determined, the rest of the unknowns can be readily obtained. For instance, Eq. (19) directly gives $\bar{\rho}$, and then Eq. (20) provides $\bar{T}$. Since we know $a_o$, $\bar{\rho}$, and $\bar{T}$, Eq. (24) gives $G/G_o$ and then $u_o$ can be obtained from Eq. (26). Eq. (31) is solved for $a_o$ on an IBM 370 time sharing terminal using a Newton's divided difference iteration scheme. Briefly, the scheme solves the equation $f(x) = o$ for $x$, given the function $f$. Starting with an initial guess of the solution $x$, the slope, $f'(x)$ is computed and its intercept with the x-axis found. This intercept then becomes the next guess. This process is repeated until the departure of $f$ from zero is less than a specified value.

Solutions were obtained for $\Gamma = 2.8$, 3.7 and 5 with $z_e = 18$. (The height of the UCSB experimental apparatus is 18 feet, consisting of a 6-foot-long truncated conical section on top of two 6-foot cylindrical sections.) The radius of the acetone dish, $r_o$, is 3 inches, and the values of the pertinent physical quantities for acetone were given previously. The solutions for $a_o$, $u_o$, $\bar{T}$, $\bar{\rho}/\rho_\infty$, and $\dot{M}_{f_m}/\dot{M}_o$ for $\Gamma = 3.7$, $z_e = 18$ are given in Table 3 for various values of C and B'. As discussed previously, $\dot{M}_{f_m} = \dot{M}_f + \dot{M}_o(1 - \Omega)$ is the total burn rate of the acetone within the dish in the presence of swirl, and $\dot{M}_o$ is the undisturbed burn rate in the absence of swirl.

Table 3 shows that, for a given value of C, $u_o$, $\bar{T}$, and $\dot{M}_{f_m}/\dot{M}_o$ decrease with B', while $\bar{\rho}$ and $a_o$ increase. The relevant temperature range of interest is from approximately 2000 to 3000 $^oR$. As C increases, the values of B' required to include this temperature range increase. For a given temperature (e.g., 2500$^oR$), there is a range of pairs of values of C, B' that result in this temperature as well as providing for reasonable values of the remaining variables. Note that the value of $a_o$ changes little as C and B' change. From Eq. (19), for $\bar{\rho}/\rho_\infty$ not close to one, $a_o^2$ varies as $\Gamma^2/z_e$, is very weakly dependent on $\bar{\rho}$, and is not directly influenced by C of B'.

Table 3. Acetone Fire Whirl Properties for $\Gamma = 3.7$, $Z_e = 18$ ft for Various Values of C and B'

| C \ B' | 18 | 19 | 20 | 20.5 | 21 | 21.5 | 22 | 23 | 24 | 25 |
|---|---|---|---|---|---|---|---|---|---|---|
| 0.6 | $a_o$ (ft) = 0.122 | 0.124 | 0.126 | 0.127 | 0.129 | | | | | |
| | $u_o$ (ft/sec)= 19.0 | 17.2 | 15.8 | 15.1 | 14.6 | | | | | |
| | $\bar{T}$ ($^oR$) = 2627. | 2318. | 2067. | 1960. | 1865. | | | | | |
| | $\bar{\rho}/\rho_\infty$ = 0.20 | 0.23 | 0.26 | 0.27 | 0.28 | | | | | |
| | $\frac{\dot{M}_{f_m}}{\dot{M}_o}$ = 2.7 | 2.5 | 2.3 | 2.2 | 2.2 | | | | | |
| 0.7 | $a_o$ = | | 0.121 | 0.121 | 0.122 | 0.123 | 0.124 | 0.127 | | |
| | $u_o$ = | | 23.2 | 22.1 | 21.0 | 20.1 | 19.2 | 17.6 | | |
| | $\bar{T}$ = | | 2835. | 2667. | 2513. | 2372. | 2244. | 2021. | | |
| | $\bar{\rho}/\rho_\infty$ = | | 0.19 | 0.20 | 0.21 | 0.22 | 0.24 | 0.26 | | |
| | $\frac{\dot{M}_{f_m}}{\dot{M}_o}$ = | | 3.1 | 2.9 | 2.8 | 2.7 | 2.6 | 2.4 | | |
| 0.8 | $a_o$ = | | | | | | | 0.121 | 0.123 | 0.125 |
| | $u_o$ = | | | | | | | 25.4 | 23.0 | 21.1 |
| | $\bar{T}$ = | | | | | | | 2701. | 2421. | 2428. |
| | $\bar{\rho}/\rho_\infty$ = | | | | | | | 0.20 | 0.22 | 0.24 |
| | $\frac{\dot{M}_{f_m}}{\dot{M}_o}$ = | | | | | | | 3.2 | 3.0 | 2.8 |

Thus, a reasonable determination of $a_o$ can be obtained directly from Eq. (19), for a given $\Gamma$ and $z_e$, by assuming a reasonable value of $\bar{\rho}$ (e.g., $\bar{\rho}/\rho_\infty = 0.2$).

Inspection of the solutions generated to date reveals that values of C and B' can be found that give reasonable values and trends of the variables with changing $\Gamma$. The variation of C and B' with $\Gamma$ is to be determined experimentally. The experimental program is not yet complete, so that the functional form of C and B' with $\Gamma$ (and $z_e$) cannot be completely determined and verified at this point in time. In particular, values of $\Gamma$ from 2 to 2.8 have been experimentally obtained, but larger values are desirable so as to minimize the effect of entrainment.

The $\Gamma = 2.8$ experimental results have been compared with the calculations. Fig. 24 demonstrates that the mean core temperature is about $2000^\circ$F ($2460^\circ$R). It was found that values of C = 0.6, B' = 18.2 produced the best comparison with the data. In order to estimate the effect of varying $\Gamma$ on the unknowns, values of C and B' were also selected for the $\Gamma = 3.7$ and 5 calculations by assuming that a slight mean core temperature increase occurs for $\Gamma = 3.7$ and 5, respectively. For increasing $u_o$ and $\dot{M}_f/\dot{M}_o$ with increasing $\Gamma$, values of 0.7 and 20.8, and 0.9 and 26.1 for C, B' were determined to be appropriate for the two values of $\Gamma$. The variation of C and B' with $\Gamma$ is plotted in Fig. 12. For $\Gamma$ greater than approximately 4.5, the C and B' slopes are nearly constant. If we assume that this trend continues for larger values of $\Gamma$, then the variation of C and B' with $\Gamma$ (for $\Gamma > 4.5$) is given by $C = 0.22\,\Gamma - 0.21$, $B' = 3.25\,\Gamma + 9.85$. Of course, this variation has to be considered as very speculative at this time. More data are necessary before the predictions can be verified.

The results for C, B', $a_o$, $\bar{T}$, $\bar{\rho}/\rho_\infty$, $u_o$, $G/G_o$, $\dot{M}_f/\dot{M}_o$, $\dot{M}_f/\dot{M}_o$, and $\dot{M}_f/\pi\bar{\rho}u_o a_o^2$ are given in Table 4 for $\Gamma = 2.8$, 3.7, and 5 and $z_e = 18$. The quantity $\dot{M}_f/\pi\bar{\rho}u_o a_o^2$ represents the ratio of the core fuel burn rate to the total core flow rate, and is a measure of the

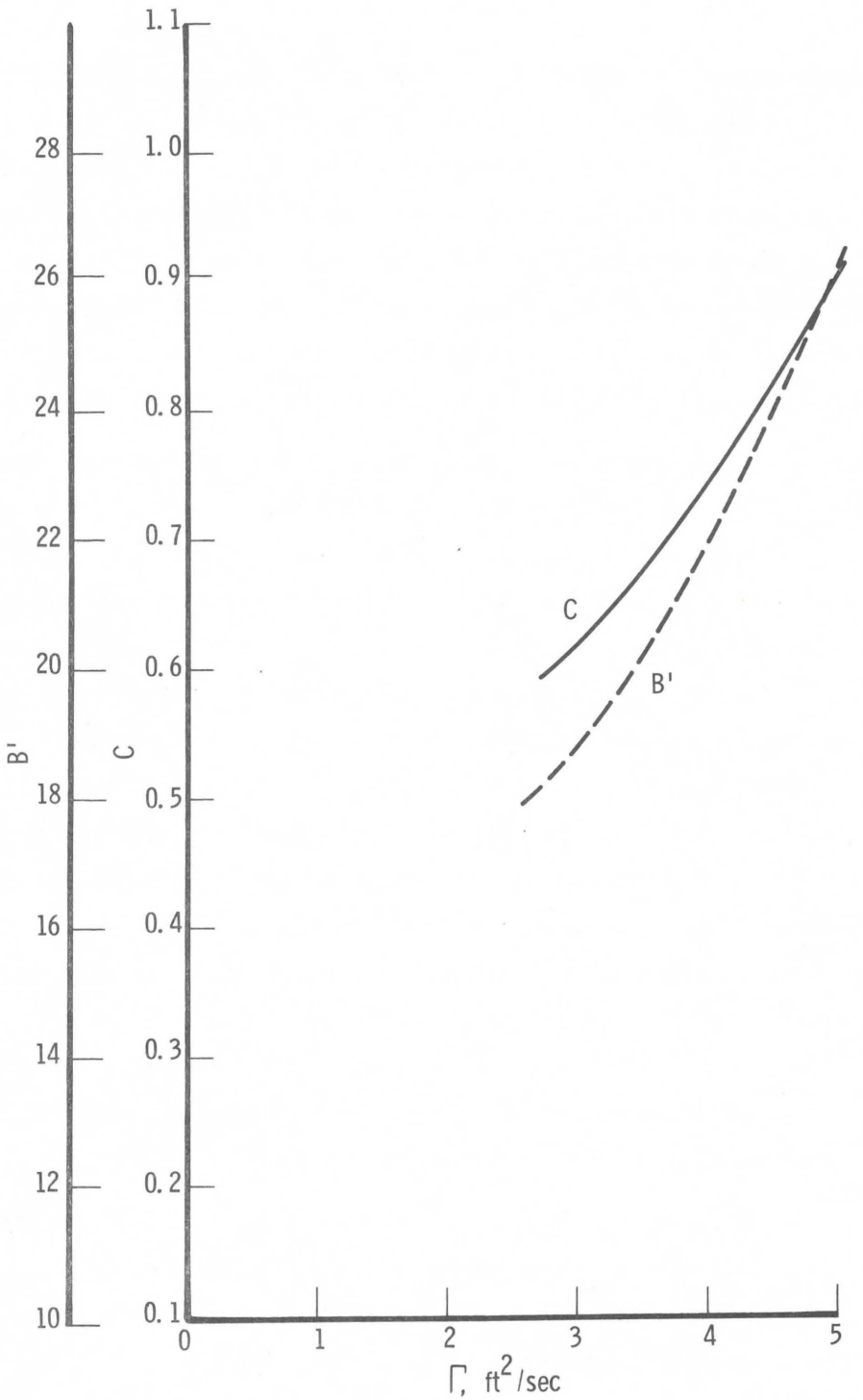


Fig. 12. Dependence of the Heat Transfer Coefficient Constant (C) and the Radial Mass Inflow Constant (B') on $\Gamma$ ($z_e$ = 18', Acetone Fuel)

Table 4. Effect of $\Gamma$ on Acetone Fire Whirl Properties

($Z_e$ = 18 ft)

| $\Gamma$, ($ft^2$/sec) | C | B' | $a_o$, (ft) | $\bar{T}$, ($^oR$) | $\bar{\rho}/\rho_\infty$ | $u_o$, (ft/sec) | $G/G_o$ | $\dot{M}_f/\dot{M}_o$ | $\dot{M}_{f_m}/\dot{M}_o$ | $\dot{M}_f/\pi\bar{\rho}u_o a_o^2$ |
|---|---|---|---|---|---|---|---|---|---|---|
| 2.8 | 0.6 | 18.2 | 0.093 | 2460 | 0.215 | 20.4 | 8.3 | 1.15 | 2.0 | 0.063 |
| 3.7 | 0.7 | 20.8 | 0.122 | 2580 | 0.205 | 21.5 | 8.8 | 2.1 | 2.9 | 0.067 |
| 5.0 | 0.9 | 26.1 | 0.164 | 2700 | 0.197 | 24.3 | 10.2 | 4.4 | 5.0 | 0.171 |

fuel mass fraction. Table 4 shows that the axial velocity increases fairly slowly and the fuel burn rate rapidly with increasing $\Gamma$. A plot of $u_o$ and $\dot{M}_f/\dot{M}_o \left(\dot{M}_{f_m}/\dot{M}_o = \dot{M}_f/\dot{M}_o + 1 - \Omega\right)$ versus $\Gamma$, for $z = 18$, is shown in Fig. 13. Note that the rate of increase of $u_o$ is increasing with increasing $\Gamma$. Since large axial velocities are needed in order to lift firebrands from the wood burn tests planned during the next phase of this study, it is seen that it is desirable to increase the circulation. The acetone burn rate, as seen from the Figure, appears to have a decreasing rate of increase with $\Gamma$ at the larger values of $\Gamma$. This is consistent with the data presented by Emmons and Ying [1966], which showed that the burn rate increase was leveling off at the larger values of $\Gamma$. Comparison of the values of $u_o$ and $\dot{M}_f/\dot{M}_o$ at $\Gamma = 2.8$ with the UCSB experimental results shown in Figs. 17, 18, and 29 shows that while the comparison between the predicted and measured burn rate ratio is adequate (a predicted 2.0 vs. a measured 2.3), the predicted velocity is almost a factor of two higher than measured. However, there are uncertainties in the calibration of the transducer used to obtain the velocity measurements (see Discussion in the Experimental Results Section of this report) which are currently in the process of being resolved. Thus, the measured velocity values are not yet finalized. The predicted axial velocity results appear to be more consistent with those experimentally obtained by Byram and Martin [1970], who measured an axial velocity of 43 ft/sec for a circulation of 7.2. Although it is difficult to accurately extend the $u_o$ plot of Fig. 13, it is seen that an axial velocity of 35 ft/sec at $\Gamma = 7.2$ is not unreasonable.

The effect of varying $z_e$ is also of interest. While the height of the experimental apparatus was not changed in this phase of the program, it will be so done in the future. Table 5 gives calculations for $z_e = 13$ at $\Gamma = 2.8$, 3.7, and 5. The variation of axial velocity and acetone burn rate ratio with $\Gamma$, for $z_e = 13$, is also shown in Fig. 14. In comparison with the $z_e = 18$ case, the axial velocity is slightly lower and the burn rate ratio slightly higher. Thus, a very weak dependence on

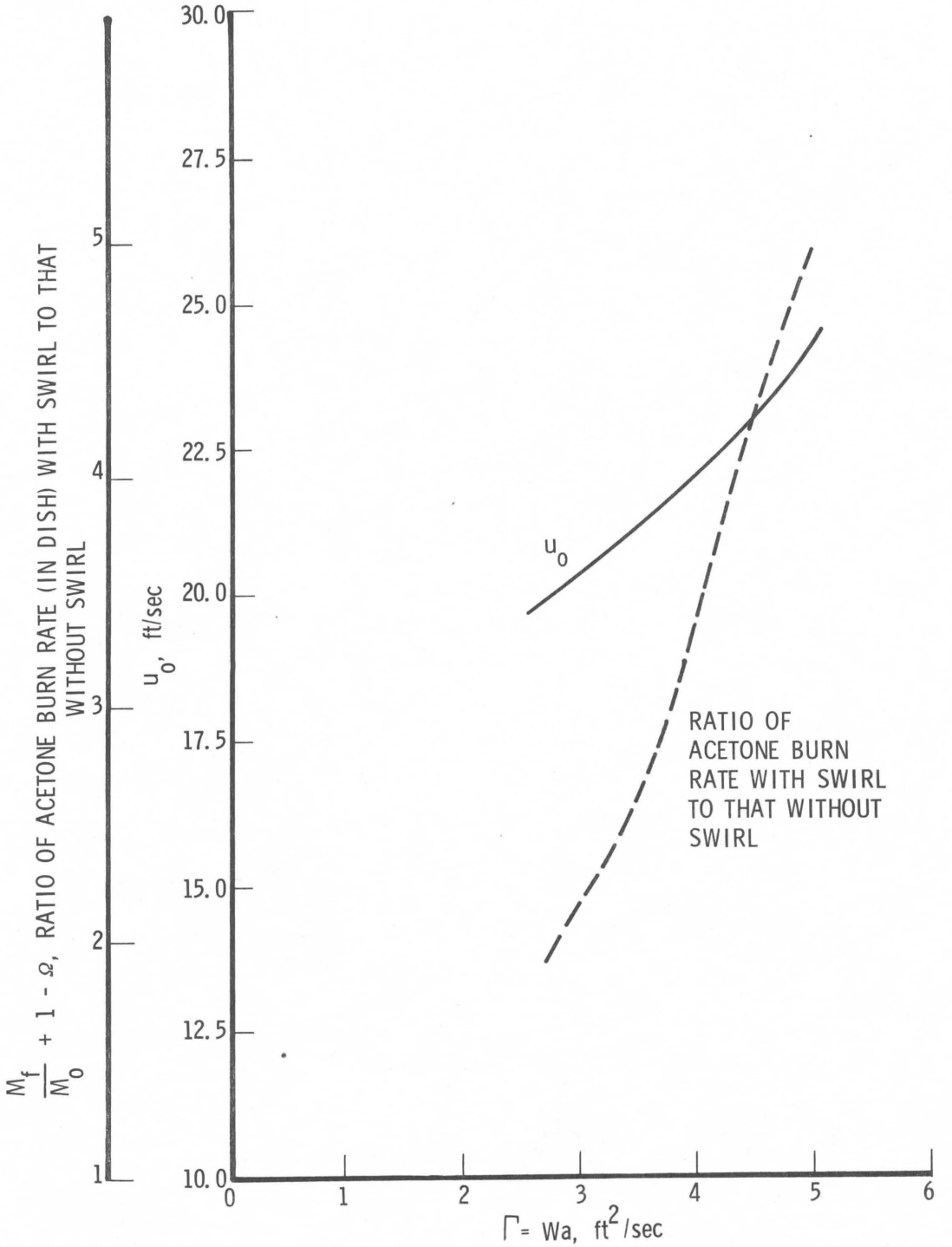


Fig. 13. Effect of $\Gamma$ on Axial Velocity and Acetone Burn Rate ($z_e = 18'$)

Table 5. Effect of $\Gamma$ on Acetone Fire Whirl Properties

($Z_e$ = 13 ft)

| $\Gamma$ ($ft^2$/sec) | C | B' | $a_o$, (ft) | $\bar{T}$, ($^oR$) | $\bar{\rho}/\rho_\infty$ | $u_o$, (ft/sec) | $G/G_o$ | $\dot{M}_f/\dot{M}_o$ | $\dot{M}_{f_m}/\dot{M}_o$ | $\dot{M}_f/\pi\bar{\rho}u_o a_o^2$ |
|---|---|---|---|---|---|---|---|---|---|---|
| 2.8 | 0.6 | 18.4 | 0.109 | 2460 | 0.22 | 17.9 | 7.4 | 1.4 | 2.2 | 0.065 |
| 3.7 | 0.7 | 21.2 | 0.144 | 2580 | 0.21 | 18.7 | 7.7 | 2.5 | 3.2 | 0.067 |
| 5.0 | 0.9 | 26.4 | 0.193 | 2700 | 0.19 | 20.9 | 8.7 | 5.2 | 5.6 | 0.071 |

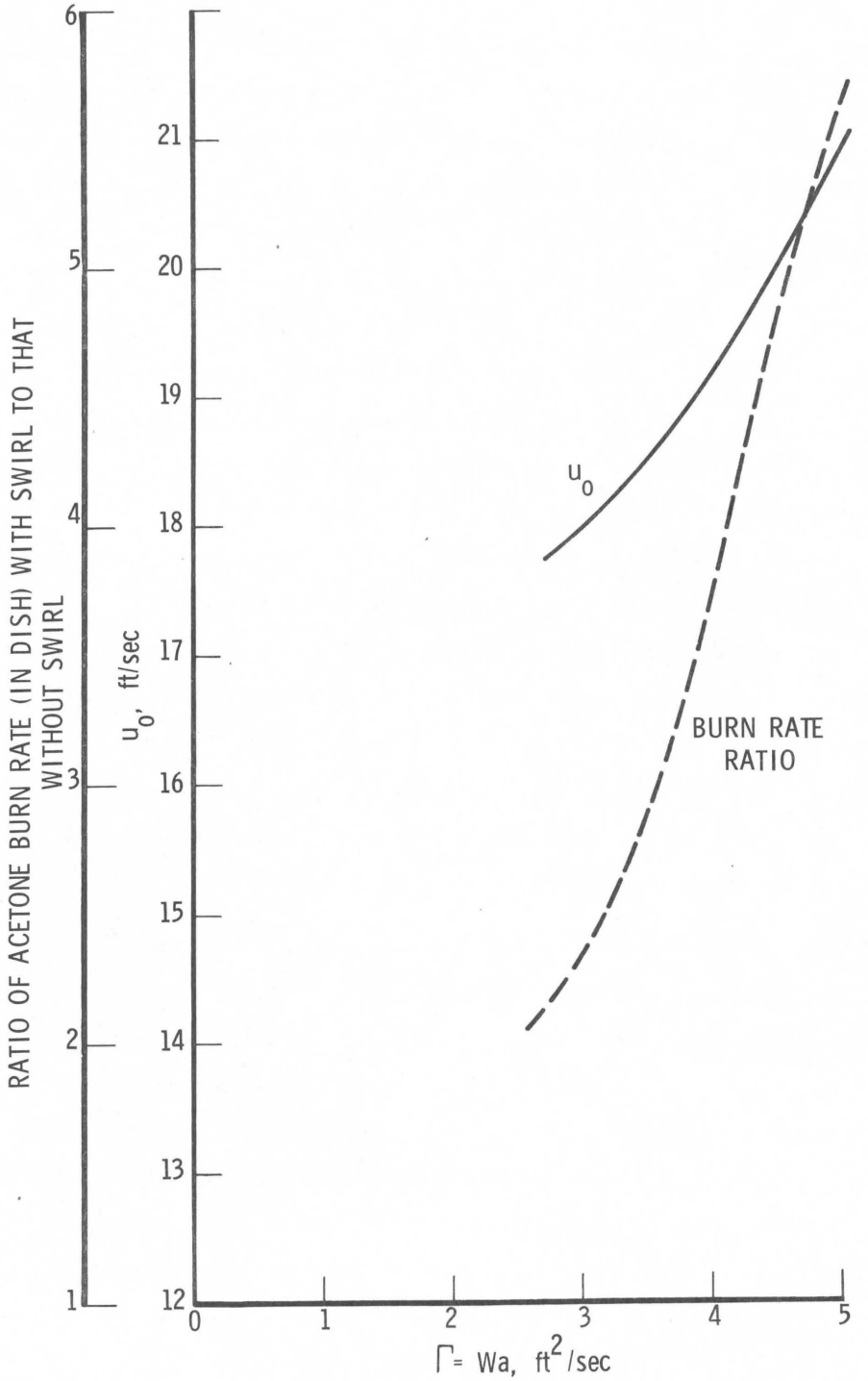


Fig. 14. Effect of $\Gamma$ on Axial Velocity and Acetone Burn Rate ($z_e$ = 13')

$z_e$ is exhibited. It is interesting to note, on comparing Tables 4 and 5, that C and B' are predicted to have negligible variation with $z_e$ over the range of variables considered.

Some of the assumptions made during the analysis can be directly checked with the experimental data. The temperature radial profile data show that the radial mean core temperature changes little with core height position. Thus, the assumption of a constant $\bar{T}$ (and hence $\bar{\rho}$) appears to be appropriate. The general trends predicted by the analytical approach also seem reasonable. Full verification of the methodology must await the forthcoming additional experimental data; in particular, a wider range and larger values of $\Gamma$, and data at varying $z_e$. If we assume validity of the procedure and adequate determination of the functional form of C and B' versus $\Gamma$, then the equations would be assumed to be directly applicable to full scale fire whirls. That is, given a value of $\Gamma$ and $z_e$, whether appropriate to a laboratory experiment or a full scale fire whirl, the pertinent core variables can be determined from the equations presented here. This presumes that the relevant physics is not dependent on overall size, so that the functional form giving the variation of C and B' with $\Gamma$ is appropriate at large $\Gamma$. The predictions tend toward a trend of a constant slope for C and B' at larger $\Gamma$, alluding to an asymptotic functional dependence of C and B' on $\Gamma$, and appropriateness of the theory at large $\Gamma$.

The analytical effort during the next phase of the study will include comparisons with both acetone and wood test data. As alluded to previously, the modifications to the analysis needed to consider wood as a fuel are minor. The major modification involves inclusion of wood size in the Reynolds number appearing in the skin friction coefficient used in the determination of the convective heat transfer coefficient. Since the modifications are minor, applicability of the procedure to full scale wood-fueled fire whirls appears feasible, albeit premature at this time.

## B. EXPERIMENTS

The initial phase of this work was directed toward two purposes: first, to develop an experimental technique and instrumentation for the study of simulated fire whirl columns; and, second, to obtain a basic understanding of the fire whirl (using acetone as a fuel) to allow development of scaling laws from which realistic experiments can be designed using natural fuels in a continuing phase.

Fire whirl characteristics have been studied in the past by Lee [1966], Emmons [1966], Byram [1970], and others using pure hydrocarbon fuels. Many of the results of these previous studies have been incorporated into initial analytical efforts which have been used to design the experimental apparatus used in this study. The features of the experimental design used herein are, in general, a combination of techniques used in the previous studies. For example, the final design included tangential boundary layer air inlets in combination with independent tangential air inlets along the bottom 6-ft region of the apparatus. By this combination, it is hoped that an independent control of the vorticity of the experiment can be obtained.

Basic measurements considered in the study were measurement of the fuel burn rate, the circulation distribution, the temperature profile, the vertical velocity, and the boundary layer velocity profiles under fire whirl conditions. Additionally, in further work, the temperature profile will be measured directly above the fuel surface to determine the effect of circulation on the heat feedback to the fuel. It should be mentioned that this temperature gradient is not required in the fire whirl analytical model described above. The measurements to be taken will be used to verify the values of the calculated heat transfer coefficients $h_o$ and h. The instrumentation for measuring the above mentioned variables is in various stages of completion, as will be discussed later in the report. Finally, as a demonstration of feasibility, three wood cribs were burned and cursory measurements taken. The results of these tests indicated that fire whirls would be generated in the apparatus using wood cribs. The discussion of wood crib tests appears in a separate section (IV. B. 5).

## 1. APPARATUS

The experimental apparatus consists primarily of two 3-ft diameter, 6-ft length cylindrical sections topped by a truncated conical section which is also 6-ft in length and has an outlet diameter of 1.5 ft. The apparatus is shown in Fig. 15. The bottom cylindrical section is fitted with five pairs of tangential forced air inlets which are fed by an air blower (Fig. 16). The mass flow rate through these tangential inlets can be controlled and the total flow measured. Additionally, the flow through each of the individual inlets can be controlled and measured when necessary.

The second cylindrical section originally was an open-screened section. It was found that this configuration damped the circulation. Later in the program, the screen was covered by a plastic sheet; and, with this new configuration, a larger circulation and more stable fire whirl core were maintained under a variety of ambient conditions.

An 8 x 8-ft flat table is installed directly below the bottom cylindrical section. This table has the capability of being raised or lowered for varying the air gap below the apparatus from zero to seven inches. In this manner, the amount of open boundary layer air space is controllable. During the program, it was determined that the forced air swirl inducers (FASI) were not capable of sustaining adequate circulation. Therefore, tangential boundary layer inlets (TBLI) were installed similar to those used by Byram. In the current configuration, there are six of these tangential inlets with an inlet area which is equivalent to a boundary layer gap of 0.9 in. With this final configuration, stable vortices have been established and maintained in the experiments.

In the center of this variable height table, the fuel is placed in a glass dish on a weighing system which will be described in more detail in the next Section. The acetone in the dish is ignited using an electric match, that is, two electrodes arcing above the surface of the fuel. The ignition of wood cribs is described in Section IV. B. 5. A typical run

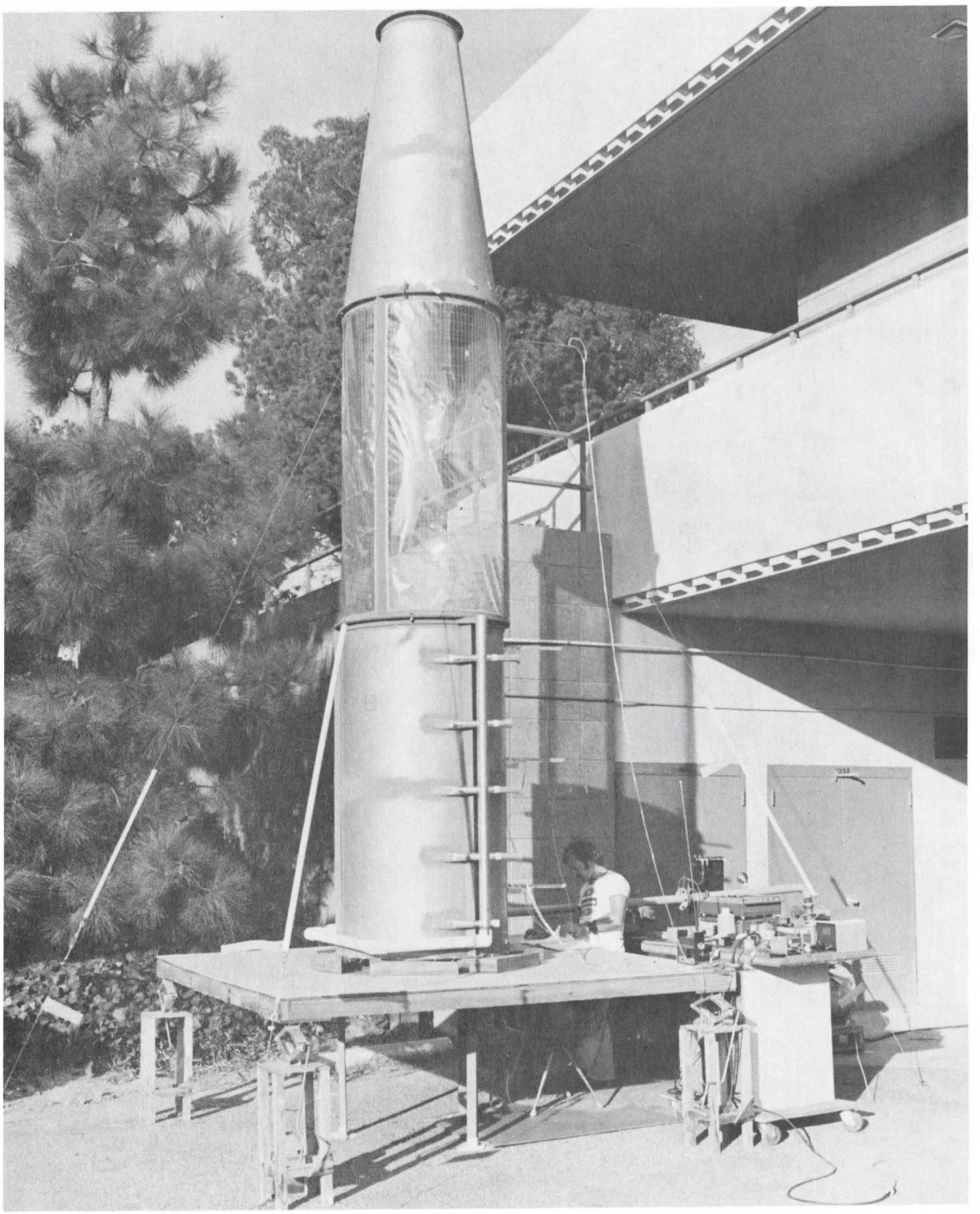

Fig. 15. Experimental Apparatus

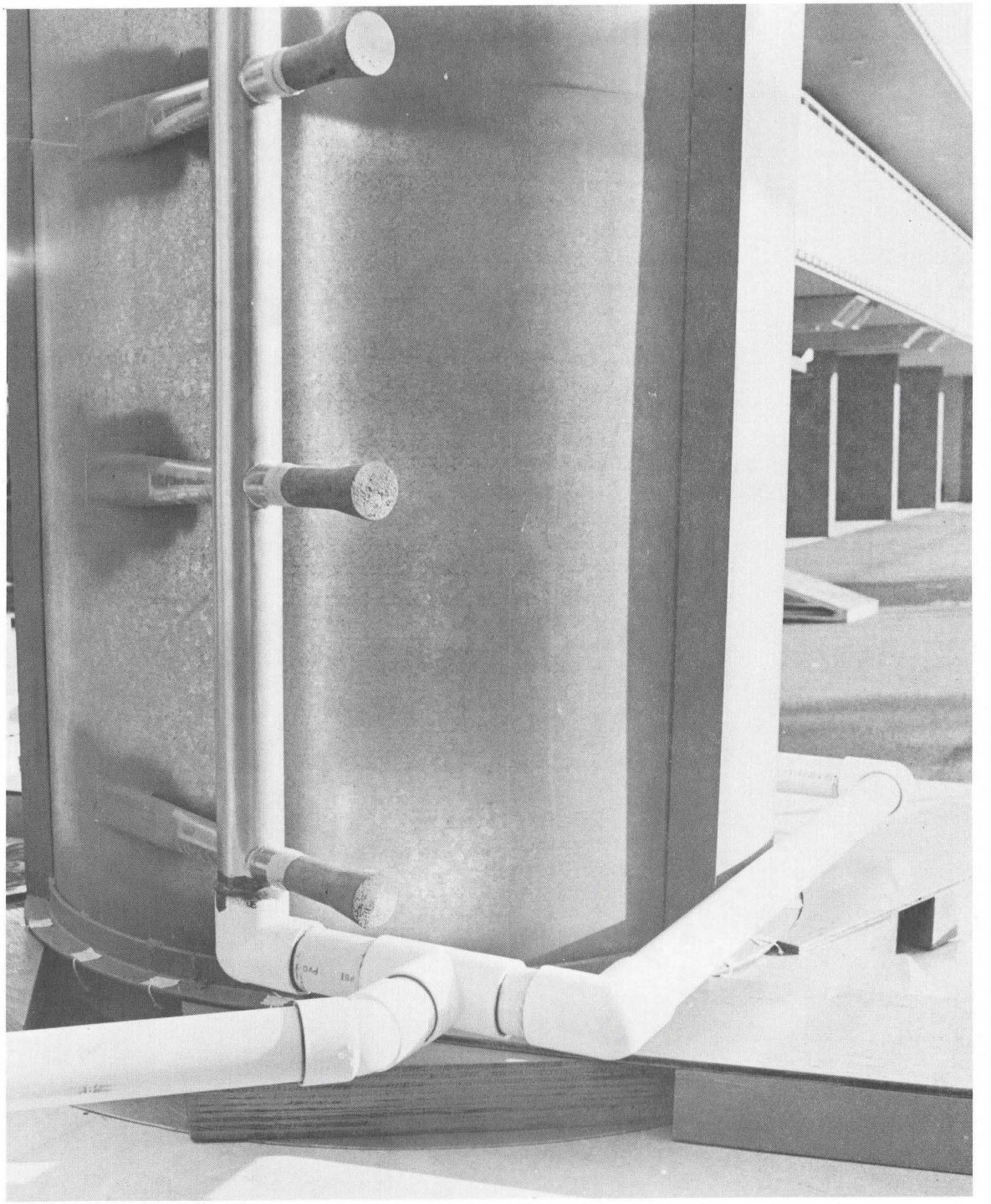

Fig. 16. Tangential Air Inlets

procedure is as follows: first, a prescribed amount of fuel is added to the weighing dish; second, the appropriate induced air flow is established and allowed to run sufficiently long to yield a steady state vortex without a burning column. When this is established, the fuel is ignited and the instrumentation started. A typical acetone run is of the order of 2 to 3 min in duration.

## 2. INSTRUMENTATION

As indicated previously, the instrumentation development is not, at this time, complete; but the following measurements are currently operational. First, the fuel burn rate is obtained by continuous weighing of the fuel during the burning process. The circulation profiles are obtained by measuring the tangential velocity at three heights within the bottom 6-ft section. These are done by the use of pitot tubes which can be positioned manually at any radius from zero to the wall position. Likewise, at the same three positions, the temperature profile can be obtained using a chromel-alumel thermocouple probe which, again, can be manually positioned at any radius from zero to the wall. Finally, a pitot tube measurement of the centerline axial velocity can be obtained at 3, 6, and 12 ft above the floor. This pitot tube is also fitted with two thermocouples to approximate the temperature of the vertical flowing gas. Additionally, three boundary layer dynamic pressure rakes have been constructed and are ready for installation in the apparatus. A rotating pitot tube is also currently being constructed to allow the measurement of the magnitude and direction of the velocity within the core as a function of radius and height. The instrument to measure the axial temperature profile above the swirl surface is still in the design stage.

The fuel burning rate is obtained by continuous measurement of the fuel weight during the burning process. This is done using a cantilever beam weighing system. A Pyrex glass dish is supported on the end of the cantilever beam which is 12 in in length and 0.194 $in^2$ and is made of 6061 aluminum. The load is actually applied 11 in from the

cantilever fix point. For this setup, the computed deflection for 100 grams is 0.108 in.

To measure the strain, Vishay Type 250B strain gages are attached to the cantilever beam. These gages are temperature compensated for aluminum and have a resistance of 120 ohms with a gage factor of 2.09 $\pm$ 0.5%. A 1/2 bridge is used on this beam with one gage on top of the beam in tension and the other on the bottom in compression. The circuit for measuring the strain gage output is given below.

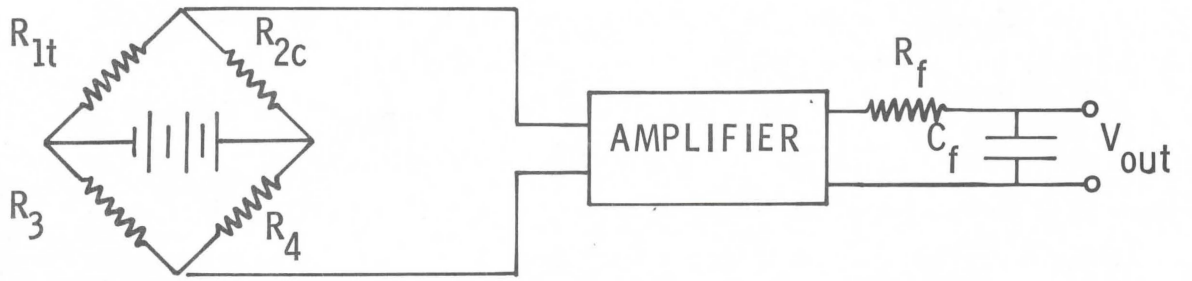


$R_{1t}$ and $R_{2c}$ represent the strain gages in tension and compression, respectively. The other half of the Wheatstone bridge ($R_3$, $R_4$) and the excitation voltage are supplied by a Vishay Type 1011 Strain Indicator. The strain indicator is also used as the amplifier in the circuit. The output is fed through a low-pass filter before being measured on a voltmeter or recorded in order to filter out the high frequency oscillation the dish may undergo during the burning process.

The cantilever beam system is attached directly below the movable floor, and the Pyrex dish which holds the acetone fuel protrudes up through a circular hole in the center of the floor. The height above the base is controlled by the use of inserts in the Pyrex dish column. For the experiments reported herein, the dish lip was initially 1/4 in above the floor. By necessity, there must be some clearance between the floor board and the Pyrex dish so that interference with the

measurement is avoided. Since the pressure just above the fuel in the burning region will be lower than the ambient pressure, air would be sucked through this gap if provisions were not made to exclude it. Consequently, the entire beam apparatus is sealed so that air cannot be admitted through the gap between the dish and the base board. Thus, a constant pressure is maintained below the dish and above the dish with no net flow around the dish. However, these two pressures are not identical due to the radial variation in pressure directly above the burning surface. Consequently, upon ignition there is a zero shift in the weight output and when the flame goes out, a negative shift occurs. However, during the steady burn period the slope of the weight curve is constant and unaffected by this variation.

As indicated, both circulation and axial velocities are measured using pitot tubes. The swirl velocity pitot tubes are 1/8-in in diameter and placed at vertical heights of 17, 45, and 71 in above the floor. These pitot tubes are capable of being manually slid to any position to obtain a radial distribution of circulation velocity in regions in which there are no other significant velocity components. For the experiments described in this report, the pitot tubes were only long enough to go to a radius of 5 in (from the center line). However, new pitot tubes are now available to allow a radial scan all the way to the center line. The axial velocity pitot tube was a 1/4-in diameter tube fitted with two chromel-alumel thermocouples for temperature measurement. This probe could be placed at the center line at three different vertical heights of 3, 6, and 12 ft above the floor. The pressure difference output of these pitot tubes was measured using a Decker $\Delta P$ Transducer Type 306 with an appropriate amplifier system.

Chromel-alumel thermocouple probes were also provided at the same three heights as the swirl velocity measurements, 17, 45, and 71 in.above the floor. These probes also are capable of being slid to any radial position from the actual core centerline to the wall. The millivolt output of the thermocouples is amplified using an operational amplifier (specifically built for this purpose) before being recorded.

In order to determine the amount of air being ingested into the flame, a boundary layer profile will be measured in future runs. This is obtained using dynamic pressure tubes at various heights above the floor. These are then referenced to a static pressure directly in line with the dynamic probe inlets. In order to obtain circumferential variation and increase the vertical detail, three probes are constructed and put into the boundary layer 120 degrees apart. In a given run, the dynamic pressures as reference to one of the static pressures will be measured sequentially. Additionally, the other two static pressures referenced to the same reference static pressure will be included in the sequential record. Thus, the velocity profile will be determined at various heights above the floor and at the three circumferential positions. Obviously, the air entering the column in the vicinity of the core is not entering in a radial direction. To compensate for this, the boundary layer rakes can be rotated so that they line up with the direction of the boundary layer flow, thus maximizing the accuracy of the velocity measurement. These pressure rakes have been constructed and are ready for installation into the apparatus.

As indicated above, the tangential velocity outside of the core and the axial velocity at the centerline can currently be measured. However, it is desired to obtain complete profiles of the velocity both in magnitude and direction. Unfortunately, one cannot use a pitot tube to measure the tangential and vertical components of a flow which is spiraling upward since each measurement would be invalidated by the flow entering the static ports. To compensate for this problem, an apparatus is being constructed which will allow the rotation of the pitot tube about its tip, thus determining the position of maximum $\Delta p$, i.e., the alignment with the actual velocity vector. By measuring this angular position and magnitude, the actual velocity can then be determined. This apparatus has been designed and is under construction at this time.

Currently, the measurements being made in a given experiment are recorded using two Hewlett-Packard XY recorders. These recorders

have their time bases ganged together so that they operate simultaneously. Various $\Delta p$'s can be recorded sequentially during a given run through the use of a 12-port solenoid drive Scanavalve system. Various temperatures can be recorded sequentially by use of an Omega Engineering thermocouple selector switch with 24 positions. Thus, several data can be recorded during a given run; but these must be done sequentially and care must be taken that the period of measurement is large compared to the fluctuation changes which occur in a given burning situation.

## 3. RESULTS

As indicated previously, one of the purposes of this first phase was to develop appropriate instrumentation for measuring the parameters of interest. In this Section, we will discuss experiments made with acetone and the results obtained.

The acetone fuel burn rate was obtained under a variety of conditions. First, the fuel burn rate was measured for various air gaps but with no circulation inducement; that is, TBLI or FASI nonoperative (Fig. 17). It is clear that for gap heights of less than 1/2-in, there is a significant change in the fuel burn rate. Similar observations were made by Emmons and Ying [1966]. However, the variation is far less at higher air gaps. As indicated previously, the TBLI give an equivalent height of 0.9 in. Therefore, the average of all runs obtained using the TBLI but with no FASI operating is also included in this Figure at 0.9 in. It would appear advisable for future runs with fuel cribs to vary the equivalent height of the TBLI to note the variation that might occur due to this parameter.

Fig. 18 shows the burn rate results for a series of runs operating with varying velocity FASI at the cylinder wall and with TBLI in place. It should be noted that the swirl air is given in terms of the pressure drop in inches of water as read directly on the manometer across the square-edged measuring orifice used in the flow apparatus. The reason for this procedure will be explained later in the Discussion

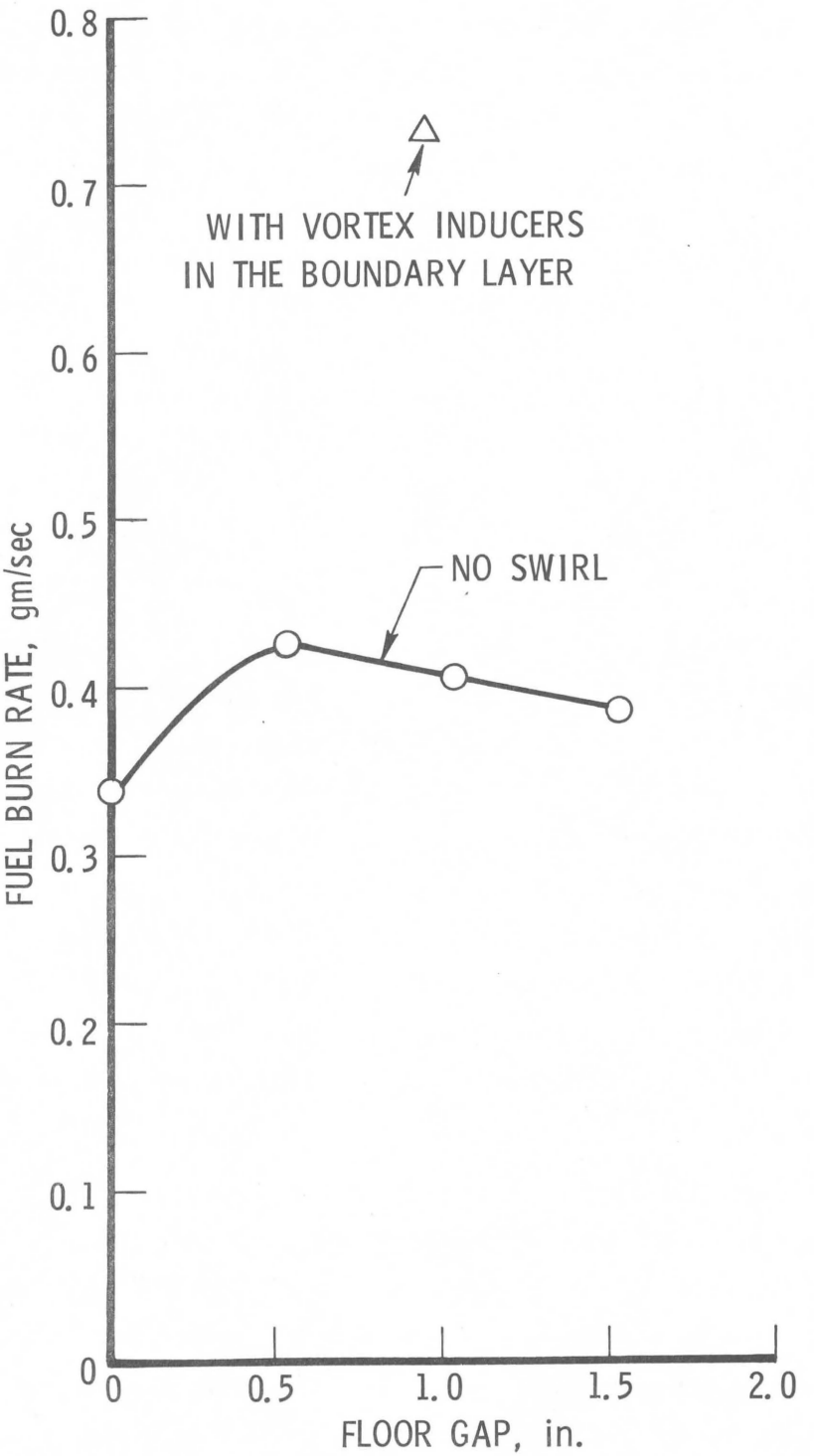


Fig. 17. Acetone Burn Rate Variation with Boundary Layer Opening with No Circulation

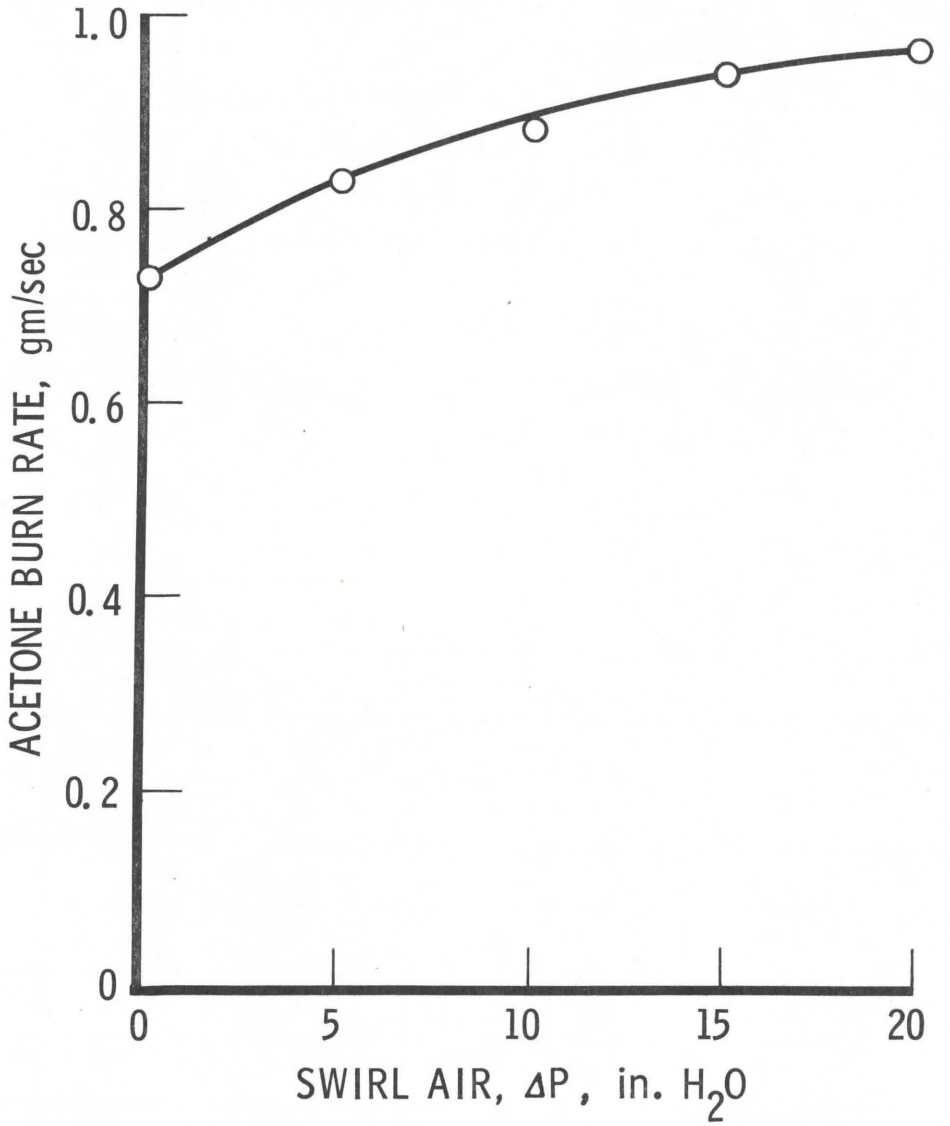


Fig. 18. Acetone Burn Rate Variation with Swirl Air Flow

Section. It is clear from these results that the FASI have modest effect on the fuel burn rate up through 20 in $\Delta p$ measured.

Table 6 shows the circulation (i.e., $\Gamma = V_t R$) that resulted for forced air flows of 0, 10, and 20 in $\Delta p$ at 17, 45, and 71 in height above the floor. Measurements were only taken at radial positions of 5 and 6 in from the centerline. These positions were chosen as most indicative of the controlling vortex based on earlier configurations of TBLI profiles from 5 in to the wall. Tangential velocities were obtained with the early TBLI, one of which is shown in Fig. 19. This complete profile shows the relative ineffectiveness of the forced air swirl inducers in producing a high circulation about the core region. By comparing actual circulation values in Table 6, it is seen that the FASI do increase the circulation with increased forced air but that the effect is small.

Table 6. Circulation Distribution-Variation with Swirl Air Flow

| Swirl Air $\Delta p$, inches $H_2O$ (FASI) | Radial Position inches | Circulation $ft^2/sec$ | | |
|---|---|---|---|---|
| | | Vertical Position, inches | | |
| | | 17 | 45 | 71 |
| 0 | 5 | 1.90 | 2.20 | 2.41 |
| | 6 | 2.17 | 2.33 | 2.69 |
| 10 | 5 | 2.38 | 2.55 | 2.55 |
| | 6 | 2.45 | 2.48 | 2.59 |
| 20 | 5 | 2.76 | 2.83 | 2.86 |
| | 6 | 2.71 | 2.86 | 2.80 |

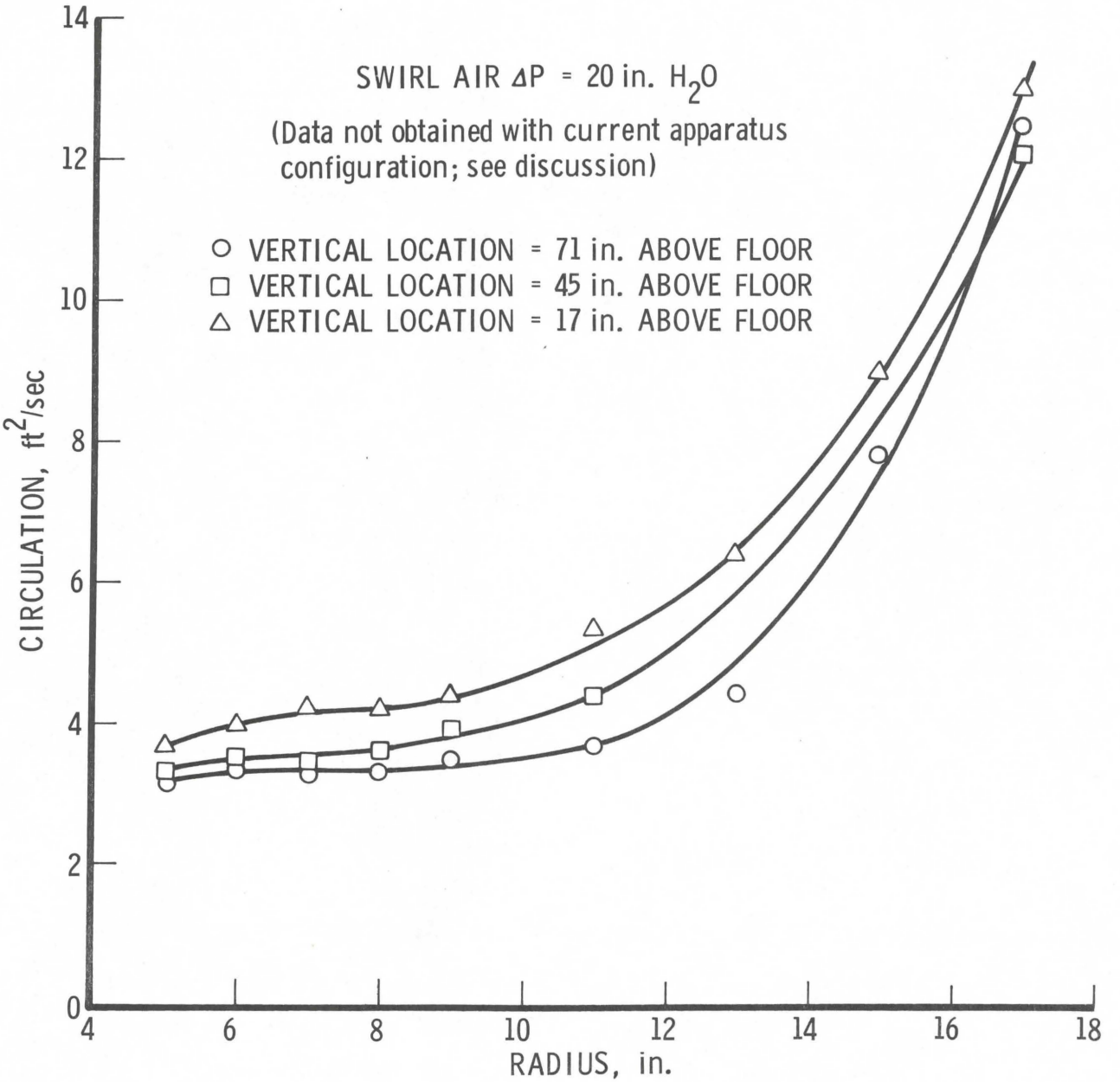


Fig. 19. Radial Circulation Distribution, Acetone Fuel

Figs. 20 through 24 give temperature profiles at the three vertical locations indicated and for the five different swirl inducers air flows. These profiles indicate that the centerline temperatures are lower than those in regions somewhat off the centerline and that the core size is approximately 3 in in diameter. This result is consistent with a phenomenological description of the core; namely, that it is fuel-rich and that the air is brought in primarily at the bottom of the core. Thus, the regions in the outer peripheral core region are less fuel-rich than the centerline flow and exhibit a higher temperature. It can also be seen that the sharpest profiles from the centerline to the outer region exist for the lowest profiles, again indicating the poor mixing within the core at the lower regions. The temperature data show that with the FASI (Figs. 21-24), the temperature in the core increased, compared to the no-FASI case (Fig. 20), and that it was highest at intermediate flow, corresponding to $\Delta p$ = 10 in. In all cases, there is a trend for flattening of the temperature profiles at the 71-in height caused by centerline dilution.

The centerline temperature variation is depicted in Fig. 25. It is seen here that the centerline position shows an increase in temperature up to 10-15 in $\Delta p$ with a significant drop at 20 in $\Delta p$. It should be noted that one data point for the top position at 15 in $\Delta p$ has been ignored since it would appear to be in error as compared to the other data.

The measurement of the core temperature as an indication of the core size is confirmed by the photographs of the core shown in Figs. 26 and 27. The acetone dish visible at the bottom is 6 in in diameter and, using this dimension as a reference, the visible core diameter size is 3 in. Figs. 26 and 27, as well as the photograph in Fig. 28, illustrate the stability of the core achieved after solution of initial stability problems.

Finally, Fig. 29 shows the axial velocity variation as a function of swirl inducers mass flow air. These results indicate that the maximum axial velocity occurs at the highest position and decreases

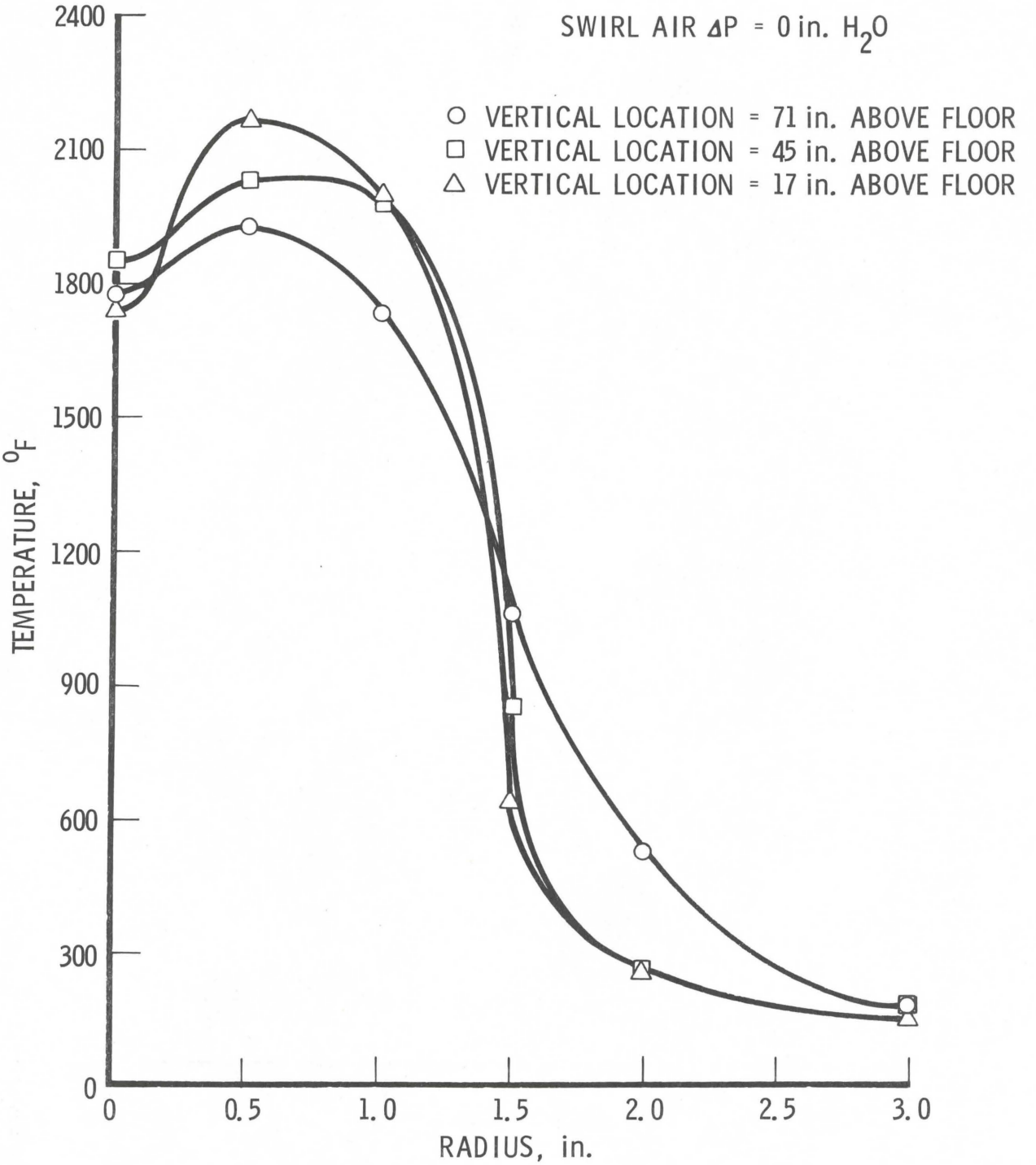


Fig. 20. Core Temperature Radial Distribution, Acetone Fuel

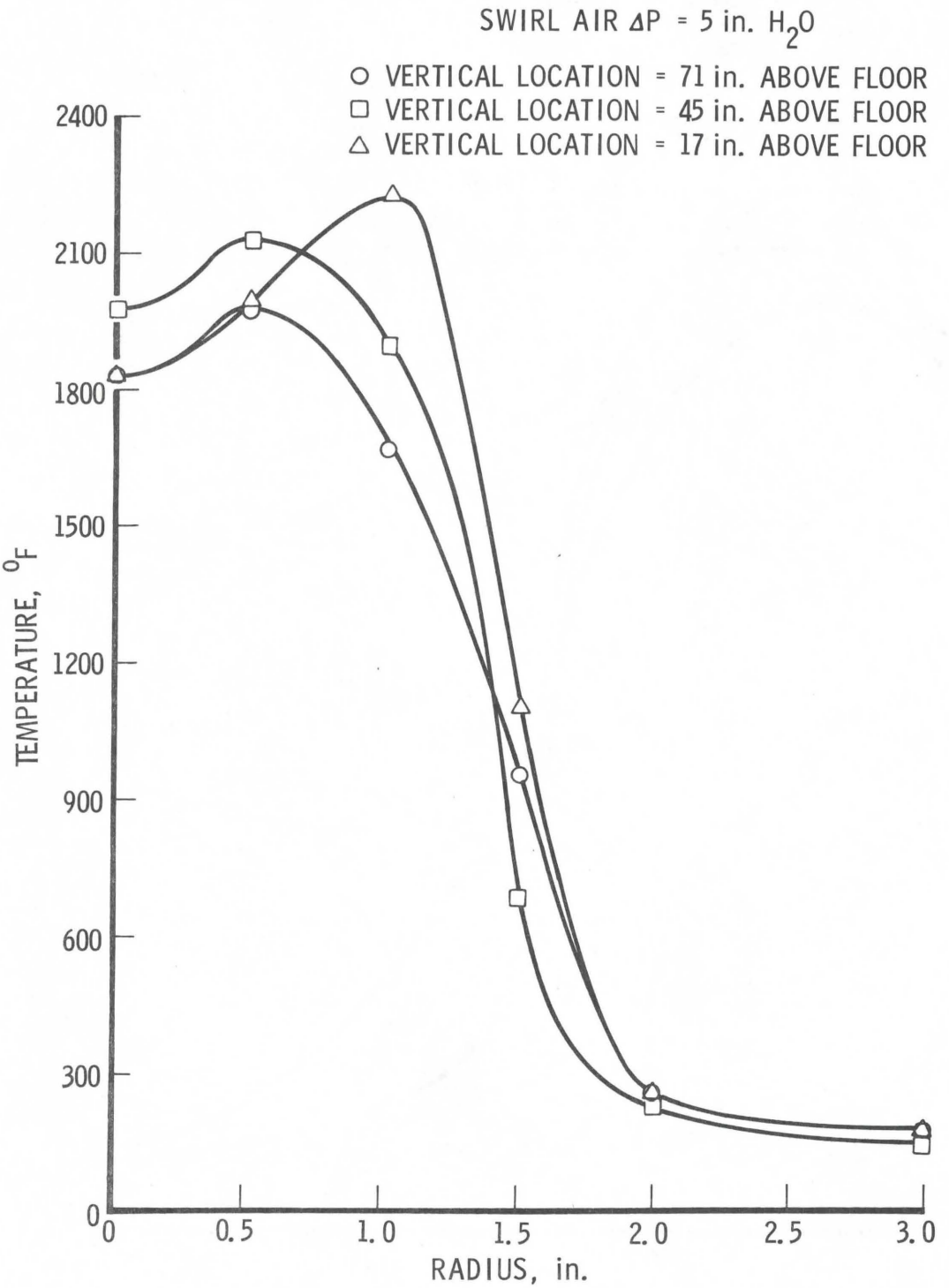


Fig. 21. Core Temperature Radial Distribution, Acetone Fuel

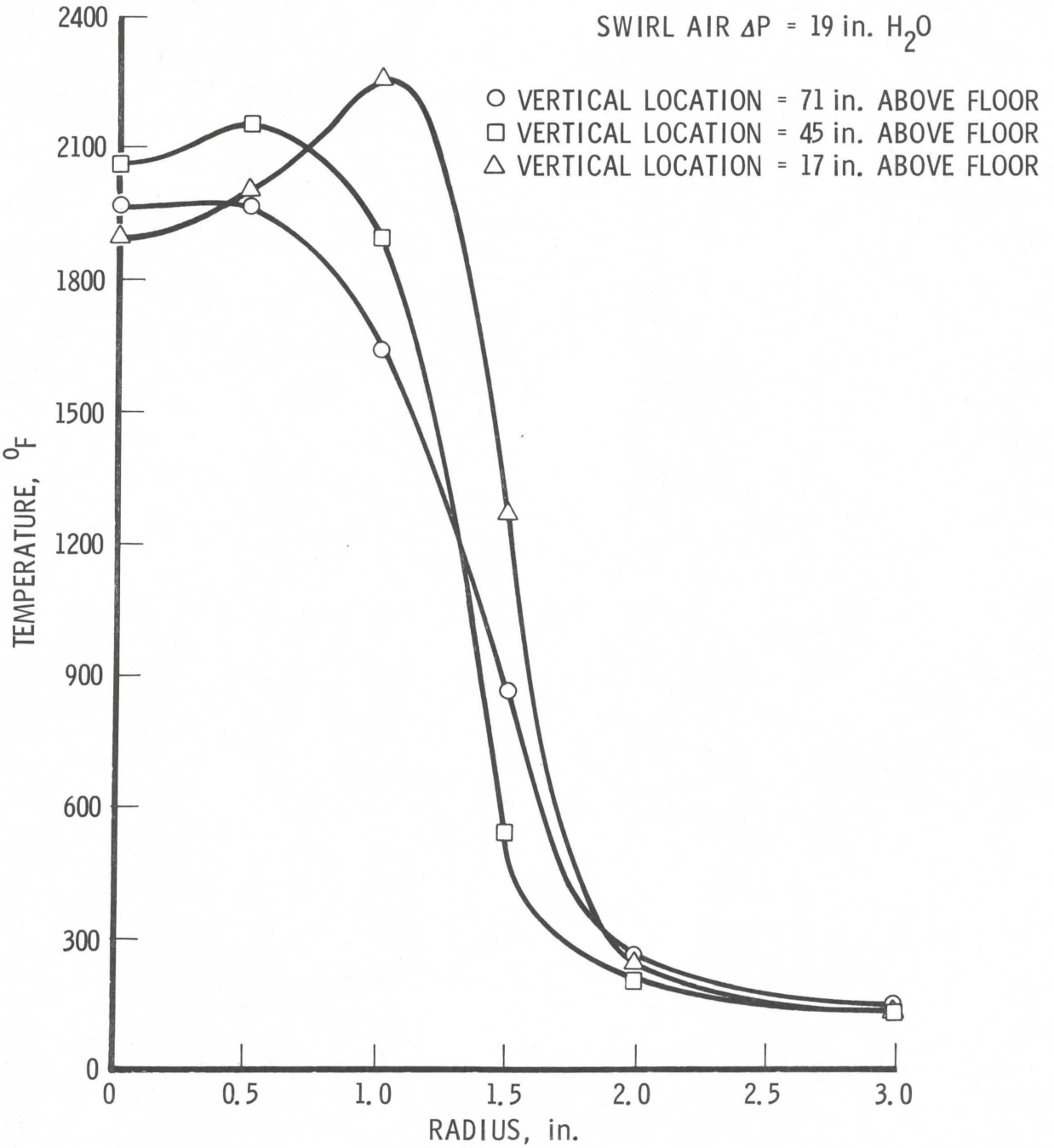


Fig. 22. Core Temperature Radial Distribution, Acetone Fuel

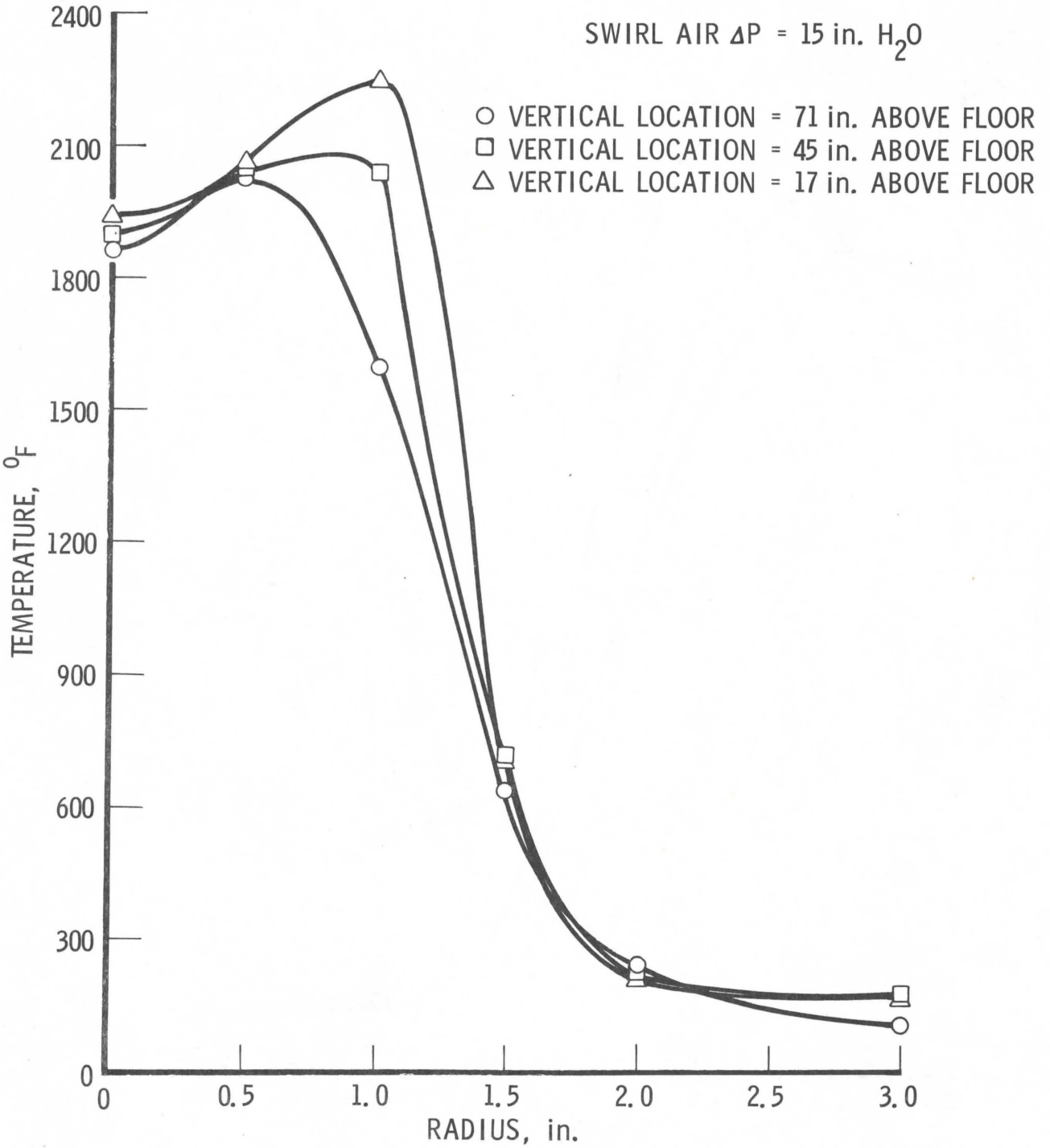


Fig. 23. Core Temperature Radial Distribution, Acetone Fuel

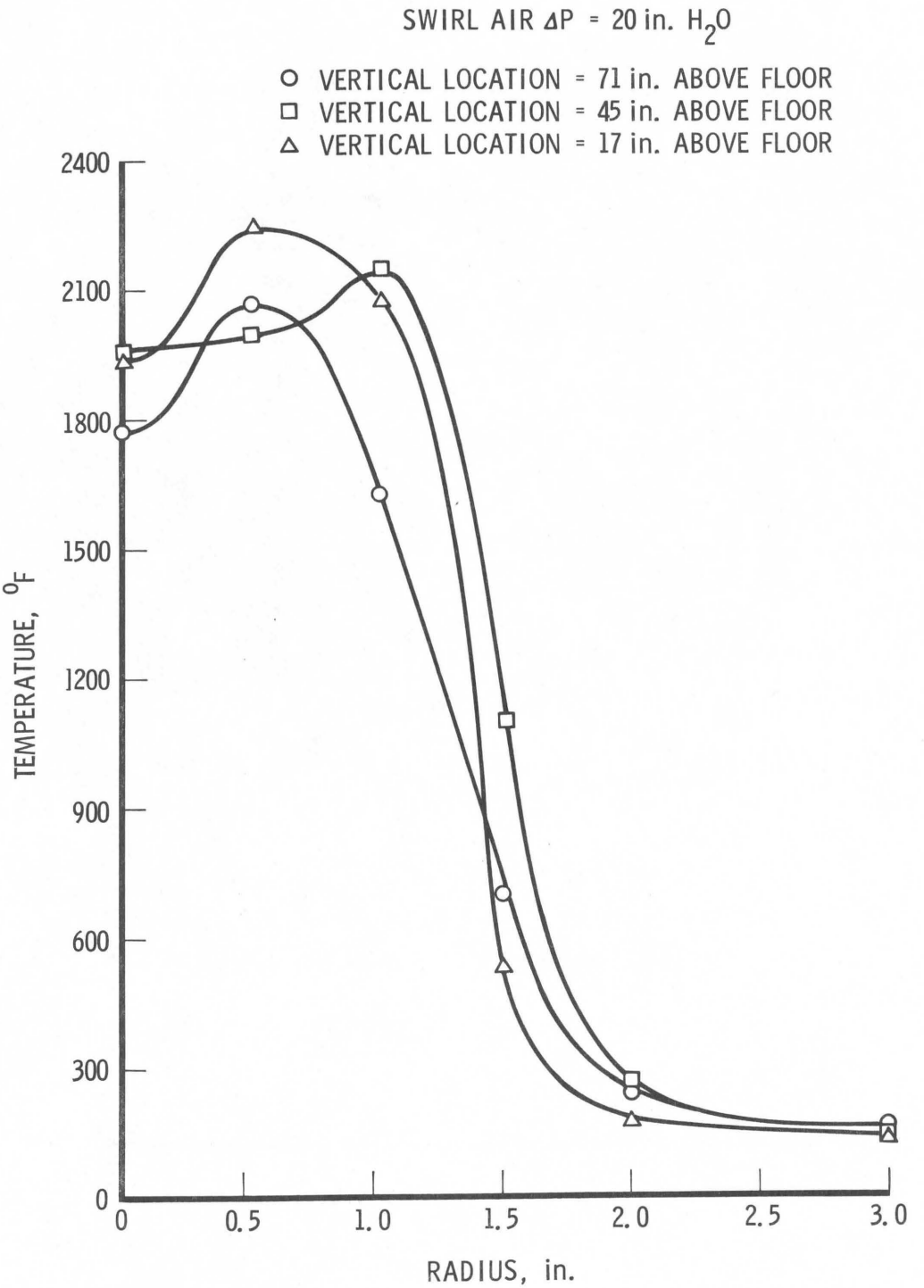


Fig. 24. Core Temperature Radial Distribution, Acetone Fuel

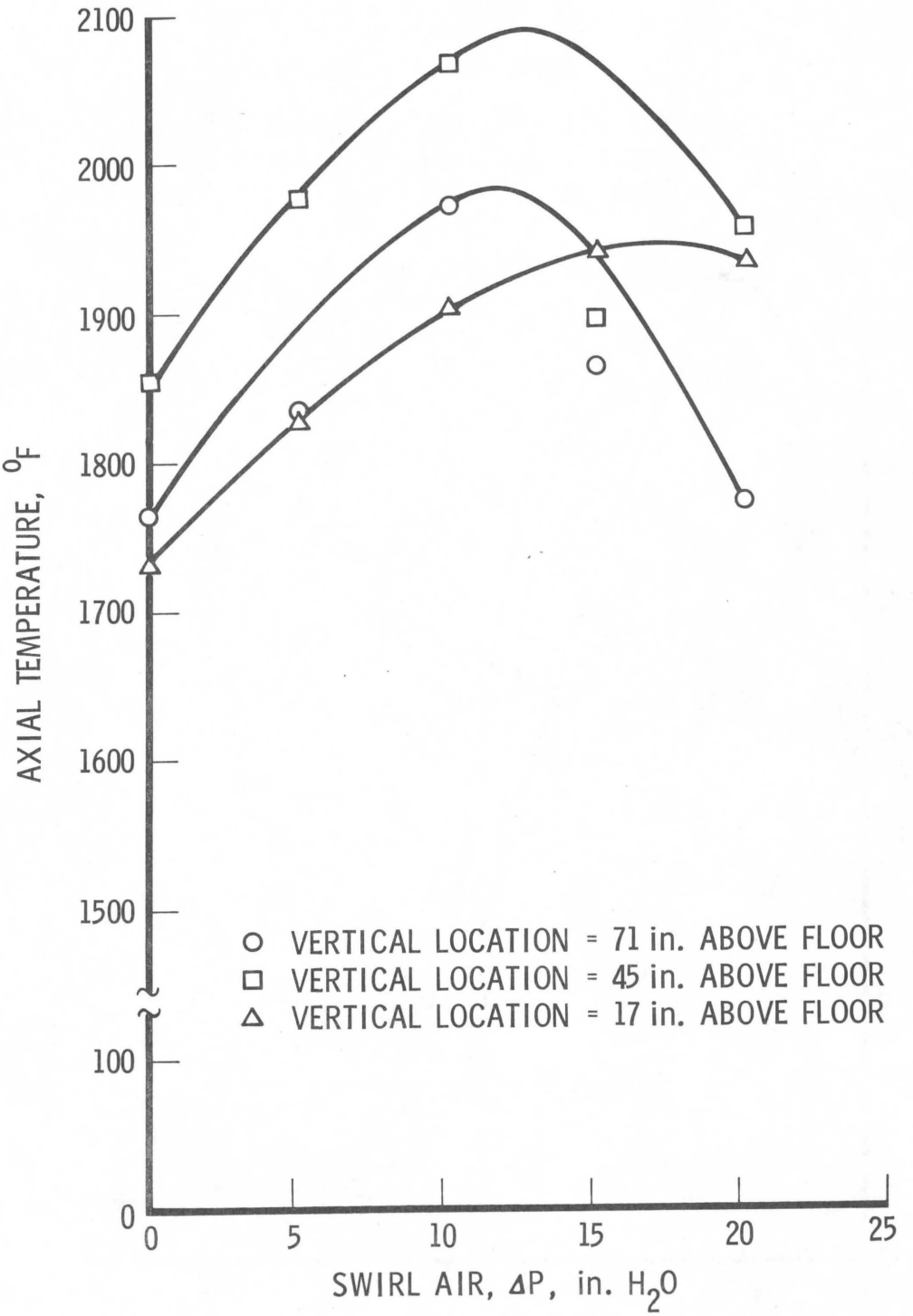


Fig. 25. Centerline Temperature Variation with Swirl Air Flow, Acetone Fuel

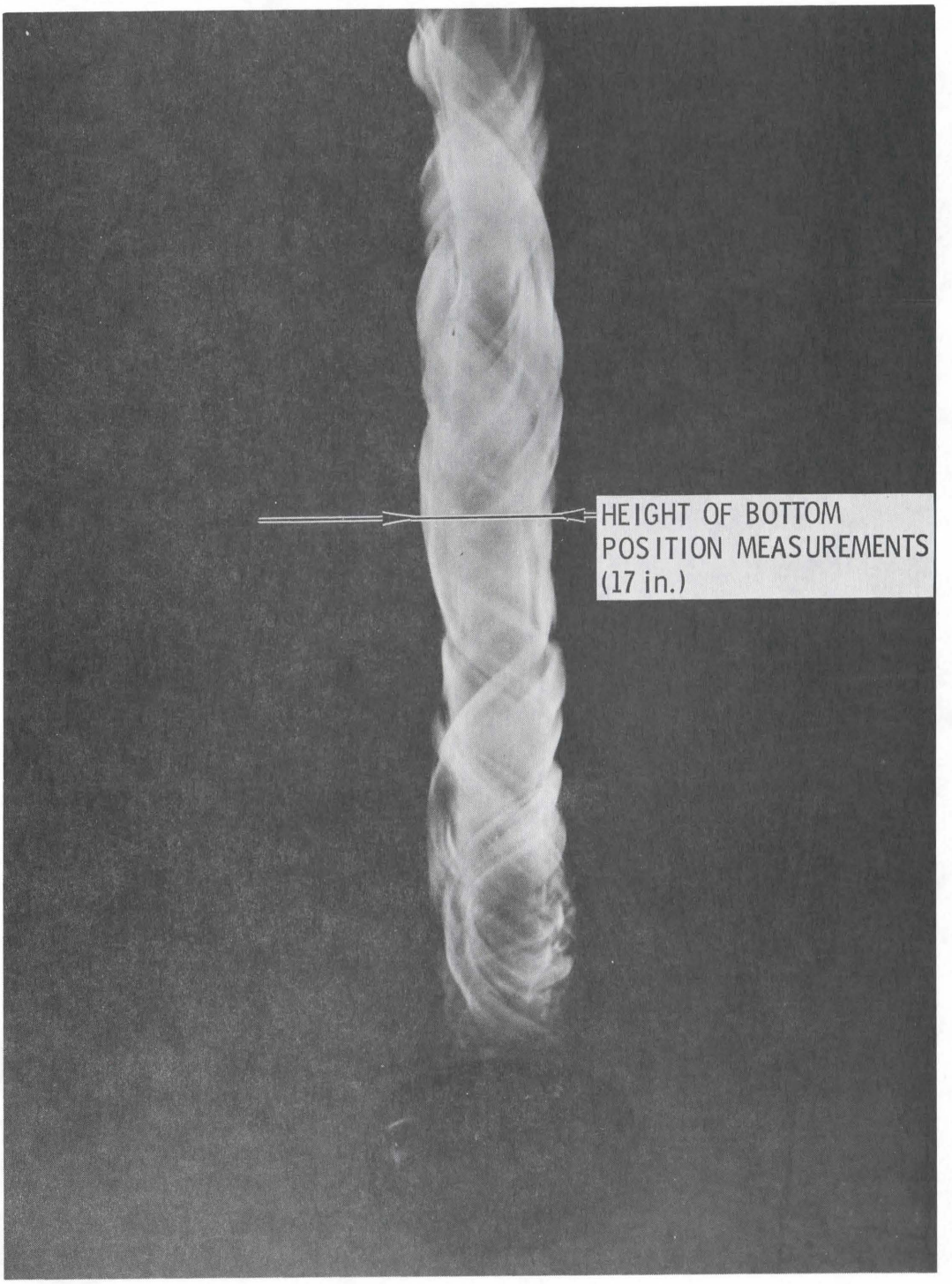


Fig. 26. Fire Whirl Experiment with Acetone Fuel

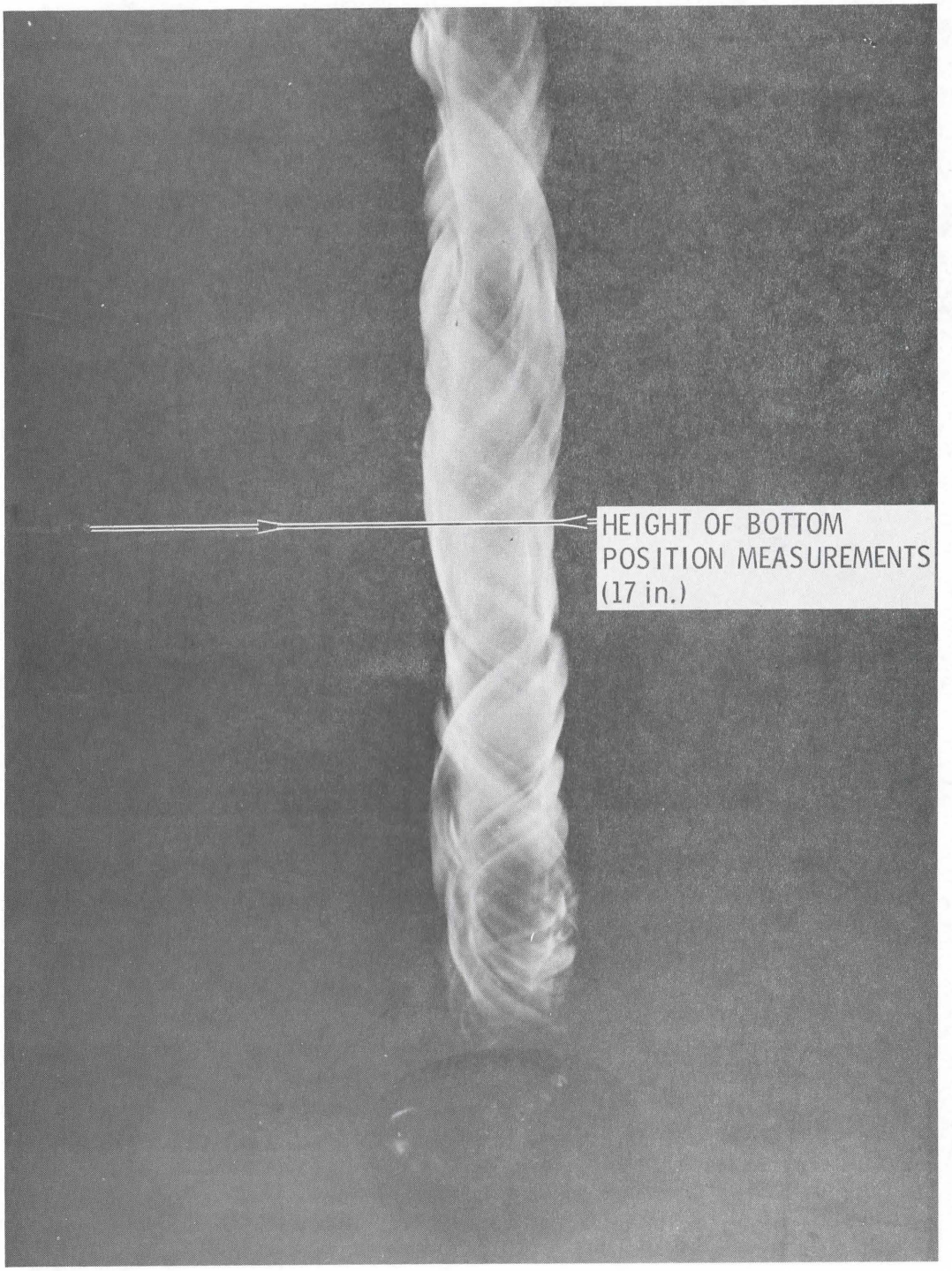


Fig. 27. Fire Whirl Experiment with Acetone Fuel

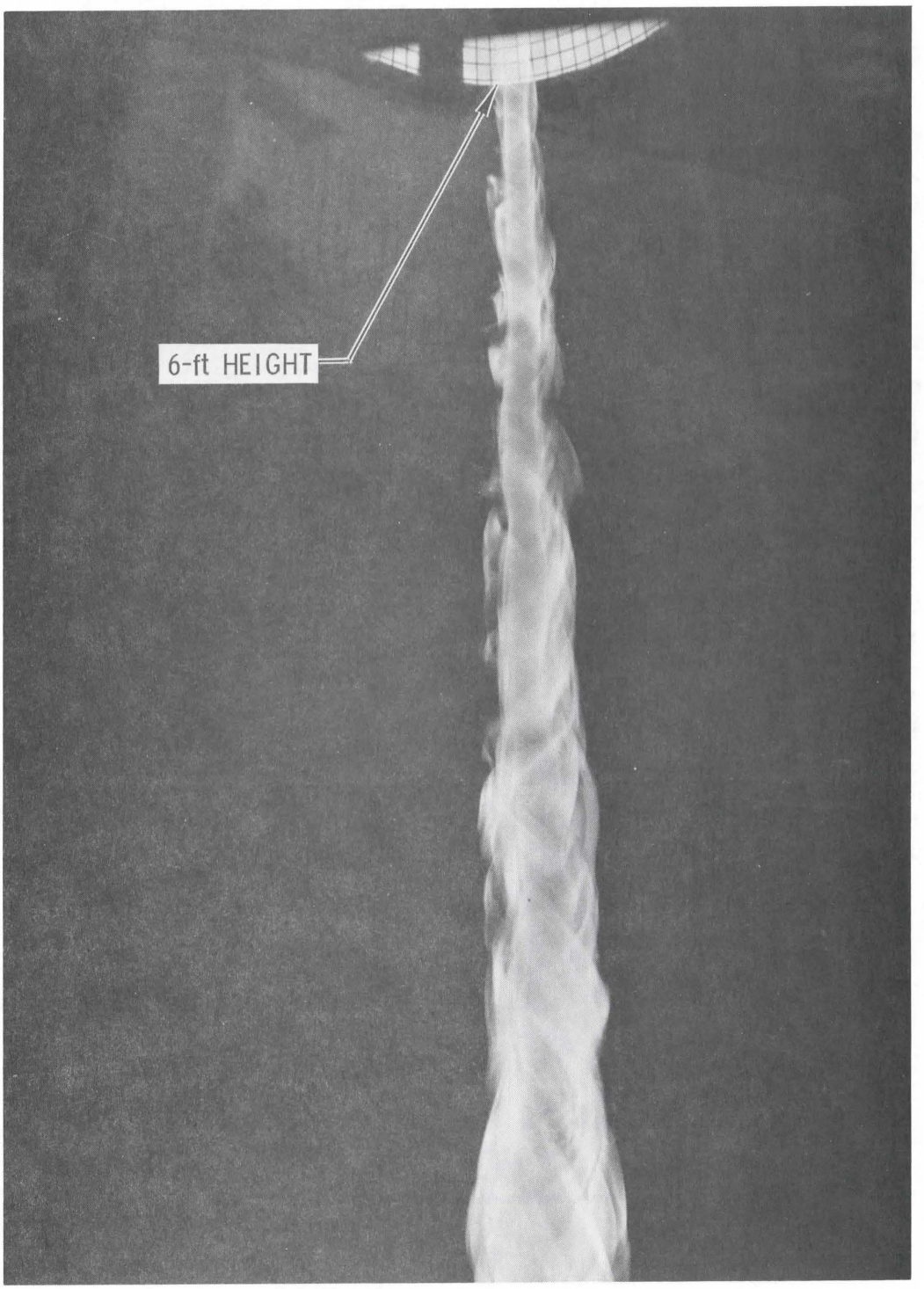


Fig. 28. Mid-Part View of the Fire Whirl Core with Acetone Fuel

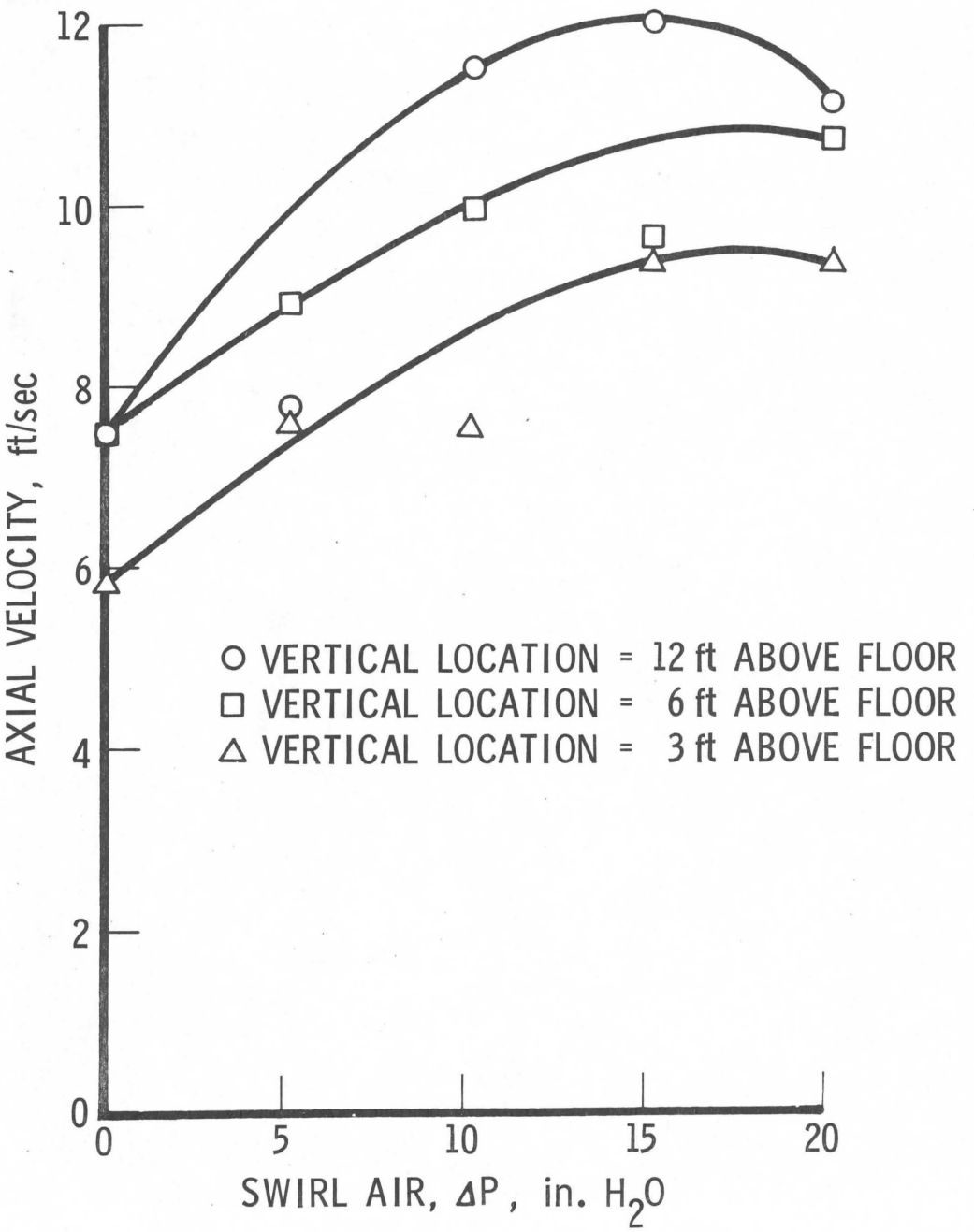


Fig. 29. Centerline Vertical Velocity Variation with Swirl Air Flow, Acetone Fuel

uniformly to the lowest height. Note again that several data points have been ignored due to their inconsistency with the remaining data.

## 4. DISCUSSION

The characterization of the swirl region using acetone fuel is incomplete and will continue concurrently with tests involving wood fuels. Therefore, the discussion will center on problems that were encountered in carrying out the experiments, the problems which are yet unsolved, and the plans for the future to eliminate these problem areas.

During the course of this study, several changes in the basic apparatus were necessitated. First, the top cylindrical section which had been open screen had to be enclosed in order to maintain an adequate circulation at higher levels. Second, TBLI inducers were incorporated to give improved circulation. The use of the TBLI came about in two design steps. The first design did not completely block the radial velocity components of the wind; and, thus, even under the mildest of wind conditions, there was an effect of the outside ambient wind which affected swirl stability. The second-stage design lengthened the inlets so that the radial direction was completely blocked, and this resulted in excellent stability and increased the burn rate of the fire whirl. Concomitant with the change in the design of the TBLI, a change in the $\Delta p$ transducer was required due to a malfunction of the previously used transducer. Thus, two changes took place at the same time. A comparison of the results obtained before and after the change is somewhat baffling. The fuel burn rates and core temperatures obtained with the initial inlet design were both lower than those obtained with the extended design. However, the swirl velocities and axial velocities decreased by approximately 30 percent. These results appear inconsistent and may be caused by an error in the calibration of either the first or second transducer. Consequently, the construction of a calibration system to verify the experimental velocity data obtained to date will be of top priority during the follow-on work.

In each of the experiments, it was noted that at the beginning of the run the acetone in the dish was fairly calm, but later it began to swirl precipitously. In a few runs, this change in the acetone system appeared to reflect a change in the burn rate; namely a higher burn rate at the onset of the run when the acetone was basically at rest and a lower burn rate later in the run when the acetone was completely swirling. This change in burn rate only manifested itself in a few of the runs in which the nonrotating acetone time period was significant. Therefore, it appears of interest to design experiments in which the nonrotating system could be stabilized for a longer period of time to give an accurate measure of this effect. This, however, will not be pursued further since the goal of this work is to burn wood cribs and generate firebrands, acetone being only a medium to provide swirl characterization.

As indicated in the Results section, the FASI air flow rates are recorded in $\Delta p$, inches of water, as measured across the square-edged orifice in the flow inlet. This was done for the following reason. The square-edged orifice was calibrated by the normal procedures, but the maximum flow rate indicated by this calibration exceeded the manufacturer's reported capacity for the blower. Because of the tight test schedule and the fact that part of the FASI air inlet system will have to be dismantled in order to cross check this result, the problem has not been resolved as of yet. However, in the near future, velocity measurements in the inlet pipe will be taken to verify the actual mass flow rates as they compare with the calibration. The current calibration is given in Fig. 30 and can be used with the above reservation.

During the early test periods, i.e., prior to the evolvement of the final test apparatus configuration, a great deal of variation in the results was obtained. One possible cause of this variation was the differences in the ambient conditions for the various days and times of day during which tests were run. In particular, the wind speed, air temperature, and humidity seem to be important. With the current configuration, it appears that the wind speed effect has been minimized, but air

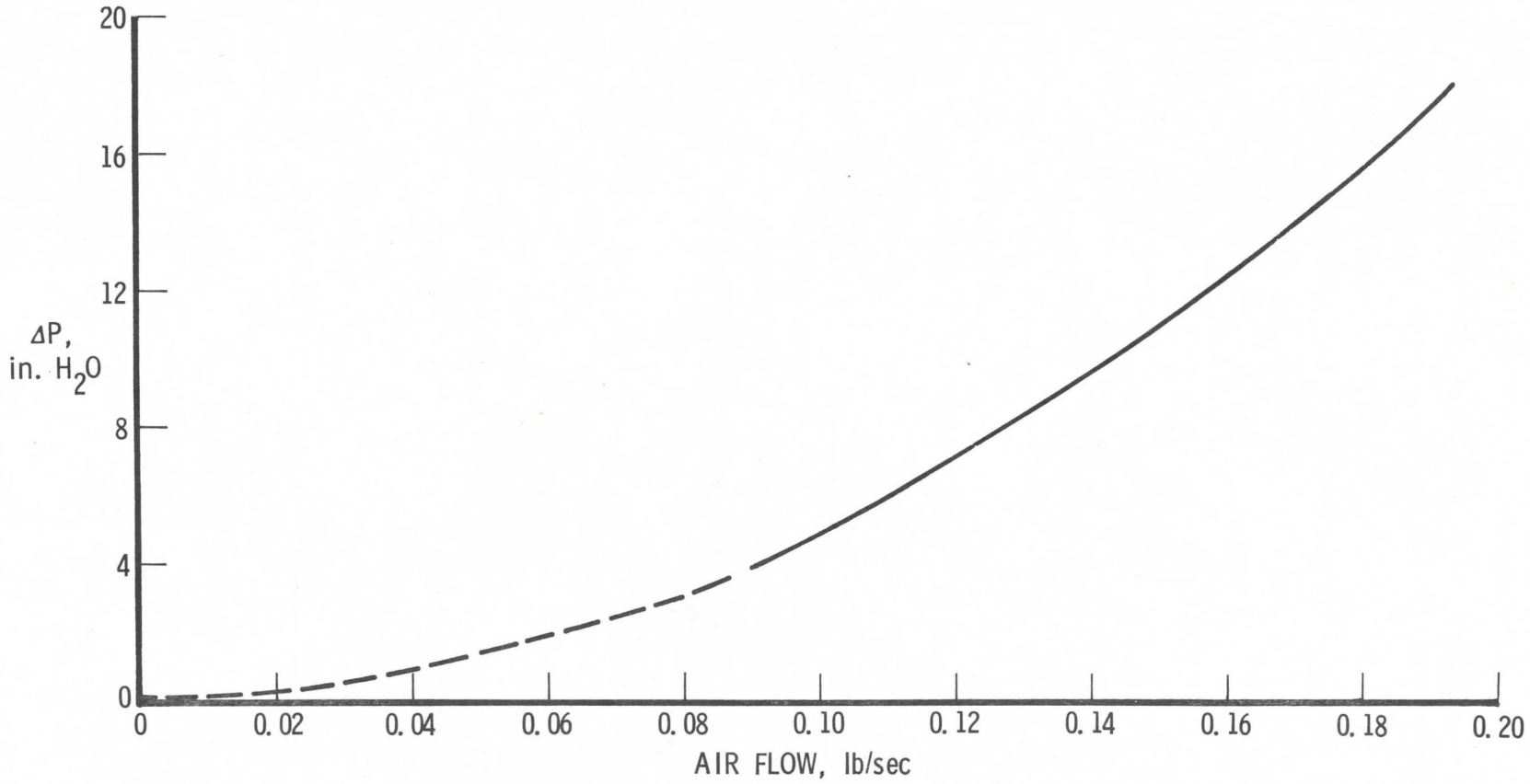


Fig. 30. Orifice Air Flow Calibration

temperature and humidity may still be important in that the ambient air is drawn directly into the combustion zone and up through the swirling core. For this reason, we now take both of these measurements during each run. The data reported herein were obtained on three different days. Unfortunately, the temperature and relative humidity (R. H. ) data must be examined on a test-by-test basis since a large variation often occurs even on the same day. For example, on one day the temperature was 70°F and R. H. 44 percent at the start, but was 56°F and 88 percent by the end of the day. To date, not enough data have been obtained to indicate any consistent variation caused by these parameters.

## 5. WOOD FUEL FEASIBILITY TESTS

As a demonstration of feasibility for the types of tests that will be run in the continuing phase of this study, three runs were made using wood cribs. The first two involved 6-in diameter cribs, as shown in Fig. 31. These cribs were set directly on the Pyrex glass dish used in the acetone experiments; and, thus, the burning rate of these cribs could be measured directly with the weighing system. In the third test, the entire floor was covered with a crib, as shown in Fig. 32. Here it should be noted that the 6-in crib still exists as a separate piece in the center and is placed directly over the dish for weighing. In each test, the crib was stuffed full of excelsior, and the ignition was accomplished by putting 20 grams of acetone in the dish and igniting it as an initiator. Alternative ignition techniques will be investigated to minimize the ignition effects on the wood burning characteristics.

In the first test, using a 6-in crib with TBLI and FASI ($\Delta p$ = 10 in), a swirl was established and the crib burned almost completely out. The burn rate was determined to be 1.9 gm/sec (based on the last 40 sec of burn) and the temperature profile at a height of 17 in is shown in Fig. 33. It is of interest to note that the core size for this wood crib is quite similar to that obtained with acetone and that the total burn time was in excess of 60 sec. During the burning, no firebrand

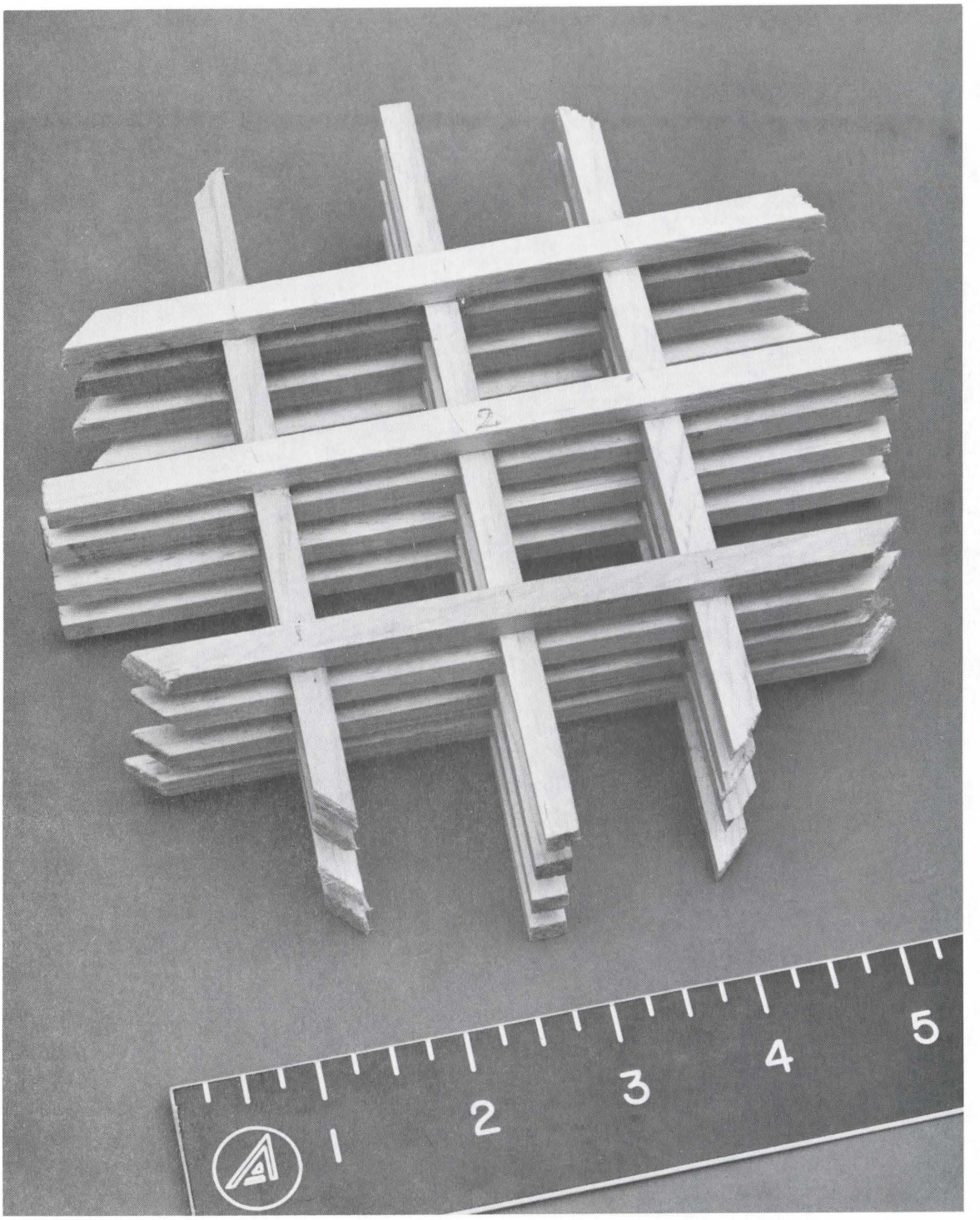


Fig. 31. Small (Six-Inch) Wood Crib

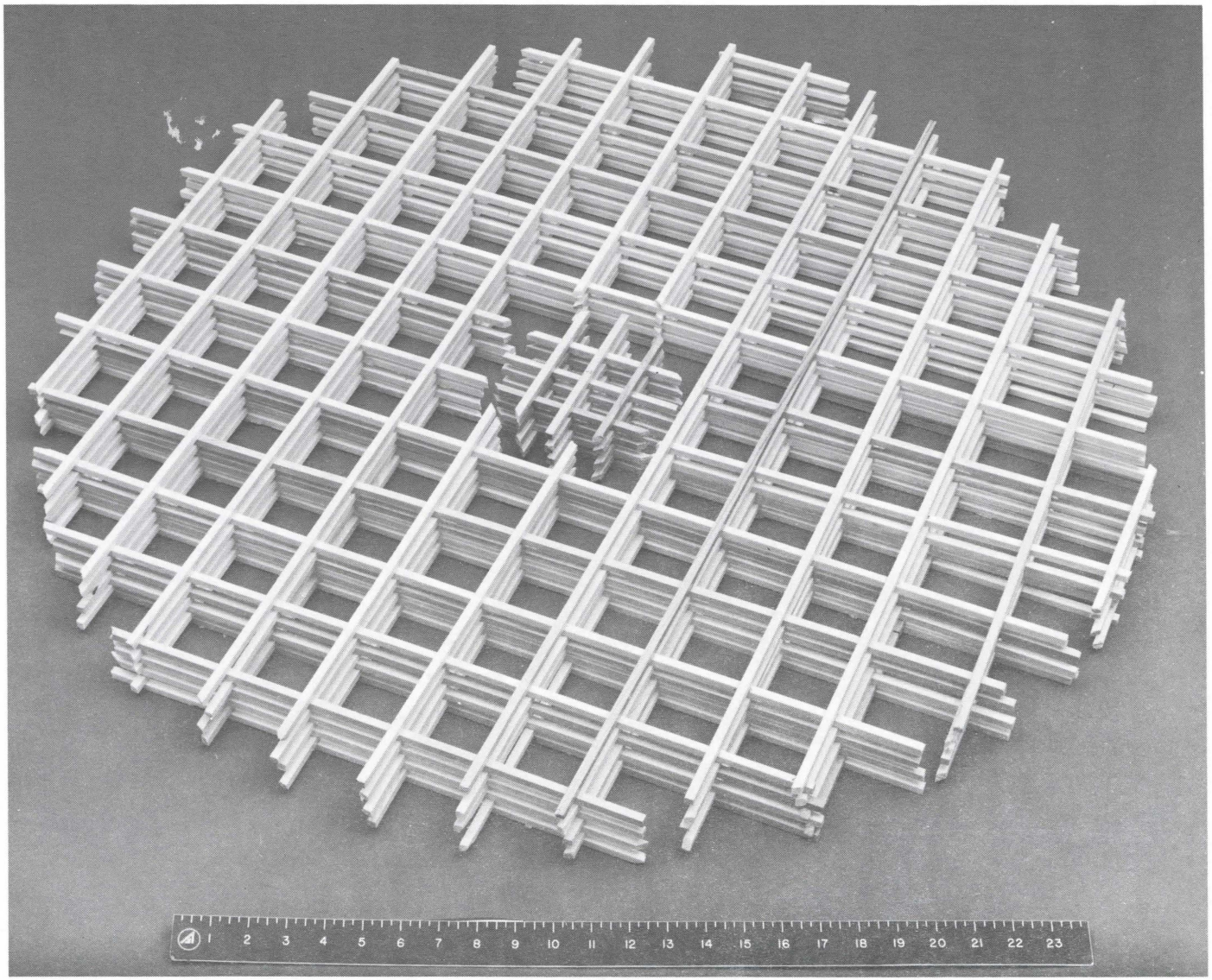


Fig. 32. Composite Wood Crib

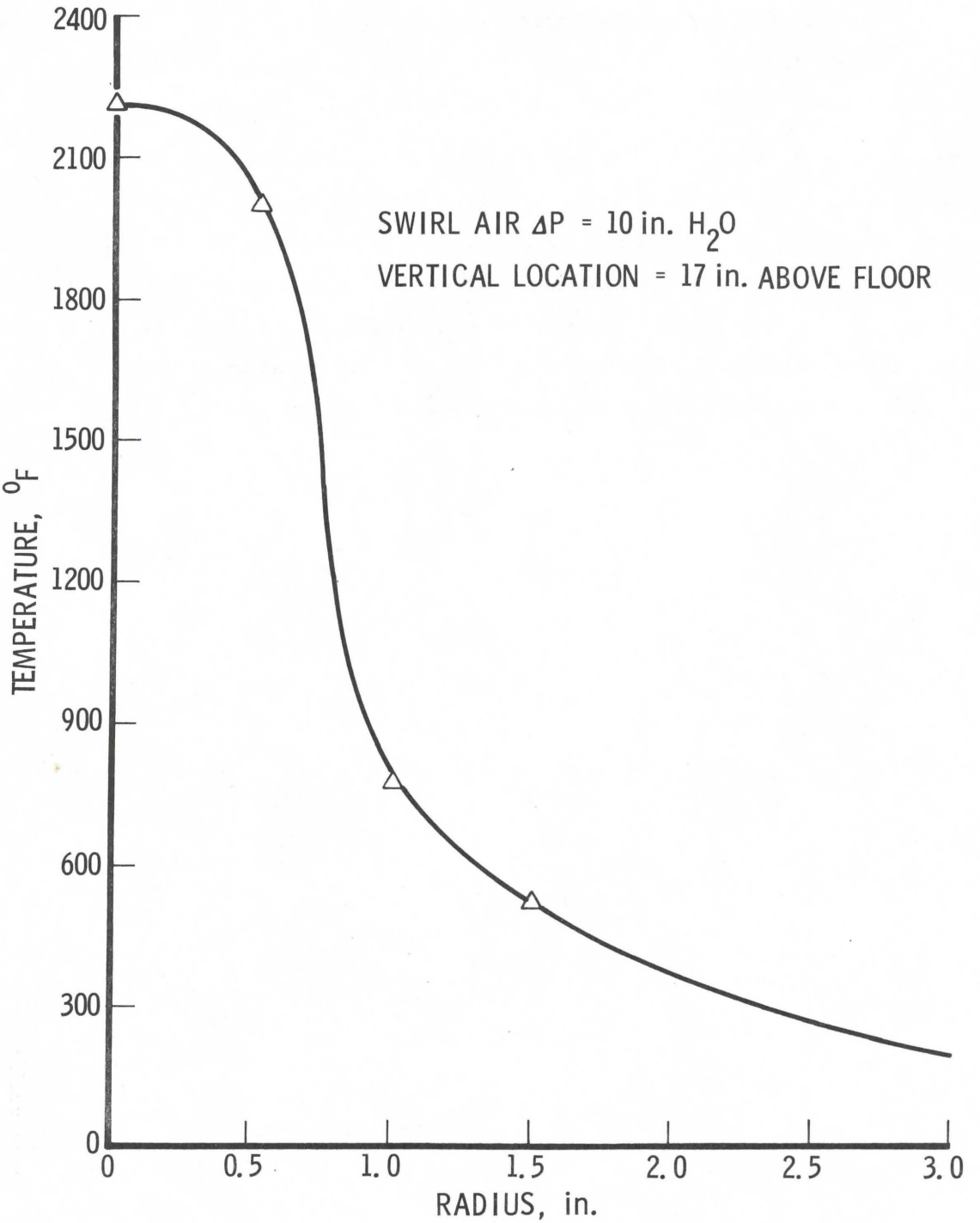


Fig. 33. Core Temperature Radial Distribution, Wood Crib Fuel

lifting was discernable; however, motion pictures of the tests showed some lifting near the end of the test.

The second test with a 6-in wood crib did not involve any circulation, i.e., both the TBLI were removed and the FASI shut off. The resulting average burn rate was 2.2 gm/sec. The maximum temperature recorded at 17 in above the floor was only 475$^{o}$F.

In the last test, in which the entire floor was covered with the crib, the fire burned all the way to the walls of the apparatus and eventually burned out the plastic windows and the plastic covering on the top cylinder. Thus, it is clear from these experiments that we can successfully burn wood cribs in this apparatus and establish fire swirls above them. However, the total diameter of the cribs must be limited so that a space exists between the crib and the wall.

# V. CONCLUSIONS

A. Burning of firebrands in flight can be represented by a relationship similar to that of wood pyrolysis (first order) with a modifying factor based on characteristic firebrand dimensions (volume/surface ratio).

B. The rate of firebrand burning in wind is lower than that in quiescent air. The burning in wind is mainly restricted to the glowing at the windward part with little or no burning at all of the leeward part. The burning in quiescent air is, on the other hand, occurring around the whole sample (mostly with flaming combustion).

C. Burning in quiescent air is characterized by a period of flaming combustion followed by glowing. For in-wind burning, a short initial period of flaming could be observed at wind velocities up to 15 mph, and was followed by windward edge glowing combustion. At higher wind velocity, there was no flaming at all.

D. The in-wind burning continues to total consumption of the material, while burning in quiescent air terminates at some final density which is a function of initial fuel size. A relationship between this density and fuel size was established.

E. After reaching the ground, the firebrand burning, if it continues, will be in most cases in a glowing combustion mode.

F. An analytical model for a fire whirl is presented which couples the vortex core flow, the ground boundary layer air inflow, and the physics of the burning fuel. Vertical uplift core velocities and enhanced fuel burn rates are predicted.

G. The tests carried out confirmed the existence of near-irrotational flow field (constant angular momentum) outside of the core.

H. The vorticity generated in the boundary layer near the ground has a primary effect on the fire whirl intensity. Air introduced tangentially along the wall of the test rig cylinder had a minor effect by reduction of wall friction losses.

I. Stabilization of the fire whirl core was achieved by increasing boundary layer vorticity and by shielding the test rig from ambient wind.

J. Wood crib ignition and burning in a fire whirl was demonstrated with swirl intensities similar to those obtained with acetone.

# VI. RECOMMENDATIONS

The primary goal of this program rests upon the demonstrated capability of not only measuring the quantity and size of firebrands lofted by the swirl, but also relating these data to burn rate, vortex strength and fuel characteristics. All tests carried out in the future must, therefore, be related to the primary goal. Considering this, the following specific recommendations are made.

A. In-wind burning data with natural fuels and with varying moisture content require further analysis to confirm or modify the relationship now established. Complete fuel ignition coupled with control of ignition time is necessary for test repeatability.

B. Fire whirl test rig modifications should be carried out to increase the swirl intensity and to provide means of its control.

C. Tests with various wood fuels burning in the fire whirl test rig should be carried out to obtain data on firebrand generation.

D. The analytical model for a fire whirl fueled by natural wood should be completed and the resulting predictions correlated with the test data.

# APPENDIX I

## WIND TUNNEL TEST INFORMATION

### Base Line Experiments

Cylinders--1/2-inch diameter x 2.5 inches and 5 inches long
1-inch diameter x 5 inches long

Materials--birch and pine

Wind Velocities--0, 5, 10, 15, 20, 25 miles per hour

Conditions--Temperature 85 to 90°F
Relative Humidity 20 to 25 percent
Oven-dry dowels

Data: Weigh and measure each dowel before test.

Record weight continuously throughout experiment.

Take 35-mm black and white photos from end of dowel and from top, periodically throughout experiment--approximately 10 exposures per test.

Take pictures simultaneously and mark weight-loss chart at time of exposure. Before igniting dowel, take one exposure of dowel and test number.

Mark weight. Record charts to show significant events such as igniter in place, igniter removed, if dowel is flaming, flame extinguishment. Also note erratic or uneven burning.

### Supplementary Experiments

#### Effect of Relative Humidity

Repeat above with 1-inch x 5-inch dowels
at 10 and 15 mph and Relative Humidity at 10 to 15 percent
30 to 35 percent
40 to 45 percent
50 to 55 percent.

Use oven-dry dowels and maintain temperature at 85 to 90°F.

#### Effect of Fuel Moisture

Precondition 1-inch x 5-inch birch and pine dowels at 20, 40, and 60 percent relative humidity and 85°F and stabilize for two weeks. Take fuel moisture samples periodically to determine the stabilized value. Set the wind tunnel conditions to match at the time of burning.

Wind Velocity--15 mph

Burning Rate of Plates

Material--flat wood cedar, pine, birch 1/4-inch x 5 x 5
1/2-inch x 5 x 5

Test conditions similar to base line experiments for cylinders. Exact conditions will be determined after some initial tests.

Natural Materials

Bark plates, pine cones, limb wood.

Conduct experiments with these materials as seems appropriate and useful. It may not be possible to obtain weight loss measurements due to odd shapes and, hence, erratic wind loads. We should be able to get burn times and photographs to show size during burning.

Flaming Characteristics

Certain tests will be repeated to determine the burning characteristics, i.e., glowing or flaming, when wind is stopped. The standard test data will be examined to aid in determining which conditions are most likely to support flaming combustion.

Data Reduction

Determine the size of the firebrand at the time each picture is taken. Obtain the weight at the same time and compute the density. The firebrand density is the primary number needed by Dr. Muraszew to substantiate the burning and aerodynamic force characteristics.

## APPENDIX II

## COMPARISON OF RADIATIVE VS. CONVECTIVE HEAT TRANSFER TO THE FUEL SURFACE

The radiative heat transfer was included in the total heat transfer coefficient without a swirl, $h_o$, and it was further assumed that the radiative contribution will remain the same when the swirl is introduced and that the increased heat transfer to the fuel surface will be due entirely to the convective term, $h_w$, only.

The radiative heat transfer is only a small fraction of the swirl convection, as is shown in the calculation below; consequently, any error resulting from the assumption made will be also small.

The direct calculation of the radiative heat transfer is difficult because of the lack of data on acetone surface absorptivity and flame emissivity. However, an indirect assessment of the radiative heat transfer can be made from experimental data on the acetone burn rate without a swirl. In that condition, conductive, convective and radiative heat transfer mechanisms existed, and in the extreme case it could be assumed that radiation is the main contributor.

Heat transfer without swirl

$$h_o\left(\bar{T} - T_s\right) = \rho_f \bullet G_o \bullet Q_i$$

$Q_i$ - pre-ignition heating - 260 Btu/lb
$\rho_f$ - acetone bulk density - 50 lb/ft$^3$
$G_o$ - experimental burn rate without swirl = $7.63 \bullet 10^{-5}$ ft/sec
$h_o\left(\bar{T} - T_s\right) = 50 \bullet 7.63 \bullet 10^{-3} \bullet 260 = 0.993$ Btu/ft$^2$-sec.

The convective heat transfer coefficient due to swirl, $\dot{q}_c$, from Eq. (23) is:

$$h_w = \bar{\rho} \bullet C_p \bullet P_r^{-2/3} \bullet N'_{(o)} \bullet \sqrt{\bar{\nu}\Gamma} \bullet \frac{1}{a_o} .$$

From Table 3 for temperature $T = 2600^{\circ}R$

$a_o = 0.121$ ft; $\Gamma = 3.7$ ft$^2$/sec

$\bar{\rho} = 0.2\,\rho_o = 0.2 \cdot 0.076 = 0.0152$ lb/ft$^3$ .

For air at temperature $\bar{T} = 2600^{\circ}R$

$\bar{\nu} = 0.0021$ ft$^2$/sec

$P_r = \dfrac{\bar{\mu}\bar{C}_p}{\bar{k}} = 0.77$

$\bar{\mu} = 34.4 \cdot 10^{-6}$ lb$_m$/ft-sec

$\bar{C}_p = 0.292$ Btu/lb$_m$, $^{\circ}R$

$\bar{k} = 0.047$ Btu/ft, hr, $^{\circ}R$

$N'_{(o)} = C$ (in Table 3) $= 0.7$ .

Acetone surface temperature at boiling $T_s = 600^{\circ}R$.

$$h_w = 0.0152 \cdot 0.292 \cdot 1.19 \cdot 0.7 \cdot \sqrt{0.0021 \cdot 3.7} \cdot \frac{1}{0.121}$$
$$= 0.0027 \text{ Btu/sec, ft}^2, {}^{\circ}R$$

$$\dot{q}_c = h_w\left(\bar{T} - T_s\right) = 0.0027(2600 - 600) = 5.4 \text{ Btu/ft}^2\text{-sec.}$$

Thus, even with radiation as the main mechanism of heat transfer, it would be less than 1/5 of the swirl convection.

## SYMBOLS

$a$ = pre-exponential constant, $sec^{-1}$ (Section III)

$a$ = core radius, ft (Section IV)

$a_o$ = core radius at z = o

$A$ = $\bar{\rho} u_o a_o^2$, $lb_m/sec$

$A_{(t)}$ = firebrand maximum cross-section, $cm^2$

$B'$ = a nondimensional constant characterizing boundary layer radial mass inflow

$C$ = $N'(o)$

$C_f$ = skin friction coefficient at the core/air interface

$C_D$ = drag coefficient

$C_p$ = specific heat, $Btu/lb_m\text{-}^oR$

$\bar{C}_p$ = core mean specific heat, $Btu/lb_m\text{-}^oR$

$D_o$ = initial firebrand diameter, cm

$E$ = activation energy in cal/g mole

$g$ = standard acceleration due to gravity, 981 $cm/sec^2$ or 32.18 $ft/sec^2$

$G$ = linear burn rate of fuel with swirl, ft/sec

$G_o$ = linear burn rate of fuel without swirl, ft/sec

$h$ = total heat transfer coefficient between the swirling flow and the burning surface, $Btu/ft^2\text{-}sec\text{-}^oR$

$h_o$ = fuel surface heat transfer coefficient without swirl, $Btu/ft^2\text{-}sec\text{-}^oR$

$h_w$ = added convective heat transfer contribution due to swirl, $Btu/ft^2\text{-}sec\text{-}^oR$

$K$ = shape factor

$L_o$ = initial firebrand length, cm

$m_{(t)}$ = firebrand mass, g

$\dot{M}_f$ = core fuel burn rate with swirl, $lb_m/sec$

$\dot{M}_{f_m}$ = total fuel burn rate, $lb_m/sec$

$\dot{M}_o$ = steady-state burn rate without swirl, $lb_m/sec$

$n$ = temperature exponent in the specific heat-temperature relationship

$N(\zeta)$ = nondimensional boundary layer azimuthal velocity profile variable

$p$ = pressure, $lb_m/ft\text{-}sec^2$ ($1\ lb_f/ft^2 = 32.18\ lb_m/ft\text{-}sec^2$)

$P_r$ = Prandtl number

$Q_c$ = net heat of combustion of the fuel which is effective in heating the core gas, $Btu/lb_m$

$Q_i$ = effective heat of ignition of the fuel, $Btu/lb_m$

$r_o$ = radius of acetone dish, ft

$R$ = universal gas constant, 1.987 cal/g-mole-$^oK$ (Section III)

$R$ = core mean gas constant, $lb_m\text{-}ft^2/sec^2\text{-}^oR\text{-}lb_m$ mole (Section IV)

$S_t$ = Stanton number

$T$ = pyrolysis temperature, $^oR$ (Section III)

$T$ = local fire whirl core temperature, $^oR$ (Section IV)

$\bar{T}$ = core mean temperature, $^oR$

$T_s$ = fuel surface burning temperature, $^oR$

$T_\infty$ = ambient temperature, $^oR$

$u$ = axial (vertical) velocity, ft/sec

$\bar{u}$ = radially averaged core vertical velocity, ft/sec

$V_{BL}$ = boundary layer radial velocity, ft/sec

SYMBOLS (concluded)

$V_\infty$ = convection characteristic velocity, ft/sec

$w_{(t)}$ = fall velocity, cm/sec

W = azimuthal velocity, ft/sec

z = axial variable, ft

$z_e$ = vertical extent of the ambient circulation, ft

$\alpha$ = nondimensional entrainment coefficient

$\beta$ = temperature exponent in the viscosity-temperature relationship

$\Gamma$ = ambient circulation, $ft^2/sec$ ($\Gamma = Wa$)

$\zeta$ = nondimensional boundary layer axial variable

$\mu_a$ = ambient air viscosity, poise

$\bar{\nu}$ = mean core kinematic viscosity

$\nu_\infty$ = ambient kinematic viscosity, $ft^2/sec$

$\bar{\rho}$ = core mean density, $lb_m/ft^3$

$\rho_a$ = ambient air density, $g/cm^3$

$\rho_c$ = final burning wood density, $g/cm^3$

$\rho_F$ = bulk density of the fuel, $lb_m/ft^3$

$\rho_\infty$ = ambient density, $lb_m/ft^3$

$\tau_o$ = fuel surface shear stress, $lb_m/ft\text{-}sec^2$

$\omega$ = angular velocity, $sec^{-1}$

# REFERENCES


Albini, F. A., 1966, "A Physical Model for Fire Spread in Brush," 11th Int. Comb. Symposium, pp. 553-560.

Anderson, H. E., 1968, "Sundance Fire," USDA Forest Service Research Paper INT-56, 25 pp.

Byram, G. M., 1959, Combustion of Forest Fuels, Forest Fire Control and Use, McGraw-Hill Book Co., Inc., New York, New York, pp. 61-69.

Byram, G. M. and Martin, R. E., 1970, "The Modeling of Fire Whirlwinds," Forest Science, Vol. 16, No. 4, pp. 386-399.

Emmons, H. W., 1965, "Fundamental Problems of the Free Burning Fire," Tenth Symposium on Combustion, The Combustion Institute.

Emmons, H. W. and Ying, S. J., 1967, "The Fire Whirl," Eleventh Symposium on Combustion (1966), The Combustion Institute, pp. 475-488.

Fons, W. L., 1946, "Analysis of Fire Spread in Light Forest Fuels," J. Agri. Res., 72(3), pp. 93-121.

Lee, S. L., 1966a, "Axisymmetrical Turbulent Swirling Natural Convection Plume," Part 1, J. of Ap. Mech., Vol. 33, September, pp. 647-655.

Lee, S. L., 1966b, "Axisymmetrical Turbulent Swirling Natural Convection Plume," Part 2, J. of Ap. Mech., Vol. 33, September, pp. 565-661.

Lee, S. L. and Hellman, G. M., 1970, "Firebrand Trajectory Study Using an Empirical Velocity-Dependent Burning Law," Combustion and Flame, 15, pp. 265-274.

Martin, S., 1964, "Ignition of Organic Materials by Radiation," Fire Research Abstracts and Review, 6.

Morton, B. R., Taylor, Sir Geoffrey and Turner, J. S., 1956, "Turbulent Gravitational Convection from Maintained and Instantaneous Sources," Proceedings of Royal Society of London, Vol. 234, pp. 1-22.

Muraszew, A., 1974, "Firebrand Phenomena," The Aerospace Corporation Report No. ATR-74(8165-01)-1, 109 pp.

Rothermel, R. C., 1967, "Sundance Fire," Eastern States Section, The Combustion Institute, 4 pp.

Rothermel, R. C., 1972, "A Mathematical Model for Predicting Fire Spread in Wildland Fuels," USDA Forest Service Res. Paper INT-115, 40 pp.

Schlichting, H., 1960, Boundary Layer Theory, McGraw-Hill Book Co., New York, New York.

Stevenson, E. A., et al, 1973, "Computer Simulation of an Actual Forest Fire," Spring Meeting of the Western States, The Combustion Institute, Tempe, Arizona, 26 pp.

Tarifa, C. S., 1965, "On the Flight Paths and Lifetimes of Burning Particles in Wood," Tenth Int. Comb. Symposium, The Combustion Institute, pp. 1021-1037.

Tarifa, C. S., 1967, "Transport and Combustion of Firebrands," U.S. Department of Agriculture, Madrid University Report, Vol. II, 90 pp.

Von Wagner, C. E., 1967, "Calculations of Forest Fire Spread by Flame Radiation," Sixth World Forestry Congress, Madrid, June 1966, 30 pp.

Young, P. H., 1973, "Firebrand Trajectory Model," The Aerospace Corporation Report No. ATR-74(8158)-1, 16 pp.

AEROSPACE CORPORATION

**INTERNAL DISTRIBUTION LIST**

(REFERENCE: COMPANY PRACTICE 7-21-1)

REPORT TITLE

FIREBRAND INVESTIGATION

| REPORT NO. | PUBLICATION DATE | SECURITY CLASSIFICATION |
|---|---|---|
| ATR-75(7470)-1 | 31 March 1975 | Unclassified |

(NOTE: FOR OFF-SITE PERSONNEL, SHOW LOCATION SYMBOL, e.g. JOHN Q. PUBLIC/VAFB)

E. B. Anderson (3)
J. B. Fedele (3)
E. G. Hertler
S. D. Huffman
A. Muraszew (6)
N. R. O'Brien
T. D. Taylor
J. Vasiliu

APPROVED BY P. Stevens DATE 4/2/25

SHEET 1 OF 1

AEROSPACE FORM 2394 REV 7-66

THE AEROSPACE CORPORATION

**EXTERNAL DISTRIBUTION LIST**

(REFERENCE: COMPANY PRACTICE 7-21-1)

REPORT TITLE

FIREBRAND INVESTIGATION

| REPORT NO. | PUBLICATION DATE | SECURITY CLASSIFICATION |
|---|---|---|
| ATR-75(7470)-1 | 31 March 1975 | Unclassified |

| MILITARY AND GOVERNMENT OFFICES | ASSOCIATE CONTRACTORS AND OTHERS |
|---|---|

(NOTE: SHOW FULL MAILING ADDRESS; INCLUDE ZIP CODE, MILITARY OFFICE SYMBOL, AND "ATTENTION" LINE.)

Press Butler
Stanford Research Institute
333 Ravenswood Avenue
Menlo Park, CA 94025

G. M. Byram
5 Cherry Lane
Asheville, NC 28804

Craig C. Chandler, Director
Division of Forest Fire and Atmospheric
Sciences Research
USDA Forest Service
Washington, D. C. 20250

Professor Howard E. Emmons
California Institute of Technology
Mail Stop 301-46
Pasadena, CA 91109

Frank Fendell
TRW, Inc.
Building R1, Room 1016
One Space Park
Redondo Beach, CA 90278

Professor Melvyn Gerstein
Associate Dean, Graduate Affairs
Engineering School
University of Southern California
University Park
Los Angeles, CA 90007

AFR 80-45 DISTRIBUTION STATEMENT X'D BELOW APPLIES

☐ NO DISTRIBUTION STATEMENT
(Classified documents only)

☐ A. APPROVED FOR PUBLIC RELEASE; DISTRIBUTION UNLIMITED

☐ B. DISTRIBUTION LIMITED TO U. S. GOV'T AGENCIES ONLY;

_____;
(Reason)

_____. OTHER REQUESTS FOR THIS DOCUMENT
(Date statement applied)

MUST BE REFERRED TO _____.
(Controlling DOD office)

APPROVED BY _____ DATE 4/2/75
(FOR THE AEROSPACE CORPORATION)

APPROVED BY _____ _____ DATE _____
(FOR COGNIZANT AF OFFICE) (SYMBOL)

IF LIST COMPRISES TWO OR MORE SHEETS, COMPLETE THIS SIGNATURE BLOCK ON LAST SHEET ONLY

THE AEROSPACE CORPORATION

**EXTERNAL DISTRIBUTION LIST**

(REFERENCE: COMPANY PRACTICE 7-21-1)

REPORT TITLE

FIREBRAND INVESTIGATION

| REPORT NO. | PUBLICATION DATE | SECURITY CLASSIFICATION |
|---|---|---|
| ATR-75(7470)-1 | 31 March 1975 | Unclassified |

| MILITARY AND GOVERNMENT OFFICES | ASSOCIATE CONTRACTORS AND OTHERS |
|---|---|
| (NOTE: SHOW FULL MAILING ADDRESS; INCLUDE ZIP CODE, MILITARY OFFICE SYMBOL, AND "ATTENTION" LINE.) | |
| | Stan Hirsch (3 copies)<br>Riverside Fire Laboratory<br>P. O. Box 5007<br>Riverside, CA 92507<br><br>James E. Kerr, Staff Director<br>Support Systems Research<br>Disaster Preparedness Agency<br>Washington, D. C. 20301<br><br>Dr. William C. Kuby (2 copies)<br>Mechanical Engineering Department<br>University of California - Santa Barbara<br>Santa Barbara, CA 93106<br><br>Professor S. L. Lee<br>State University of New York at Stony Bro<br>Stony Brook, NY 11790<br><br>Peter H. Kourtz, Research Officer<br>Canadian Forestry Service<br>Forest Fire Research Institute<br>Ottawa, Canada<br><br>R. E. Martin<br>College of Forestry Resources<br>University of Washington<br>Seattle, WA 98195 |

| AFR 80-45 DISTRIBUTION STATEMENT X'D BELOW APPLIES | |
|---|---|
| ☐ NO DISTRIBUTION STATEMENT (Classified documents only) | ☐ B. DISTRIBUTION LIMITED TO U. S. GOV'T AGENCIES ONLY; _____ (Reason); _____ (Date statement applied). OTHER REQUESTS FOR THIS DOCUMENT MUST BE REFERRED TO _____ (Controlling DOD office). |
| ☐ A. APPROVED FOR PUBLIC RELEASE; DISTRIBUTION UNLIMITED | |

APPROVED BY O. Stevens (FOR THE AEROSPACE CORPORATION) DATE 4/2/75

APPROVED BY _____ (FOR COGNIZANT AF OFFICE) _____ (SYMBOL) DATE _____

IF LIST COMPRISES TWO OR MORE SHEETS, COMPLETE THIS SIGNATURE BLOCK ON LAST SHEET ONLY



AEROSPACE FORM 2380 REV 7-71

THE AEROSPACE CORPORATION

**EXTERNAL DISTRIBUTION LIST**

(REFERENCE: COMPANY PRACTICE 7-21-1)

REPORT TITLE

FIREBRAND INVESTIGATION

| REPORT NO. | PUBLICATION DATE | SECURITY CLASSIFICATION |
|---|---|---|
| ATR-75(7470)-1 | 31 March 1975 | Unclassified |

| MILITARY AND GOVERNMENT OFFICES | ASSOCIATE CONTRACTORS AND OTHERS |
|---|---|

(NOTE: SHOW FULL MAILING ADDRESS; INCLUDE ZIP CODE, MILITARY OFFICE SYMBOL, AND "ATTENTION" LINE.)

Dr. William G. O'Regan
Forest Service
P.O. Box 245
Berkeley, CA 94701

Dr. P. P. Pagni
College of Engineering
University of California - Berkeley
Berkeley, CA 94720

Charles W. Philpot (5 copies)
Division of Forest Fire and Atmospheric Sciences Research
USDA Forest Service
Washington, D.C. 20250

Richard C. Rothermel (50 copies)
Research Project Leader
USDA Forest Service
Intermountain Forest and Range Experiment Station
Northern Forest Fire Laboratory
Drawer G
Missoula, MT 59801

AFR 80-45 DISTRIBUTION STATEMENT X'D BELOW APPLIES

☐ NO DISTRIBUTION STATEMENT
(Classified documents only)

☐ A. APPROVED FOR PUBLIC RELEASE; DISTRIBUTION UNLIMITED

☐ B. DISTRIBUTION LIMITED TO U. S. GOV'T AGENCIES ONLY;

_____;
(Reason)

_____. OTHER REQUESTS FOR THIS DOCUMENT
(Date statement applied)

MUST BE REFERRED TO _____.
(Controlling DOD office)

APPROVED BY P. Stevens (FOR THE AEROSPACE CORPORATION) DATE 4/2/75

APPROVED BY _____ (FOR COGNIZANT AF OFFICE) _____ (SYMBOL) DATE _____

IF LIST COMPRISES TWO OR MORE SHEETS, COMPLETE THIS SIGNATURE BLOCK ON LAST SHEET ONLY